LBL-32877
UC-404

Center for Advanced Materials

CAM

Model Heterogeneous Acid Catalysts and Metal-Support Interactions: A Combined Surface Science and Catalysis Study

I. Boszormenyi
(Ph.D. Thesis)

May 1991

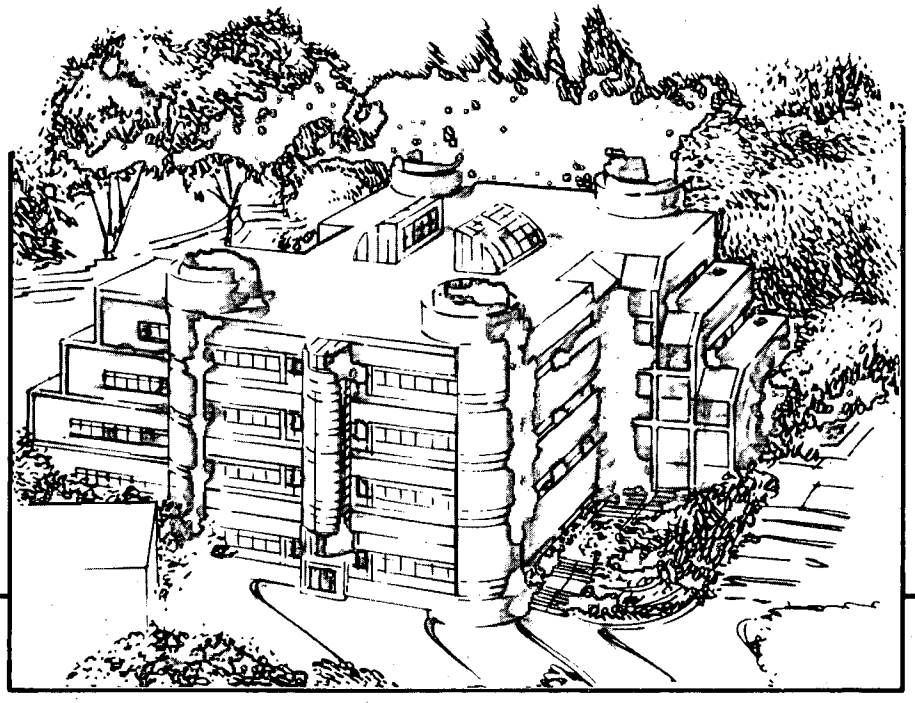

Materials and Chemical Sciences Division

Lawrence Berkeley Laboratory • University of California

ONE CYCLOTRON ROAD, BERKELEY, CA 94720 • (415) 486-4755

Prepared for the U.S. Department of Energy under Contract DE-AC03-76SF00098

| LOAN COPY |
|Circulates |
|for 4 weeks| Bldg. 50 Library.

LBL-32877
Copy 2

DISCLAIMER

This document was prepared as an account of work sponsored by the United States Government. Neither the United States Government nor any agency thereof, nor The Regents of the University of California, nor any of their employees, makes any warranty, express or implied, or assumes any legal liability or responsibility for the accuracy, completeness, or usefulness of any information, apparatus, product, or process disclosed, or represents that its use would not infringe privately owned rights. Reference herein to any specific commercial product, process, or service by its trade name, trademark, manufacturer, or otherwise, does not necessarily constitute or imply its endorsement, recommendation, or favoring by the United States Government or any agency thereof, or The Regents of the University of California. The views and opinions of authors expressed herein do not necessarily state or reflect those of the United States Government or any agency thereof or The Regents of the University of California and shall not be used for advertising or product endorsement purposes.

Lawrence Berkeley Laboratory is an equal opportunity employer.

This report has been reproduced directly from the best available copy.

DISCLAIMER

This document was prepared as an account of work sponsored by the United States Government. While this document is believed to contain correct information, neither the United States Government nor any agency thereof, nor the Regents of the University of California, nor any of their employees, makes any warranty, express or implied, or assumes any legal responsibility for the accuracy, completeness, or usefulness of any information, apparatus, product, or process disclosed, or represents that its use would not infringe privately owned rights. Reference herein to any specific commercial product, process, or service by its trade name, trademark, manufacturer, or otherwise, does not necessarily constitute or imply its endorsement, recommendation, or favoring by the United States Government or any agency thereof, or the Regents of the University of California. The views and opinions of authors expressed herein do not necessarily state or reflect those of the United States Government or any agency thereof or the Regents of the University of California.

LBL-32877
UC-404

MODEL HETEROGENEOUS ACID CATALYSTS AND METAL - SUPPORT INTERACTIONS: A COMBINED SURFACE SCIENCE AND CATALYSIS STUDY

ISTVAN BOSZORMENYI
Ph.D. Thesis

DEPARTMENT OF CHEMISTRY
University of California

and

MATERIALS SCIENCE DIVISION
Lawrence Berkeley Laboratory
University of California
Berkeley CA 94720

MAY 1991

This work was supported by the Director, Office of Energy Research, Office of Basic Energy Sciences, Materials Sciences Division, of the U.S. Department of Energy under Contract No. DE-AC03-76SF00098.

Model Heterogeneous Acid Catalysts and Metal - Support Interactions: A Combined Surface Science and Catalysis Study

by

Istvan Boszormenyi

Abstract

Thin (< 100 Å) silica-alumina layers have been prepared, characterized and tested as potential model heterogeneous acid catalysts for combined surface science and catalysis studies. Three methods have been developed for their preparation: 1) Oxidation of r3xr3 R30 Al/Si(111) structure in ultra-high vacuum (UHV) using water and oxygen. 2) Deposition on Si(111) from aqueous solution. 3) Argon ion beam sputter deposition in UHV.

The homogeneous thin layers are amorphous by LEED and XRD. Based on XPS, the chemical environment of surface atoms in the thin films is similar to that of silicon, aluminum and oxygen atoms on high surface area acid catalysts.

Since the ion beam deposited thin layer of silica-alumina has the same composition as the target zeolite, and the chemical shifts in XPS indicate similar atomic environments on both surfaces this deposition method appears to be a promising tool to prepare model catalysts using practical catalyst targets.

The silica-alumina layers are active in cumene cracking, a typical acid catalyzed reaction. In order to clearly distinguish background reactions taking place on the reactor walls and the acid catalyzed reaction occurring on the model acid catalyst, at least 20 cm^2 catalyst surface area is needed.

The interaction of platinum and alumina has also been studied. Two series of model platinum-alumina catalysts have been prepared in a combined UHV - high pressure reactor cell apparatus by 1) depositing alumina on a polycrystalline platinum foil and by 2) vapor depositing platinum on a thin layer of alumina on gold. Both model surfaces have been prepared in the presence and in the absence

of chlorine. Auger electron spectroscopy, temperature programmed desorption of CO, as well as methyl cyclopentane (MCP) hydrogenolysis studies indicate that the platinum surface area is always higher if the catalyst preparation and regeneration involved a chlorination step. This observation can be explained in terms of chlorine assisted redispersion of platinum.

The selectivity patterns in MCP ring opening on 'platinum-on-alumina' and on 'alumina-on-platinum' are different, and only the former can be described as a linear combination of selective and statistical ring opening. The product distribution, however, changes with coverage and reaction time. The properties of the two model catalyst systems and the role of chlorine, as a source of Lewis acidity at the platinum alumina boundary, in MCP hydrogenolysis are also discussed.

Acknowledgements

There are many people I would like to thank for their help during these years in Berkeley. It has been a great experience to work with Professor Gabor Somorjai and his international group. I am thankful for his guidance, enthusiasm and patience throughout my stay. He has been a constant source of ideas and encouragement. I would also like to thank Professor Laszló Guczi for his understanding and support. Without Gabor and Laszló my coming to Berkeley would never have realized.

My deepest thanks go to Judit Böszörményi for the sacrifices she has made, for her efforts to help me through difficulties and for her willingness to have put up with me despite my cranky moods when nothing seemed to work. I am also grateful for all the great times we have had together.

I thank Dr. Miquel Salmeron and Dr. Michel Van Hove who were always available for valuable discussions. Then I would like to thank past and present members of the Somorjai group for their help and for valuable scientific and not so scientific discussions. I feel very fortunate to have been able to work with this distinguished group of people. Because of limited space here, I cannot acknowledge everyone who directly or indirectly contributed to this work. But I wold like to mention a few of them. Brian Naasz, Brian Bent, Ken Lewis and Greg Blackman helped me go through the first confusing weeks, perhaps months, here in Berkeley. Bruno Marchon and Brian Naasz taught me the UHV basics and I inherited their chambers.

Discussions with Dr. Jule Rabo of UOP and Dr. Juan Garces of DOW lead to the development of both aqueous and ion beam depositions. The zeolite targets for the sputter deposition were kindly provided by them. Gil Vandentop helped me take electron microscopy pictures of thin silica-alumina films prepared in aqueous solution. Some of these films were carefully prepared by Yusing Ko. The time consuming ion beam sputter deposition work could not have been completed

without the devoted assistance of Brian McIntyre and Dr. Taisei Nakayama. Dave Kelly and Dave Jentz, saved me trips by turning off the bake-out at ungodly hours.

When I had problems related to catalysis I could always turn to Pedro Pereira for ideas and suggestions. The first attempts to study the alumina on platinum system were made with the help of Gerard Vurens during a Christmas break. I have learned a great deal from stimulating conversations with Sabrina Fu, Michael Quinlan and Colette Knight. I will miss them with all their spicy humor and sarcasm.

The electrical problems were handled by Jim Severens and Bob Ybarra in electronic shop on the Hill. The new manifold, numerous small UHV parts and the differentially pumped manipulator were built by Bob Wright and Dan Colomb in the Hill machine shop. For giving advice on rewiring the entire system, the Instrument Repair Shop on campus needs to be thanked.

I also wish to thank Brigid Tung for making her printer available for printing this manuscript, for the delicious treats, and, in general, for her kind support over the years.

Outside the lab, Leslie and Greg, Sue and Ken, Pamela and Mike, Pauline and Bruno, Marinella and Roberto, Chin-Chi and Peter, Karina and Albert, Marti and Lennon, Satomi, Patti, and Mark have been great to go out with. We could always count on them to do some hiking, camping, gardening, mushroom hunting or anything relaxing at home.

This work was supported in part by the Director, Office of Energy Research, Office of Basic Energy Sciences, Materials Sciences Division, of the U.S. Department of Energy under Contract No. DE-AC03-76SF00098.

Contents

List of Figures ix

1. Introduction **1**

1.1 Acid Catalysis 2

1.2 Typical High Surface Area Catalysts 4

1.2.1 Alumina 4

1.2.2 Silica-alumina 6

1.2.3 Zeolites 9

1.3 Characterization of High Surface Area Acid Catalysts 12

1.3.1 Determination of Acidity 12

1.3.2 Techniques to Study Heterogeneous Acid Catalysts 18

1.4 Model Catalyst Approach to Study Heterogeneous Acid Catalysts 21

References. 24

2. Experimental **30**

2.1 Ultra-High Vacuum - High-Pressure Catalytic Reactor Apparatus 30

2.2 Surface Analysis Techniques 35

References 39

3. Model Silica-Alumina Catalysts **40**

3.1 $Al_xSi_yO_z/Si(111)$ 43

3.1.1 Preparation in UHV:

$Al_{(v)} + Si(111) + O_2(H_2O)_{(g)} \rightarrow Al_xSi_yO_z/Si(111)$ 43

3.1.1.1 Experimental 44

3.1.1.2 Results and Discussion 46

3.1.2 Preparation in Aqueous Solution:

$Al_{(s)} + Si(111) + NaOH_{(aq)} \rightarrow Al_xSi_yO_z/Si(111)$ 54

3.1.2.1 Experimental. 58

3.1.2.2 Results and Discussion 60

3.1.3 Reactivity of Model Catalysts 72
3.1.3.1 Experimental 74
3.1.3.2 Results and Discussion 75
References 78
3.2 $Al_xSi_yO_z$/Au
Preparation in UHV by Ar^+-ion Beam Sputter Deposition 80
3.2.1 Experimental 80
3.2.2 Characterization of Sputter Deposited Thin Films 83
3.2.3 Reactivity in Cumene Cracking 92
References 96
3.3 Summary 97

4. Model Pt-Cl-Al_2O_3 catalysts 100
4.1 Introduction 101
4.2 AlO_x/Pt and AlO_x/Cl/Pt 104
4.2.1 Experimental 104
4.2.2 Results and Discussion 106
4.3 Pt/AlO_x/Au and Pt/Cl/AlO_x/Au 121
4.3.1 Experimental 122
4.3.2 Results and Discussion 123
4.4 AlO_x/(Cl/)Pt and Pt/(Cl/)AlO_x/Au - Summary 132
References 140

List of Figures

1.1 Interaction of a silanol group with a neighboring aluminum ion. - p. 6.

1.2 The formation of a Lewis acid site from Bronsted sites on the surface of silica-alumina. - p. 7.

1.3 Preparation of a highly acidic OH group on silica-aluminas. First the sodium ions are exchanged with ammonium ions, then the ammonium salts are decomposed at 670-770 K. - p. 8.

1.4 Primary (a) and secondary (b) building units of zeolite Y (c). - p. 9.

1.5 The ratio of the volume of the surface detected by surface sensitive electron spectroscopies and the total volume of a spherical particle as a function of diameter for 30 Å mean free path electrons. - p. 20.

2.1 Schematic diagram of the ultra-high vacuum - high pressure cell apparatus for combined surface science and catalysis studies. *Italic letters* and *numbers* indicate stainless steel bellows valves (Nupro), **A**, **B** and **C**:leakvalves, DP I and DP II: Diffusion pumps for pumping the UHV system and the gas manifold, respectively, HPC: High Pressure Cell, MP III: Mechanical pump for pumping the reactor loop and the manifold, MP IV: Mechanical pump for differential pumping of the manipulator and providing the reference vacuum for the differential pressure gauge, RFA: Retarding Field Analyzer, QMS: Quadrupole Mass Spectrometer. - p. 31.

2.2 Same as Figure 2.1, but only the reactor loop with the closed high-pressure cell (HPC), and part of the gas introduction system are shown. p. 33.

2.3 Sample mounting. On the right we show the temperature profile when a 0.025 mm Au foil was heated to a) 300 C and b) 600 C in air. - p. 34.

3.1 Mounting of the Si (111) wafers in the UHV - high pressure cell apparatus. The thermocouple is spotwelded to the gold foil. - p. 45.

3.2 a) The relative Auger peak intensity of the Al and Si Auger lines as a function of deposition time. b) Three examples of Auger spectra in the 20-110 eV region taken after 0, 37 and 143 s of deposition. c) Area of Al TPD peak as a function of aluminum coverage. - p. 47.

3.3 LEED patterns of a) clean silicon (111) showing the 7x7 reconstruction and b) r3xr3 R30 Al-Si(111). (E_p=122 eV) - p. 48.

3.4 Auger spectrum of the r3xr3 R30 Al-Si(111) structure before oxidation (a) and after 4 L oxygen exposure at 570 K (b). - p. 50.

3.5 LEED patterns before (a) and after (b) 4 L oxygen exposure of r3xr3 R30 Al/Si(111) at 570 K. (E_p=66 eV) - p. 51.

3.6 The intensity of the (0,0) beam of the LEED patterns obtained for the four samples as a function of the electron energy. (Raw data, not normalized to constant beam current!) - p. 52.

3.7 AES spectra obtained using the LEED electron gun after the oxidation of 2 ML Al/Si(111) at two different areas on the sample. a) an area that exhibit a 1x1 LEED pattern shown in c) and , b) another area of the same sample showing no ordering by LEED. (E_p=122 eV) - p. 53.

3.8 The apparatus used to deposit thin silica-alumina layers on silicon single crystals. - p. 58.

3.9 Kinetic equations to describe the rate of chemical reactions taking place when a silicon single crystal and a piece of aluminum is immersed in sodium hydroxide solution. See corresponding chemical reactions in text: *(I) - (1), (II)* and *(V) - (3), (III)* and *(VI) - 7* and *(IV) - 5.* - p. 61.

3.10 XPS spectra obtained from a thin film deposited in 0.5 M NaOH solution at room temperature. The deposition time was 5 hours. a) survey spectrum, b) the silicon 2p, c) aluminum 2p, d) oxygen 1s, e) sodium 1s, and f) carbon 1s lines. The spectra are not charge corrected. - p. 62.

3.11 a) The $Al_{ox}/(Al_{ox}+Si_{ox})$, b) Si_{ox}/Si ratios and c) the concentration of sodium ions in the surface layers as a function of time for two sets of experiments using 0.5 and 1.M NaOH solutions. - p. 63.

3.12 Charge corrected binding energies for the O 1s, Si 2p, Al 2p and Na 1s lines, obtained from thin films prepared using 0.5 M and 1.0 M NaOH solutions. The literature values for the Si, O, Al and Na containing solids are also given, as reported by Wagner *at al.* and Barr *at al.* [49a and 49b in Chapter 1.] - p. 66.

3.13 SEM image of a thin layer on silicon (111). After 21 hours of deposition according to the modified method described in the Experimental section. Auger spectra from areas 1, 2 and 3 were taken and are shown in Fig. 3.14. - p. 68.

3.14 Auger spectra obtained from areas 1, 2 and 3 in fig. 3.13. - p. 69.

3.15 The intensity of the O (512 eV), Al (1396 eV), Si (92 eV) and SiO_y (80 eV) peaks was determined after repeated argon ion bombardment of a 1x1 mm selected area away from deposits (see Fig. 3.13). The beam energy was 0.5 kV and the pressure was 14 mPa (PHI 660), measured in the differentially pumped raster ion gun. - p. 70.

3.16 Sodium KLL Auger lines before (a) and after (b) $Na^+ \rightarrow NH_4^+$ ion exchange and the nitrogen 1s region before ion exchange (c), after ion exchange (d) and after thermal decomposition at 660 K. - p. 71.

3.17 Benzene (a) and propylene (b) accumulation curves for a 1 cm^2 surface area silica-alumina layer prepared on Si(111). Silica-alumina layer was deposited in aqueous media. - p. 76.

3.18 Argon ion beam sputter deposition of silica-alumina. - p. 81.

3.19 Ion beam sputter deposition of silica-alumina on gold foil using Y zeolite (Y-62) as target. Integrated XPS peak intensities as a function of deposition time: a) O 1s and Au 4f peak areas, and b) Si 2p and Al 2p peak areas. - p. 84.

3.20 Ion beam sputter deposition of silica-alumina on gold foil using Y zeolite (Y-62). Atomic concentration ratios as a function of deposition time: a) O/Si atomic ratio, and b) Si/Al atomic ratio. Horizontal lines indicate values obtained for the target. - p. 85.

3.21 Binding energies of the O 1s, Si 2p and Al 2p electrons in the sputter deposited silica-alumina film as a function of deposition time. - p. 87.

3.22 Characteristic O KVV Auger transitions in different Al-Si-O compounds [9]. I. Aluminum oxides, hydroxides and silicates. II. Uncharged silica network and silicones. III. Oxygen in AlO_4^- tetrahedra such as in zeolites. - p. 89.

3.23 Oxygen O KVV Auger transitions: a) dealuminated Y zeolite target b) sputter deposited thin film using dealuminated Y zeolite. (Electron kinetic energy = 1253.6 eV - Binding energy). - p. 90.

3.24 Oxygen O KVV Auger transitions: a) Y-82 target, b) thermally decomposed Y-82 (1470 K, 10 hours), c) sputter deposited silica alumina film on gold foil using Y-82 as target, and d) sputter deposited silica alumina film on gold foil using a mechanical mixture of SiO_2 and Al_2O_3. (Electron kinetic energy = 1253.6 eV - Binding energy.) - p. 91.

3.25 Product accumulation curves for cumene cracking reaction at 570 K over blank reactor (a) and over sputter deposited silica-alumina layers (b) deposited on gold foil using zeolite Y-82 as target. - p. 93.

3.26 Initial rate of cumene cracking at 570 K a) for high surface area catalysts: zeolite Y-82, decomposed zeolite Y-82 (in He at 1470 K for 10 hrs), alumina and silica, and b) for sputter deposited thin films using Y-82, a mixture of alumina and silica, alumina, silica as targets and the initial rate for the background reactions as well. - p. 94.

4.1 Methyl cyclopentane ring opening selectivities [17]. - p. 103.

4.2 Preparation of model catalysts a) AlO_x/Pt and b) AlO_x/Cl/Pt. - p. 105.

4.3 Characteristic Auger spectra. a) after accumulative deposition of 30 min AlO_x on platinum foil, b) after chlorine deposition, and c) after MCP hydrogenolysis. - p. 107.

4.4 Relative intensity of the chlorine Auger peak (181 eV) as a function of the platinum Auger peak (237 eV) intensity. Pt_o and Cl_o are the intensity of the platinum and chlorine Auger peaks before deposition of AlO_x, respectively. - p. 108.

4.5 Auger uptake curves for annealed platinum foil a) in the absence and b) in the presence of chlorine. - p. 109.

4.6 Relative CO TPD areas as a function of AlO_x deposition time for annealed platinum foil. - p. 110.

4.7 Relative MCP hydrogenolysis rate and relative CO TPD area as a function of AlO_x deposition time for samples prepared with and without chlorine deposition on an annealed platinum foil. Initial rate on the clean foil was 0.2 MCP molec/Pt/sec. ($T=620K$, $p_{H2}=1$ atm, H_2/MCP = 240) - p. 111.

4.8 Two possible mechanisms to explain the larger platinum surface area when the catalysts were prepared in the presence of chlorine. - p. 112.

4.9 The relative rate of MCP hydrogenolysis as a function of AlO_x deposition time for argon ion beam sputtered platinum substrate. - p. 115.

4.10 Model for 'redispersion' of AlO_x/Pt catalysts. - p. 116.

4.11 Selectivity of MCP hydrogenolysis over model catalysts prepared on an annealed platinum foil in the absence and in the presence of chlorine. ($T=620$ K, $p_{H2}=1$ atm, H_2/MCP=240) - p. 117.

4.12 Comparison of MCP ring opening selectivities on platinum. 3MP = 3-methyl-pentane, 2MP = 2-methyl-pentane and nHx = n-hexane. - p. 118.

4.13 MCP selectivity over model catalysts prepared on sputtered platinum foil in the presence and in the absence of chlorine. - p. 120.

4.14 Platinum source. - p. 122.

4.15 Typical CO TPD peak shapes a) before and b) after hydrogen treatment. - p. 124.

4.16 a) Relative CO TPD areas as a function of catalyst treatments. For conditions see text. b) Total platinum surface area after hydrogen treatment and MCP hydrogenolysis. Lost surface area refers to the decrease of surface area. - p. 125.

4.17 Total CO TPD area before and after MCP hydrogenolysis as function of platinum deposition time and regeneration conditions. **A** and **B** refer to sample preparation and regeneration procedures (Chapter 4.3.1). - p. 127.

4.18 Platinum (237 eV) to oxygen (512 eV) Auger peak ratio and initial MCP hydrogenolysis rate as a function of platinum deposition time and catalyst regeneration conditions. - p. 128.

4.19 Product distribution for methyl cyclopentane (MCP) hydrogenolysis over model platinum catalysts. **A** and **B** refer to sample preparation and regeneration procedures described in Chapter 4.3.1. - p. 129.

4.20 The intensity of the Pt (237 eV) peak before reaction, after reaction and after regeneration as a function of deposition time. **B** and **C** refer to sample preparation and regeneration procedures described in Chapter 4.3.1. - p. 130.

4.21 MCP ring opening selectivity on (Cl/)Pt/Cl/AlOx/Au model catalysts as a function of platinum deposition time. **C** refer to sample preparation and regeneration procedures described in Chapter 4.3.1. - p. 131.

4.22 3MP/2MP and 3MP/nHx ratios for catalysts AlO_x/Pt, Pt/AlO_x/Au and Pt/Cl/AlO_x/Au as a function of MCP conversion. - p. 133.

1. Introduction

Acid catalyzed reactions are by far the most important hydrocarbon conversion reactions in the chemical industry. These reactions use and produce the largest volume of hydrocarbons and demand the largest amount of catalysts. Isomerization, cracking, alkylation, and polymerization of aliphatic and aromatic hydrocarbons all belong to this group of reactions. Although in general the term 'acid catalyst' includes both homogeneous (e.g. aqueous solutions of sulfuric, phosphoric acids and superacids) and heterogeneous catalysts (e.g. alumina, silica-aluminas, halogenated aluminas, and most importantly zeolites), from the point of view of the petrochemical industry, the heterogeneous catalysts are of real interest.

The application of single crystals and atomically clean metal foils as model catalysts, and specially the combination of surface and catalysis studies have greatly contributed to the understanding of elemental catalytic processes taking place on metal surfaces. The major goal of the work presented here has been to explore if a similar approach to heterogeneous acid catalysts is feasible.

In this thesis we report the first attempts to build, characterize and test low surface area silica-alumina model catalysts as thin layers. Both ultra-high vacuum and aqueous preparation methods have been developed to deposit a homogeneous mixture of silica and alumina on Si(111) and gold substrates. The model surfaces have been characterized using surface science techniques and compared with practical high surface area catalysts. The catalytic properties of these catalysts have been tested in typical acid catalytic reactions using a classical ultra-high vacuum (UHV) - high pressure catalytic reactor system developed for the study of metal single crystal model catalysts.

We have found that although the surface properties of these models agreed well with the that of the high surface area catalysts, in order to comfortably measure

catalytic reaction rates at least one order of magnitude larger catalyst surface area is necessary than it is customary in metal single crystal studies. The main reason for this is that the number of active sites on both the practical and model catalyst surfaces is two to three orders of magnitude lower than on metals. And while in metal single crystal studies the background activity due to metal reactor components can be neglected, here the rates on the model surface and on the reactor walls are comparable. Thus the study of acidic oxides calls for improved reactor designs and materials to minimize background activities.

The current reactor system is well-suited, however, to model interactions between metal particles and high surface area supports. In Chapter 4 of this thesis, we compare two complex platinum-alumina-chlorine model catalytic systems and relate their properties to practical platinum catalysts supported on chlorinated alumina.

In this introductory chapter first we give an overview of the acid catalytic process, then we describe the high surface area industrial acid catalysts relevant to this thesis. Then we turn our attention to the techniques used to characterize these materials, and finally we introduce our approach to prepare and study model acid catalysts. Introduction to the metal-support interaction study will be given in Chapter 4.

1.1 Acid Catalysis

Both homogeneous and heterogeneous catalysts can either provide H^+-ions (Bronsted acids) or accept a pair of electrons (Lewis acids). It is generally accepted that acid catalyzed reactions proceed via positively charged ionic intermediates having tetra- or pentacoordinated carbon atoms. These carbonium ions have various lifetimes in solution or on the surface of the heterogeneous catalysts as they undergo inter- or intramolecular transformations. In the final step of the catalytic cycle, they lose the positive charge and the acid catalyst is regenerated. A general cycle for Bronsted and Lewis acid catalyzed reactions are shown below [1,23]:

1. Carbonium ion formation:

Bronsted acid:

$$R + H^+ \rightarrow RH^+$$

Lewis acid:

$$RX + L \rightarrow R^+ + LX^-$$

where X=H or halogen

2. Carbonium ion rearrangements and/or intermolecular reactions:

a) $RH^+ \rightarrow R'H^+$

b) $RH^+ + R'' \rightarrow R''H^+ + R'''$

$RH^+ + R'' \rightarrow R''^+ + R'''H$

c) $R^+ \rightarrow R''^+$

d) $R^+ + R'X \rightarrow RX + R'^+$

3. Regeneration of the catalyst:

Bronsted acid:

$$R'H^+ \rightarrow R' + H^+$$

Lewis acid:

$$R^+ + LX^- \rightarrow RX + L$$

The stability, i.e. the lifetime of the carbonium ion is of crucial importance as far as the reaction path is concerned. The trends of stability of the carbonium ions are very similar in the gas phase, in solution and on the surfaces of solid acids, as it has been suggested by the product distributions of many reactions that have been studied to date (tertiary > secondary> primary carbon atom). This also implies that the nature of the counter ion plays only a minor role in the catalytic cycle [2]. Infrared spectroscopy and ^{13}C MASNMR (Magic Angle Spinning Nuclear Magnetic Resonance) studies have verified the formation of surface stabilized carbonium ions [3] as intermediates on the surfaces of solid catalysts.

1.2 High Surface Area Acid Catalysts

What is the source of Bronsted and Lewis acidity on oxide surfaces?

Early infrared studies of oxides revealed [24c] that their surfaces are covered with OH groups. When these oxides are heated, neighboring OH groups combine to form water, which then desorbs leaving behind an oxygen vacancy. To completely dehydrate an oxide, temperatures as high as 1400-1600 K are necessary.

Acid-base indicator studies and infrared spectroscopy data indicated that surface OH groups can be regarded as proton sources, that is Bronsted acid sites, and the oxygen vacancies as electron acceptors, Lewis acid sites.

This dissertation focuses on acidic oxide catalysts containing silica and alumina, thus in this chapter we will concentrate only on the properties of these oxides.

1.2.1 Alumina

Alumina is the most simple heterogeneous acid catalysts. It has been long known that it becomes active in hydrocarbon conversion reactions if heated to 570-770 K. In this activation process, two adjacent OH groups combine, form a water molecule, and as the water desorbs an anion vacancy, i.e. a coordinatively unsaturated cation remains on the surface. The appearance of catalytic activity coincides with the decrease in the surface OH concentration and the increase in the anion vacancy concentration [25].

The Bronsted and Lewis sites can be interconverted by the following dehydration/hydration

$$\underline{\underline{\text{OH OH}}} \leftrightarrow \underline{\underline{\text{O}}}{+}{=} + \text{HOH}$$

$$\text{Bronsted} \leftrightarrow \text{Lewis} + \text{HOH}$$

The first and most often cited study of the structure and texture of aluminas was performed by Lippens [26]. Based on theoretical calculations, infrared spectroscopy and thermal gravimetry results, five different OH environments have been postulated by Peri [27a]. This model was later refined by Zamora and Cordoba [27b], but the assignment of IR bands to five basic OH structures, that differ only in the number of OH, O or vacancy neighbors, was unchanged.

Knözinger and Ratnasamy [28] review the surface properties of catalytic aluminas and speculate what configuration of the active site in different hydrocarbon conversions might be. They argue that not every surface acid site is active, only ones with special local coordination (defects) can be held responsible for hydrocarbon reactions: The total number of Bronsted and Lewis sites on alumina is in the same order of magnitude as the number of atoms on close packed metal surfaces: $10^{15}/cm^2$. Yet, selective catalytic poisoning experiments indicated that the number of active sites on the surface of alumina is two to three orders of magnitude lower: 10^{12}-10^{13}.

Recently, Cocke *at al.* [29a] gave a comprehensive review of the preparation, structure and chemistry of aluminas fabricated in a planar morphology. Alumina has several modifications, depending upon the arrangement of the aluminum ions in an O^{2-} lattice [26]. Most of these structures can be interconverted in the appropriate temperature and H_2O partial pressure regime, and can be prepared in a planar morphology. There is a wide variety of methods to prepare planar model aluminas ranging from direct oxidation of aluminum [29c] to plasma spraying [29d]. The thickness of these layers can be varied between 30 Å and 10,000 Å.

To enhance the acidity of aluminas, often halogen is incorporated in the surface layers by using HCl, CCl_4 or chloroform treatments at 570-770 K [29a]. Tanaka and Ogasawara [30a] demonstrated that the adsorption of HCl on .gamma.-alumina increases the Bronsted acidity. Parallel with this enhanced Bronsted acidity, they found an increase in the initial rate for double bond isomerization of 1-butene. These results are in contrast with the findings by Knözinger and Kaerlein

[29b] who show that chlorinated aluminas have more Lewis sites, and no new Bronsted sites are present.

As we will see in Chapter 4, when a transition metal such as platinum is supported on chlorinated alumina, the change in acidity can have implications on the stability of platinum particles. In addition, the selectivity pattern can change rather dramatically. For example, in n-hexane reaction over alumina supported platinum catalysts, chlorine treatment brings about an enormous increase in the isomerization activity [31].

1.2.2 Silica-Alumina

Silica-aluminas are intimate mixtures of silica and alumina. Many preparation methods have been reported in the literature for the preparation of silica-alumina catalysts [23,33] in both non-aqueous and aqueous solutions. According to the most common method, silica-alumina is co-precipitated from a sodium silicate and sodium aluminate solution.

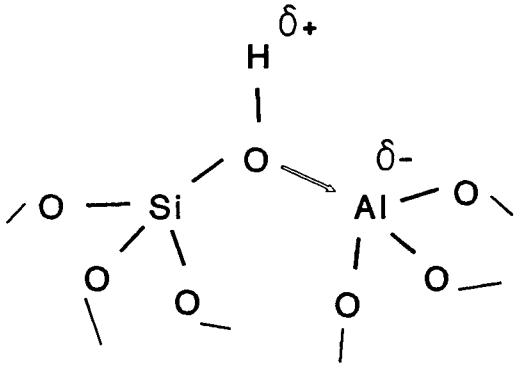

Fig. 1.1

Silica-alumina catalysts consist of a random three dimensional network of SiO_4 and AlO_4^- tetrahedra, and their acidity is higher than that of the two individual oxides. It is now generally accepted that the increased acidity of silica-aluminas is due to aluminum ions in tetrahedral coordination. In Fig. 1.1 we show the interaction of a silanol group with a neighboring aluminum ion. This interaction is takes place in an intimate mixture of the two oxides, especially since aluminum ions energetically favor tetrahedral over planar or pyramidal threefold coordination. This interaction causes the weakening of the O-H bond, which in turn increases the proton donating

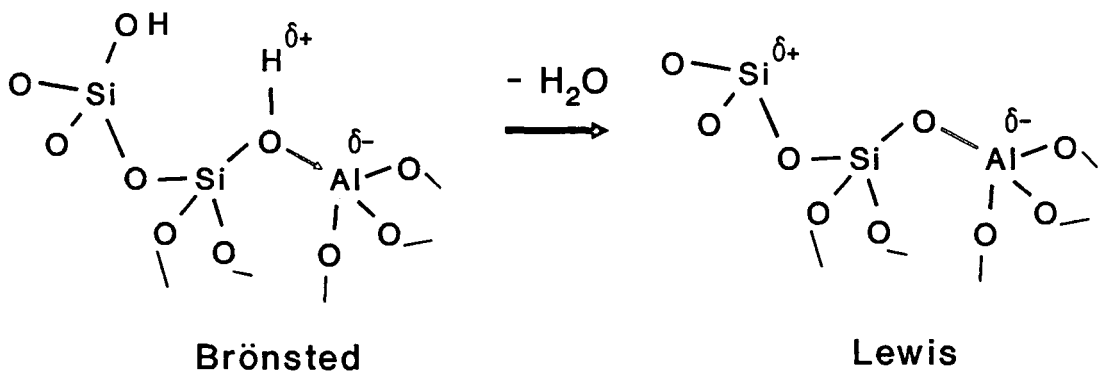

Fig. 1.2

Although the surface of silicon dioxide is also covered with OH groups and when heated water leaves the sample, it does not show significant acidity nor does it power of the silanol group. As the silica-alumina is heated (Figure 1.2), two adjacent OH groups combine, form water, and a strong Lewis site is left behind. have catalytic activity in typical acid catalyzed reactions. If silica is intimately mixed with alumina the activity increases and there are several catalytic reactions for which the activity *vs.* Si/(Al+Si) curves go through a maximum, indicating a significant promotional effect. The surface acidity of silica-aluminas have been studied the most.

Peri [34] postulated eight structures possibly present on the surface of a 3D random network of silica and alumina. In agreement with experimental titration data, the concentration of these acid sites was on the order of 10^{11}-$10^{13}/cm^2$.

After precipitation from basic solutions the sodium salt of the acid undergoes a $Na^+ \leftrightarrow NH_4^+$ ion exchange process to form the ammonium salt which is then decomposed to generate the highly acidic OH groups. This ion exchange followed by calcination is also used in the preparation of crystalline alumino silicates, zeolites. The chemical reaction taking place is shown in Fig. 1.3.

The properties of the final catalyst greatly depend on the preparation conditions and parameters. For example, pH 3 and high silicate concentration favor the formation of the desired Al-O-Si bonds, but the resulting material has a very low specific area. At higher pH, however, a more desirable porous material can be prepared with high surface area. By choosing the proper synthesis conditions [35], the pore size distribution of these amorphous silica-aluminas can be optimized for a given catalytic process.

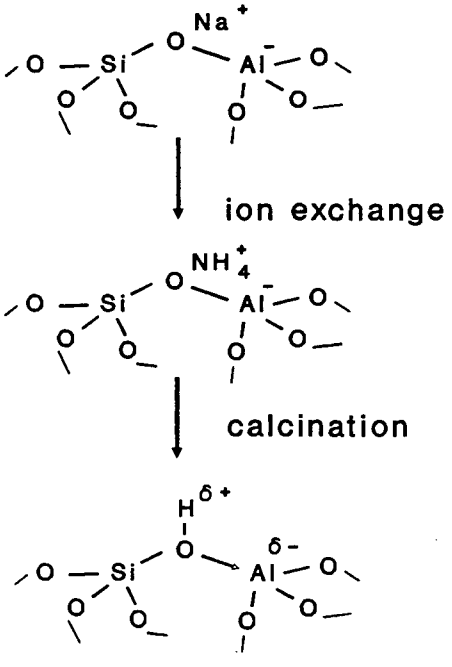

Fig. 1.3

Amorphous silica-aluminas are active in every type of acid catalyzed reaction. An important question is how the activity changes with the composition of the catalyst Höffkes *at al.* [22] found that in 1-hexene cyclization and cracking silica was inactive and alumina showed some activity. When some silica was added to alumina, the activity increased, and went through a maximum at about 70 wt% silica content.

Similar trend was observed by Sato and co-workers in isopropanol dehydration and cumene cracking [21c], but in these reactions the maxima occurred at 15-20 wt% silica for the cumene reaction and at around 20-30 wt% silica for the dehydration, respectively.

It is known from surface science studies that the surface composition of a multicomponent system can be dramatically different form that of the bulk. Since the catalytic reactions take place only on the surface, instead of the bulk compositions, it would be more appropriate to know what the surface compositions are. This kind of information is hardly ever available in the literature dealing with high surface area catalysts. We will return to the discussion of this problem of surface composition in Chapter 1.4.

1.2.3 Zeolites

Zeolites are the largest volume of catalysts used and produced in the chemical industry. We do not attempt to review all aspects of their preparation, characterization, properties and use, but refer the reader to the extensive literature available addressing these questions [37]. Here we would like to summarize only the most important aspects relevant to this dissertation.

Zeolites are crystalline alumino silicates. The primary building blocks of zeolites are the same as the building blocks of amorphous silica-aluminas: SiO_4^{4-} and AlO_4^{5-} tetrahedra. In zeolites, however, these are connected to form ordered

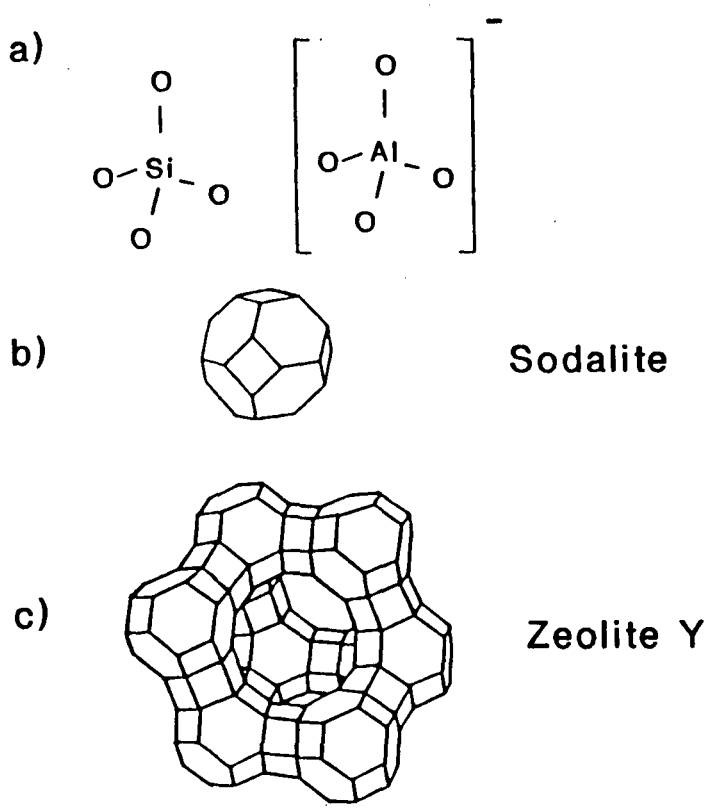

Fig. 1.4 Primary (a) and secondary (b) building units of zeolite Y (c).

secondary building blocks which in turn are linked together and form a large three dimensional open framework. The difference between the large number of zeolite structures is the sequence by which the primary and secondary building units are connected to each other. As an example, in Fig. 1.4, we show the sodalite cage, which is the secondary building unit of Y zeolites. In the figure the lines represent oxygen bridges between Si and Si or Si and Al atoms.

In some freshly synthesized zeolites, the negative charge of the framework aluminum ions is balanced by an alkali metal cation. Similarly to amorphous silica-aluminas this cation is exchanged with an ammonium ion and finally the ammonium salt is heated to yield acidic OH groups (Fig. 1.3).

The acidity and catalytic activity of zeolites are orders of magnitude higher than a similar composition amorphous silica-alumina. Despite the large body of knowledge available on zeolites, the basic question, why this proton in the zeolitic framework is more acidic than the one on amorphous silica-alumina, has remained unanswered.

Rabo and Gajda recently reviewed what is known about the acid function in zeolites [38]. They point out that in addition to the number of sites and the acid strength of the individual sites two other factors have to be taken into account to understand the exceptional catalytic properties of these materials: diffusion effects and solvent effects.

Since zeolites are very porous materials, reactants or probe molecules have to diffuse into the three dimensional network to reach the acid site. Depending on the size of the molecules relative to that of the pores, the diffusion rate can be very different for the reactants and/or the products [41]. In addition, the diffusion process folds into the kinetics of the reaction, making the determination of the absolute reaction rates difficult.

As the reactants and products diffuse in the channels and pores, they interact very strongly with the walls. As Rabo and Gajda [38] describe it, this interaction resembles the interaction between solvated molecules and high polarity solvents.

Thus the lifetime of intermediates due to both solvent and diffusion effects can be very different on zeolites and on silica-aluminas.

The synthesis of zeolites was more like an art of cooking than science for a long period of time. Today with the help of modern NMR and FTIR techniques it is a fast growing field of science. These alumino silicates are crystallized from an aqueous gel of sodium aluminate and sodium silicate at elevated temperatures and often high pressures. The most important factor governing the type of zeolite forming is the concentration of the different species in the gel. Table I. shows the typical synthesis conditions for Zeolite A, X, and Y.

Table I.

	mol/mol Al_2O_3				
Zeolite type	Na_2O	SiO_2	H_2O	Temp. K	Time (hours)
A	2	2	35	373	3
X	4	3	144	373	7
Y	8	20	320	373	7
Mordenite	6	27	61	373	168

Table I. Typical Zeolite Synthesis Conditions [37a].

Although the Si/Al ratio in the zeolite frame work is not strictly specific to structure, there is an experimentally observed limit as to how rich the zeolite can be in aluminum ions. For example, zeolite A can be prepared with a ratio as low as 1, but ZSM-5 zeolites can be made having very high (>100) Si/Al ratios. Furthermore, the Si/Al ratio of a zeolite can be increased by dealuminating the framework, yet maintaining the crystallinity [40].

The distribution of aluminum ions is most likely random in zeolites, but some authors report some local ordering. In addition, it has been postulated that 1) there are no Al-O-Al bridges (Lövenstein's rule) and 2) the number of Al-O-Si-O-Al units is minimized (Dempsey's rule) throughout the zeolite framework [37c].

Thermodynamically zeolites are metastable structures. When heated, the highly porous zeolitic framework collapses and turns into an amorphous low surface area mixture of silica and alumina [37a].

1.3 Characterization of High Surface Area Acid Catalysts

The techniques used to characterize oxides can be divided into the following two groups:

1) The acidic properties are described by the interaction of the surface and a probe molecule.

2) The structure and composition of the material and the chemical environments of the its constituents are directly determined.

A brief overview of these techniques is given in Chapters 1.3.1 and 1.3.2., respectively.

1.3.1 Determination of Acidity

Acidity cannot be measured on an absolute scale. Only in comparison with a base, can we rate how easily a molecule gives up a proton (Bronsted acids) or accepts a pair of electrons (Lewis acid). For a Bronsted acid-base pair, Hammet's H_o acidity function [4] describes the

$$HA + B \leftrightarrow BH^+ + A^-$$

equilibrium:

$$H_o = -\log (a_{H^+}.f_B)/f_{BH^+} = pK_{BH^+} - \log (c_{BH^+}/c_B) \qquad (1)$$

where a_{H^+} is the activity of the proton (in solution or on surface of solid), f_B and f_{BH^+} are the activity coefficient of the base and its conjugate acid, respectively, pK_{BH^+} is the pK_a for the conjugate acid and c_{BH^+} and c_B are the concentrations.

By determining these concentrations and looking up pK_{BH}^+, H_o can be calculated. For dilute aqueous solutions of inorganic acids $f_B = f_{BH}^+ = 1$ and the numeric value of H_o, becomes that of the pH. For solid acids, however, the determination of H_o is more complicated, because there is a wide distribution of Bronsted and Lewis acid sites present on the surface, due to the different OH environments. Some techniques are suitable to determine only the strength of the acid sites, but others can be used to estimate their concentrations as well.

The most frequently used qualitative and quantitative methods are as follows:

A. Volumetric titrations of aqueous [5] or non-aqueous [6] suspension of the solid.

This is the simplest method and uses traditional indicators, electrochemical or spectrophotometrical endpoint determination techniques. The bases range from aqueous solutions of inorganic hydroxide solutions to amines such as pyridine dissolved in benzene.

B. Change of color of indicators adsorbed from non-aqueous solvents [7].

The change of color of acid - base indicators adsorbed on solid acids determined by spectrophotometry can be related to the c_{BH}^+/c_B ratio and according to eq. *(1)*, Hammet's function can be determined. To map out the site distribution, a series of indicators is used on the same sample and by running the same tests on different oxides and homogeneous acids one can quantitatively (or at least semi-quantitatively) compare them. The technique has been developed for both Bronsted and Lewis acids [8f]. In Table II., on the next page, we collected Hammet's functions for common homogeneous and heterogeneous acid catalysts.

Most heterogeneous acid catalyzed reactions are carried out in the 500-800 K temperature range. In spite of the differences in the conditions of the above methods and that of the catalytic reactions Moscon and Mone [9] found remarkable correlation between the number and strength of acid sites determined by indicator methods and the cracking activity of rare earth exchanged zeolites.

C. Adsorption of bases

Although ammonia or pyridine adsorption capacities are often used as a quick measure of acidity [12a], the method by itself does not give information about the energetics and the distribution of adsorption sites. Combined with more sophisticated techniques, however, it becomes a powerful research tool. Instead of observing simply the color change of an indicator, the following techniques are used

Table II.

	$-H_o$
Superacids	
SbF_5 10 mol %/HF	24.3
SbF_5/HSO_5F	18.6
BF_3/HF	16.8
Strong acids	
HSO_5F	12.8
H_2SO_4(100%)	11.0
H_2SO_4(96%)	8.98
HY Zeolites	<8.2
Silica-Alumina	<8.2
Hydrogen montmorillonite	5.6-8.2
Weak acids	
H_3PO_4	5.0
Al_2O_3-TiO_2	>3
Silica-Magnesia	-1.5-3
H_2CO (formic acid)	2.2

Table II. Hammet's acidity function for acids measured by titration or indicator adsorption at room temperature [6b,8].

most frequently to examine the changes that accompany the adsorption of the probe molecule:

1) Infrared Spectroscopy

Even without a probe molecule, IR is a very valuable tool in the study of solid acids. It can provide information on the types of OH^- groups present on the surface and their relative concentration. Further details of acidity are revealed when an appropriate probe molecule such as ammonia or pyridine is adsorbed on the acidic surface. The infrared spectra clearly show the formation of NH_4^+ ions on Bronsted sites and the change in the vibrational modes of the NH_3 molecules as the they interact with Lewis sites. This method proved first the coexistence of Lewis and Bronsted acid sites on silica-alumina [10].

A large number of acidic oxides have been investigated [10,11]. While ammonia can interact with not only Bronsted and Lewis sites, but with surface O^{2-} ions as well to give NH_2 and an OH groups, pyridine or pyridine analogues do not have this reaction path available. Amines are also used as probe molecules, but here the formation of alkenes is observed as a side reaction on stronger acid sites [11c].

The great advantage of this technique is that the surface - adsorbate interaction can be studied under more reaction-like conditions. As we see more molecular detail, however, it becomes more difficult to assign a numeric value, such as the H_o function, to describe the acidity of the material.

2) Temperature programmed desorption (TPD)

In this technique, the oxide is exposed to the vapor of the base, then the temperature is increased at a constant rate under vacuum or a flow of an inert gas, and the desorption rate is measured by means of mass spectrometry or a thermal conductivity detector [12]. The maximum rate of desorption is related to the activation energy of desorption, which is a good measure of how strongly the adsorbate is held on the surface [13]. Multiple desorption maxima indicate the presence of different adsorption sites, and the concentration of these sites is proportional to the area under the desorption peak.

Amenomiya *at al.* [14a] and Contour *at al.* [14b] found that ammonia TPD line shapes can be explained by an exponential acid site distribution on .gamma.-

alumina surfaces. The heat of adsorption varies between 7 and 18 kcal/mol. While ammonia desorption gives one single TPD peak, amines desorb in two distinct TPD features detected by a thermal conductivity detector (TCD). The first one is a molecular desorption peak at 380 K and the other peak at around 530 K is due to chemisorbed molecules [14c and 12c]. The determination of the heat of adsorption of ammonia or amines using TPD is often a difficult task if the solid is a porous material. For example in the case of zeolites, when analyzing TPD data one have to keep in mind that the rate limiting step is not necessarily the desorption process, but it can be the diffusion of species in the pores. Activation energies of up to 36 kcal/mole have been reported for diffusion of ammonia [14d]. In addition, a model describing the TPD peaks has to include a term that allows partial readsorption of the adsorbate [14d and 14e].

3) Calorimetric methods

Two types of calorimetric techniques are used most frequently: thermometric titration and differential scanning calorymetry (DSC).

In the first, the heat of adsorption of a base, such as n-butylamine dissolved in an organic solvent is determined [15] by measuring the heat evolved during titration. The heat of adsorption ranges between 20-40 kcal/mol on different acidic materials, and it has been found that the higher the acidity of the surface, determined by other methods, the higher the heat of adsorption.

In a DSC measurement, similar to TPD, the temperature is raised linearly with time, but instead of following the evolution of a previously adsorbed gaseous base, the heat necessary for the desorption process is monitored. From the amount of heat and the desorption temperature the concentration and the strength of the surface acid sites can be determined [16].

4) X-ray Photoelectron Spectroscopy (XPS)

The binding energy of the N 1s electron is sensitive to the chemical environment of the nitrogen atom. Thus, at least in principle, one could distinguish nitrogen atoms adsorbed on Bronsted and Lewis sites. Unfortunately, this technique has not been proved to be very successful on practical catalysts because 1)

there is a broad site distribution which broadens the peaks and 2) XPS is a surface sensitive technique tha provides information about the topmost <50 Å of the solid, which is not necessarily characteristic of the entire sample.

Yet, Defosse and Canesson [17] found a quantitative correlation between the area under the two N 1s lines in the XPS spectra and the infrared absorption intensities for Bronsted and Lewis acid sites.

D. Test reaction method

The above techniques have one common problem. Even though the general correlation between the number and strength of acid sites and the acid catalytic properties is rather good, Holm and Clark [18] point out that the active sites in an acid catalytic reaction may not be the same as the acid sites responsible for the

Table III.

	References
1. Isomerization:	20
Double bond shift	
e.g. cis-2-butene, dimethyl butenes	
Positional	18
e.g. dimethyl benzenes	
Skeletal	20
e.g. n-paraffins	
2. Dehydration of alcohols	21
e.g. *iso*-propanol, methanol	
3. Catalytic cracking	23
Alkyl aromatics	23
Alkenes	22
Alkanes	19

adsorption of indicators or nitrogen containing bases. They found, for example, that the isosteric heat of ammonia adsorption on silica-alumina catalysts of different silica/alumina ratios, is the highest for alumina and the lowest for silica. The rate of

o-xylene isomerization, however, showed a maximum at 15% Al_2O_3-85% SiO_2 composition and no activity was observed on either pure component.

Thus, the real test of the catalysts, we believe, is the test of its activity in a series of appropriately chosen reactions requiring different acid strength. In Table III. we list the test reactions most often used in high surface area catalysis research.

Reaction rate studies alone, however, cannot provide quantitative information on the number, distribution and strength of the acid sites. In order to obtain quantitative data, selective poisoning experiments are needed. According to this method a base is introduced with the reactant feed, and the number of base molecules necessary to completely suppress the catalytic activity gives the number of active sites.

In Chapter 3.1.3, we will discuss the reactions we used in this study in more detail.

1.3.2 Techniques to Study High Surface Area Acid Catalysts

In Table IV, without the intention of providing a complete list, we give examples of how the properties of high surface area acidic oxides have been studied. The techniques are complementary to each other, and can be divided into two groups based on how deeply they sample the material: 'bulk' and 'surface' techniques. Barr and Lishka [49b] point out, however, that the region between 50 and 1000 Å cannot be explored by any techniques available today.

The use of bulk techniques can be fully justified when studying an infinitely porous material. In this case the results can be readily correlated with catalytic data. But to find correlations between results obtained from surface and catalytic studies is more difficult, because they sample different segments of the material. From this point of view, one can define two kinds of surfaces: 1) internal surface of the pores and channels, on which the catalytic reaction and adsorption processes take place,

and 2) external surface of the particles or crystallites which is detectable by the surface sensitive techniques. These two are not necessarily identical or similar as to their structure, chemical composition or chemical environment.

Table IV.

	Information	Examples
	'Bulk' Techniques	
IR, Raman	OH geometries, framework vibrations	24b, 42, 43
^{1}H-NMR	Proton environments	44
^{29}Si, ^{27}Al-NMR	Si and Al environments,	45
X-ray diffraction	bulk structure	37a
HREM, SAED	atomic structure	46
DTA, DTG	thermal properties, dehydration process	37a
EXAFS	local structure	47
	'Surface techniques'	
AES	surface composition, valence band structure	48, 49a
XPS	surface composition, chemical environments, oxidation states	49
SIMS, FABMS	composition, local structure	50, 51
AFM	real space surface structures	52

MASNMR	Magic Angle Spinning Nuclear Magnetic Resonance
HREM	High Resolution Electron Microscopy
SAED	Selected Area Electron Diffraction
DTA(G)	Differential Thermal Analysis (Gravimetry)
EXAFS	Extended X-ray Absorption Fine Structure
AES	Auger Electron Spectroscopy
XPS	X-ray Photoelectron Spectroscopy
SIMS	Secondary Ion Mass Spectroscopy
FABMS	Fast Atom Beam Mass Spectroscopy
AFM	Atomic Force Microscopy

The use of surface techniques is most appropriate if the sample is non porous or the thickness of the layer under investigation is comparable with the sampling depth. Since most surface analysis techniques utilize low energy electrons (30-2,000 eV), the sampling depth is determined by the mean free path of these electrons. In Fig. 1.5 we show the ratio of the volume of the material sampled by the surface sensitive electron spectroscopies and the volume of a spherical particle as a function of the particle size. Assuming that every electron leaving the sample can be

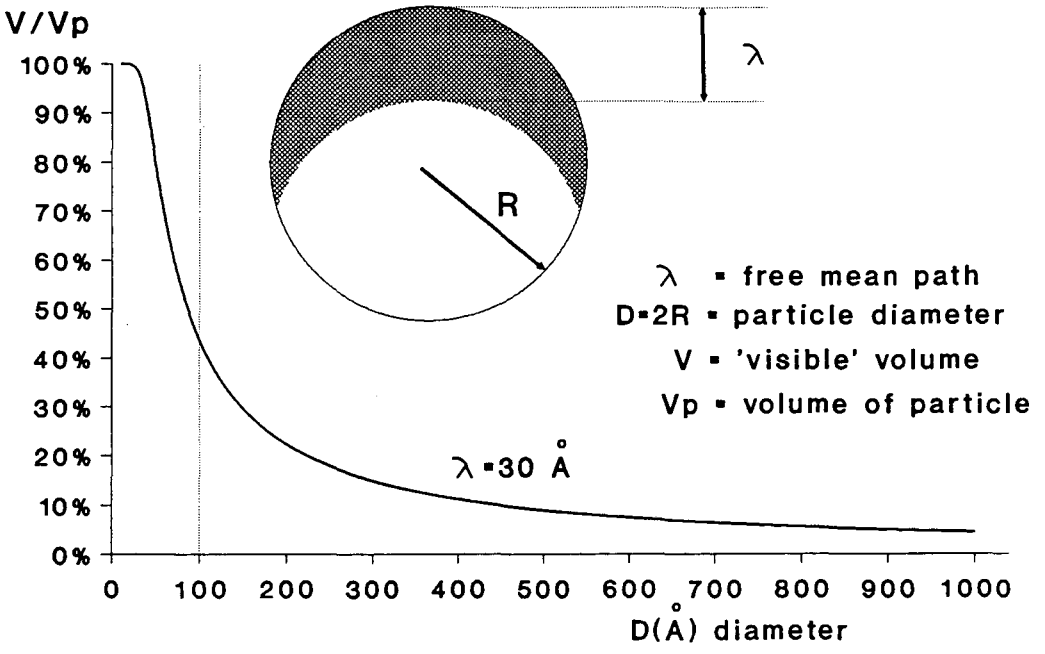

Fig. 1.5 The ratio of the volume detected by surface sensitive electron spectroscopies and the total volume of a spherical particle as a function of diameter for 30 Å mean free path electrons.

detected, for a 10,000 Å diameter particle, the size of typical zeolite crystallites, the fraction of volume 'visible' to us is less than 0.1 %. There is no reason to believe that this outmost volume is a representative sample of the whole particle. Thus, in the case of highly porous materials, it is very difficult to find convincing correlations between the catalytic properties and the surface composition.

1.4 Model Catalyst Approach to Study Heterogeneous Acids catalysts

Metal single crystals and foils have been successfully used as model catalysts [53]. According to this approach, instead of studying the complex supported metal particles, one uses an approximately 1 cm^2 surface area single crystal of the metal as a model catalyst. After cleaning under ultra-high vacuum conditions and characterization by surface sensitive techniques, the catalyst is tested in a catalytic reaction. This combined surface science and catalysis approach allows one to correlate the structure and composition of the model catalyst to its catalytic properties.

One of the major goals of this dissertation is to explore the feasibility of a similar approach in the field of heterogeneous acid catalysis. In the next paragraphs we will elaborate on the model systems we considered at the start of this project, and finally we briefly describe the ones we prepared and tested.

The simplest system that comes to mind as a potential acid catalyst is a single crystal of alumina. French and Somorjai [54] studied the composition and surface structure of .alfa.-alumina, and found that the surface reconstructs at high temperatures in ultra-high vacuum. Since alumina is an insulator it cannot be heated resistively. In their study, they heated the alumina radiatively by a tungsten foil and they report that the error in the temperature measurement was estimated to be 100 K. This would be unacceptable in a catalysis study, especially if one considers that most metals would be active in hydrocarbon conversion reactions in one way or the other. Because of these technical difficulties associated with heating and temperature measurement, we did not use the single crystal approach.

The other possibility is to prepare the model catalyst under controlled ultra-high vacuum (UHV) conditions on a conductive substrate which can be heated resistively. From the surface science point of view, ideally one would like to prepare and study a thin (<100 Å) layer of an acid catalytic material on a conductive substrate, a thin layer, so even if the model catalyst was porous a much larger

fraction of the material would be 'visible' than in the case of high surface area acid catalysts, and on a conductive substrate, so the charge buildup would be minimized during surface analysis using low energy electrons.

Aluminum metal would be a natural substrate in this approach. Cocke *at al.* [29a] reviewed the methods developed to build thin layers of all the different types of alumina on aluminum. In a preliminary study we oxidized an aluminum foil under controlled ultra-high vacuum conditions with oxygen and/or water, and found that the activity of the thin oxide layer was extremely low in 1-butene isomerization.

High surface area silica-aluminas have higher activity than alumina alone. And zeolites are even more active. In our subsequent efforts, we concentrated on the preparation and characterization of model silica-alumina catalysts, and in the rest of this dissertation we will deal with this system only.

Since zeolites are the most active and most important heterogeneous acid catalysts, a thin (<100 Å) zeolite layer would be a perfect model catalyst. The surface science techniques would provide information from ca. >30% of the sample and the catalytic activity in the catalysis study would be clearly distinguishable from the background activity.

Recently Davis *at al.* [55] developed synthesis methods for thin zeolite layers on polycrystalline copper, silver and platinum substrates. The layers were characterized by XRD, SEM, luminescence spectroscopy and surface area measurements and the film thickness could be varied between 1000 Å to 1 mm by stopping the synthesis at different times. The thinner films were not uniform by SEM: 0.5-1 micrometer zeolite particles were present on copper substrates and large areas of copper were still exposed. It is likely that these particles were supported on a thin layer of amorphous silica-alumina. No significant charging during the characterization of the films by SEM was observed.

From surface science point of view, using these films would not have any advantage over industrial zeolites, because the size of these particles is the same as for practical catalysts. In both cases, only << 1% of the total volume of the catalyst could be analyzed by the surface sensitive tools. Our goal is to prepare model acid

catalysts as < 100 Å thin films such that a much larger fraction of the catalyst would be 'visible' by our surface science techniques. We characterize these layers using surface science techniques and test their catalytic properties in typical acid catalyzed reactions. In this thesis we report three methods:

1) $Si(111) + Al_{(v)} + O_2(H_2O)_{(g)} \rightarrow Al_xSi_yO_z/Si(111)$
2) $Si(111) + Al_{(s)} + NaOH_{(aq)} \rightarrow Al_xSi_yO_z/Si(111)$
3) Preparation by Ar^+ ion Beam Sputter Deposition

Methods 1) and 3) are carried out under Ultra-High Vacuum (UHV) conditions. According to method 2) we deposit the thin layer of silica-alumina in aqueous solution, and then the samples are transferred for surface analysis and catalytic testing into the UHV - high pressure catalytic reactor. A more detailed description to these methods will be given in Chapter 3.

From extrapolation of high surface area catalytic data we can predict that the basic difficulty associated with this approach is that the active site concentration is one to two orders of magnitude lower than on metals. In industrial applications, very large surface area catalysts are used to compensate for this low active site density. In our model studies, however, we are limited to very small (1-2 cm^2) surface area samples by the apparatus used.

We found that the model silica-alumina samples were active in typical acid catalytic reactions, but in order to detect a significantly higher activity than that of the background, a minimum of 20 cm^2 surface area was necessary. In Chapter 4, we show how the existing reactor systems can be used to investigate the interaction of acidic oxides and transition metals, and compare two very complex model systems: AlO_x/(Cl/)Pt and (Cl/)Pt/(Cl/)AlO_x/Au.

References

1. Pines, H., "The Chemistry of Catalytic Hydrocarbon Conversions", p. 2, Academic Press, New York, 1981.
2. Bethell, D. and Gold, V., "Carbonium Ions: An Introduction", Academic Press, New York, 1967.
3. a) Lombardo, E. A., Dereppe, J. M., Marcelin, G., and Hall, W., K., *J. Cat.*, **114**, 167-175 (1988).

   b) Kramer, G. M., McVicker, G. B., and Ziemiak, J. J., *J. Cat.*, **92**, 355-363 (1985).

   c) Hindin, S. G., Mills, G. A., and Oblad, A. G.., *J. Am. Chem. Soc.*, **73**, 278 (1951).

   d) Haw, J. W., Richardson, B. R., Oshiro, I. S., Lazo, N. D. and Speed, J. A., *J. Am. Chem. Soc.*, **111**, 2052-2058 (1989).
4. Hammet's, L. P., and Deyrup, A. J., *J. Am. Chem. Soc.*, **54**, 2721 (1932).
5. a) Ryland, L. B., Tamele, W. W., and Wilson, J. N., *Catalysis* **7**, 214, 1960

   b) Forni, F., *Cat. Rev.*, **8**, 69, (1973).
6. a) Johnson, O., *J. Phys. Chem.*, **59**, 827, (1955).

   b) Benesi, H. A., *J. Am. Chem. Soc.*, **78**, 5490 (1956).

   c) Murrell, L. L., Dispenziere, Jr., N. C., *J. Cat.*, **117**, 275-280, (1989).

   d) Kreis, W. K., and Unger, K. K., pp. 373-382 in "Adsorption at the gas - solid and the liquid - solid interface" Edited by Rouquerol, J., and Sing, K. S. W., Elsevier, Amsterdam, 1982.
7. a) Benesi, H. A., *J. Phys. Chem.*, 970, (1957).

   b) Walling, C., *J. Am. Chem. Soc.*, **72**, 1164, (1950).
8. a) Gillespi, R. J., and Peel, T. E., *Adv. Phys. Org. Chem.*, **9**, 1, (1971).

   b) Siskin, M., *J. Am. Chem. Soc.*, **100**, 1838, (?)

   c) Otouma, H., Arai, Y., and Ukihashi, H., *Bull. Chem. Soc. Jpn.*, **42**, 2449, (1969).

d) Take, J., Tsuruya, T., Sato, T., and Yoneda, Y., *Bull. Chem. Soc. Jpn.*, **45(11)**, 3409, (1972).

e) Walvecar, S. P., and Halgeri, A. B., *Indian J. Chem.*, **11**, 662, (1973).

f) Hashimoto, K., Masuda T. and Sasaki, H., *Ind. Eng. Chem. Res.*, **27**, 1792 1797 (1988).

9. Moscon, L., and Mone, R., *J. Cat.*, **30**, 417, (1973).
10. Mapes, J. E. and Eischens, R. P., *J. Phys. Chem.*, **58**, 1059 (1954).
11. a) alumina - ammonia: Peri, J. B., *J. Phys. Chem*, **69(1)**, 231 (1965).

    b) alumina - pyridine: Parry, E. P., *J. Cat.*, **2**, 371 (1963).

    c) Morimoto, T., Imai, J., and Nagao, J., *J. Phys. Chem.*, **78**, 704 (1974).
12. a) Mills, G. A., Boedeker, E. R., and Oblad, A. G., *J. Am. Chem. Soc.*, **72**, 1554, (1950).

    b) Clark, A., Holm, V. C. F., and Blackburn, D. M., *J. Cat.*, **1**, 244, (1962).

    c) Takahashi, M., Iwasawa, Y., and Ogasawara, S., *J. Cat.*, **45**, 15-24 (1976)
13. a) Cvetanovic, R. J. and Amenomiya, Y., *Cat. Rev.*, **6(1)**, 21-48 (1972).

    b) Cvetanovic, R. J. and Amenomiya, Y., "Advances in Catalysis", **17**, p. 103, Academic Press, New York, 1967.

    c) Redhead, P. A., *Vacuum*, **12**, 203 (1962).
14. a) Amenomiya, Y., Chenier, J. H. B., and Cvetanovic, R. J., *J. Phys. Chem*, **68**, 52 (1964).

    b) Contour, J.-P., Pagniet, J., and Pannetier, G., *Bull. Soc. Chim. France*, 75 (1970).

    c) Mieville, R. L. and Meyers, B. L., *J. Cat.*, **74**, 196-198 (1982).

    d) Forni, L and Magni, E., *J. Cat.* 112, 437-443 (1988).

    e) Criado, J. M., Malet, P., and Munuera, G., *Langmuir* **3**, 973-975 (1988).
15. a) Bezman, R., *J. Cat.*, **68**, 242 (1981).

    b) Yoshizumi, H., Shimada, Y., and Shirasaki, T., *Chem. Lett.*, p. 107 (1973).
16. Aboul-Gheit, A. K., *J.Cat.*, **113**, 490-496 (1988).
17. Defosse, C., and Canesson, P., *J. Chem. Soc., Farad. Trans. I.*, **11**, 2565 (1976).
18. a) Holm, V. C. F., and Clark, A., *J. Cat.*, **2**, 16 (1963).

b) Babu, G. P., Kulkarni, S. B., and Ratnasamy,. P., *J. Cat.*, **79**, 215 (1983).

c) Akolekar, D. B. and Choudhary, V. R., *J. Cat.*, **105**, 416-431 (1987).

19. a) Lombardo, E. A., and Hall, W. K., *J. Cat.*, **112**, 565-578 (1988).

b) Lombardo, E. A., Pierantozzi, R., and Hall, W. K., *J. Cat.*, **110**, 171-183 (1988).

20. a) Perot, G., Guisnet, M., and Maurel, R., *J. Cat.*, **41**, 14-21 (1976)

b) Medemia, J., *J. Cat.*, **37**, 91-100 (1975).

c) Corado, A., Kiss, A., Knötzinger, H., and Müller, H.-D., *J. Cat.*, **37**, 68-80 (1975).

d) Gati, Gy. and Knözinger, H., "Proc. V. Intern. Congr. Catalysis, Palm Beach, 1972." p. 819. North-Holland, Amsterdam, 1973.

e) Abbot, J. and Wojciechowski, B. W., *J. Cat.,* **107**, 451-462 (1987).

21. a) Hall, W. K., Lutinski, F. E., and Garberich, H. R., *J. Cat.*, **3**, 502 (1964).

b) Moravek, V., *React. Kin. Catal. Lett.*, **30(1)**, 71-75 (1986).

c) Sato, S., Toita, M., Yu Y.-Q., Sodasewa, T., and Nozaki, F., *Chem. Lett.*, 1535-1536 (1987).

d) Luy, J. C. and Parera, J. M., *Appl. Cat.*, **26**, 195-304 (1986).

22. Höffkes, H., Baumgarten, E., and Hollenberg, D., *J. Cat.*, **77**, 257-262 (1982).

23. a) Corma, A., and Wojciechowski, B. W., *Catal. Rev.-Sci. Eng.*, **27(1)**, 29-150 (1985).

b) Corma, A., and Wojciechowski, B. W., *Catal. Rev.-Sci. Eng.*, **24(1)**, 1-65 (1982).

24. a) Peri, J. B., *J. Phys Chem.*, **69(1)**, 211-219 (1965).

b) Knözinger, H., Adv. Catal., **25**, 184 (1976).

c) Peri, J. B. Hannan, R. B., *j. Phys. Chem.*, **64**, 1526 (1960).

25. Maciver, D. S., Wilmot, W. H., and Bridges, J. M., *J. Cat.*, **3**, 502 (1964).

26. Lippens, B. C., Ph. D. Thesis, Delft, 1961.

27. a) Peri, J. B., *J. Phys Chem.*, **69(1)**, 220-230 (1965).

b) Zamora, M. and Cordoba, A., *J. Phys. Chem.*, **82(5)**, 584-585 (1978).

28. Knözinger, H., and Ratnasamy, P., *Catal. Rev.- Sci.* Eng., **17(1)**, 31-70 (1978).
29. a) Cocke, D. L., Johnson, E. D., and Merrill, R. P., *Catal. Rev.- Sci. Eng.*, **26(2)**, 163-231 (1984).
    b) Knözinger, H. and Kaerlein C. P., *J. Cat.*, **25**, 436 (1972).
    c) e.g. Hall, J. T. and Hansma, P. K., *Surf. Sci.*, **71**, 1 (1978).
    d) e.g. Vardelle, M. and Beeson, J. L., *Ceram. Int.*, **7, 48** (1981).
30. a) Tanaka, M. and Ogasawara, S., *J. Cat.*, **16**, 157 (1970).
    b) Myers, J. W., *In*d. Eng. Chem., *Prod. Res. Dev.*, **10**, 200 (1971).
31. Goble, A. G. and Lawrence, P. A., *Proc. Int. Congr. Catal., 3rd*, Amsterdam, 1964, p. 320 (1965).
32. a) Tanabe, K., "Solid Acids and Bases.", Academic Press, New York, 1970.
    b) Benesi , H. A. and Winquist, H. C., *Adv. Cat.*, **27**, 97-182 (1978).
33. Ryland, L. L. B., Tamele, M. W., and Wilson, J. N., "Cracking Catalysts," in *Catalysis*, **7** (Emmett, P. H., Ed.), Reinhold, New York, 1960.
34. Peri, J. B., *J. Cat.*, **41**, 227 (1976).
35. Plank, C. J. and Drake, L. C., *J. Colloid Sci.*, **2**, 399, (1947).
36. Leonard, A. J., Ratnasamy, P., Declerek, F. D., Fripiat, J. J., *Discuss. Farad. Soc.*, **52**, 98 (1971).
37. a) Breck, D. W., "Zeolite Molecular Sieves: Structure, Chemistry and Use", Hiley, New York, 1974.
    b) Gould, R. F., ed. "Molecular Sieves - II," ACS Symposium Series, no. 40, ACS, Washington, D.C., 1977.
    c) Stucky, G. D. and Dwyer, F. G., eds. "Intrazeolite Chemistry," ACS Symposium Series, no. 218, ACS, Washington, D.C., 1977.
    d) Drzaj, B., Hocevar, S., and Pejovnik, S. eds. "Zeolites, Synthesis, Structure, Technology and Application," Studies in Surface Science and Catalysis, no. 24, Elsevier, Amsterdam, 1985.
    e) Rabo, J. A. ed. "Zeolite Chemistry and Catalysis", ACS Monograph 171, Washington, D. C., 1976.
38. Rabo, J. A. and Gajda, G. J., *Catal Rev.-Sci. Eng.* 31(4), 385-340 (1989-90).

40. e.g. Beyer, H. K. and Belanykaja, *Catalysis by Zeolites*, ed. Imelik., B., Naccache, Taarit, B. Y., Vedrine. J. C., Coudurier, and Pralia, H., p. 203, Elsevier, Amsterdam, 1980.
41. Kaeding, W. W. and Holland, R. E., *J. Cat.*, **109**, 212-216 (1988).
42. a) Hair, M. L., "Infrared spectroscopy in surface chemistry", Ekker, New York, 1967.
    b) Peri, J. B., *J. Phys. Chem.*, **70**, 3168 (1966).
    c) Ward, J. W., in "Zeolite Chemistry and Catalysis," ACS Monograph 171, ed. Rabo, J. A., pp. 118-287, Washington, D. C., 1976.
43. a) Wengui, G., Juan, L., Hongyuan, L., Muliang, Y., and Jiehan, H. in "Zeolites, Synthesis, Structure, Technology and Application," Studies in Surface Science and Catalysis, eds. Drzaj, B., Hocevar, S., and Pejovnik, S., no. 24, p. 279, Elsevier, Amsterdam, 1985.
    b) Zi, G. and Yi, T, *Zeolites*, **8**, 232-237 (1988).
44. Freude, D., Hunger, M., and Pfeifer, H., *Chem. Phys. Lett.*, **128(1)**, 62-66 (1986).
45. Engelhardt, G. and Michel, D., "High Resolution Solid State NMR of Silicates and Zeolites", Wiley, New York, 1987
46. Thomas, J. M., Millward, G. R., Ramadas, S., Audier, M., in "Intrazeolite Chemistry," ACS Symposium Series, eds. Stucky, G. D. and Dwyer, F. G., no. 218, pp181-198, ACS, Washington, D.C., 1977.
47. Kampers, F. W., Englen, C. W.R., Van Hooff, J. H. C., Konigsberger, D. C., *J. Phys. Chem.*, **94(23)**, 8574-8 (1990).
48. Suib, S. L., Stucky, G. D. and Blattner, R. S., *J. Catal.*, **65(11)**, 174-178 (1980).
49. a) Wagner, C. D., Passoja, D. E., Hillery, H. F., Kinisky, T. G., Six, H. A., Jansen, W. T., and Taylor, J. A., *J. Vac. Sci. Tech.*, **21(4)**, 933-944 (1982).
    b) Barr, T. L., and Lishka, M. A., *J. Am. Chem. Soc.*, **108**, 3178-3186 (1986).
50. Suib, S. L., Coughlin, D. F., Otter, F. A. and Conopask, L. F., *J. Cat.*, **84**, 410-422 (1983).

51. a) Dwyer, J., Elliott, I. S., Fitch, F. R., van den Berg, J.A., and Vickerman, J. C., *Zeolites*, **3**, 97-98 (1983).
b) Dwyer, J., Fitch, F. R., Machado, F., Qin, G., Smyth, S.M., and Vickerman, J. C., *J. Chem. Soc., Chem. Comm.*, **1981**, 422.
52. Weisenhorn, A. L., Mac Dougall, J. E., Gould, S. A. C., Cox, S. D., Wise, W. S., Massie, J., Maivald, P. Elings, V. B., Stucky, G. D., Hansma, P. K., *Science*, **247(4948)**, 1330-1333 (1990).
53. Godbey, D. J., Garin, F. and Somorjai, G. A., *J. Catal.,* **117**, 144-154 (1989).
54. French, T. M. and Somorjai, G. A., *J. Phys. Chem.*, **74(2)**, 2489-2495 (1970).
55. Davis, S.P., Borgstedt, E. V. R., and Suib, S. L., *Chem. Mater.*, **2**, 712-719 (1990).

2. Experimental

The research described in this thesis was carried out using several pieces of equipment. In this general experimental section we will introduce the ultra-high vacuum (UHV) - high pressure reactor cell (HPC) apparatus and the surface science techniques used in this study. The detailed description of the experiments can be found in the experimental sections preceding the 'Results and Discussion' chapters.

2.1 Ultra-High Vacuum - High Pressure Reactor Cell Apparatus

The apparatus is shown in Fig. 2.1. For the record we note that the UHV part of the apparatus, with the exception of the manipulator, was 'inherited' from Dr. Brian M. Naasz [1,2], but the gas introduction system and the reactor loop have been redesigned and rebuilt.

In general, the model catalysts were prepared on a 10x10 mm surface area substrate under ultra-high vacuum conditions and were characterized by Auger electron spectroscopy (AES), Low Energy Electron Diffraction (LEED) and Temperature Programmed Desorption (TPD).

After characterization (Fig. 2.2) the sample was isolated from UHV by closing the high pressure cell (HPC). Valves *7* and *8* were opened, and valve *9* and *2* were closed. The reactor was filled with 1 atm of N_2 or H_2. (The pressure was monitored using a Wallace-Tiernan manometer.) Then valve *3* was closed and the circulation pump was started. The reactants (most often 1-6x10^{-3} ml liquid cumene or methyl cyclopentane) were injected using a microsyrenge via a septum. The temperature of the sample was raised to reaction temperature (within a minute or so), and during the course of the reaction samples were taken with an automatic

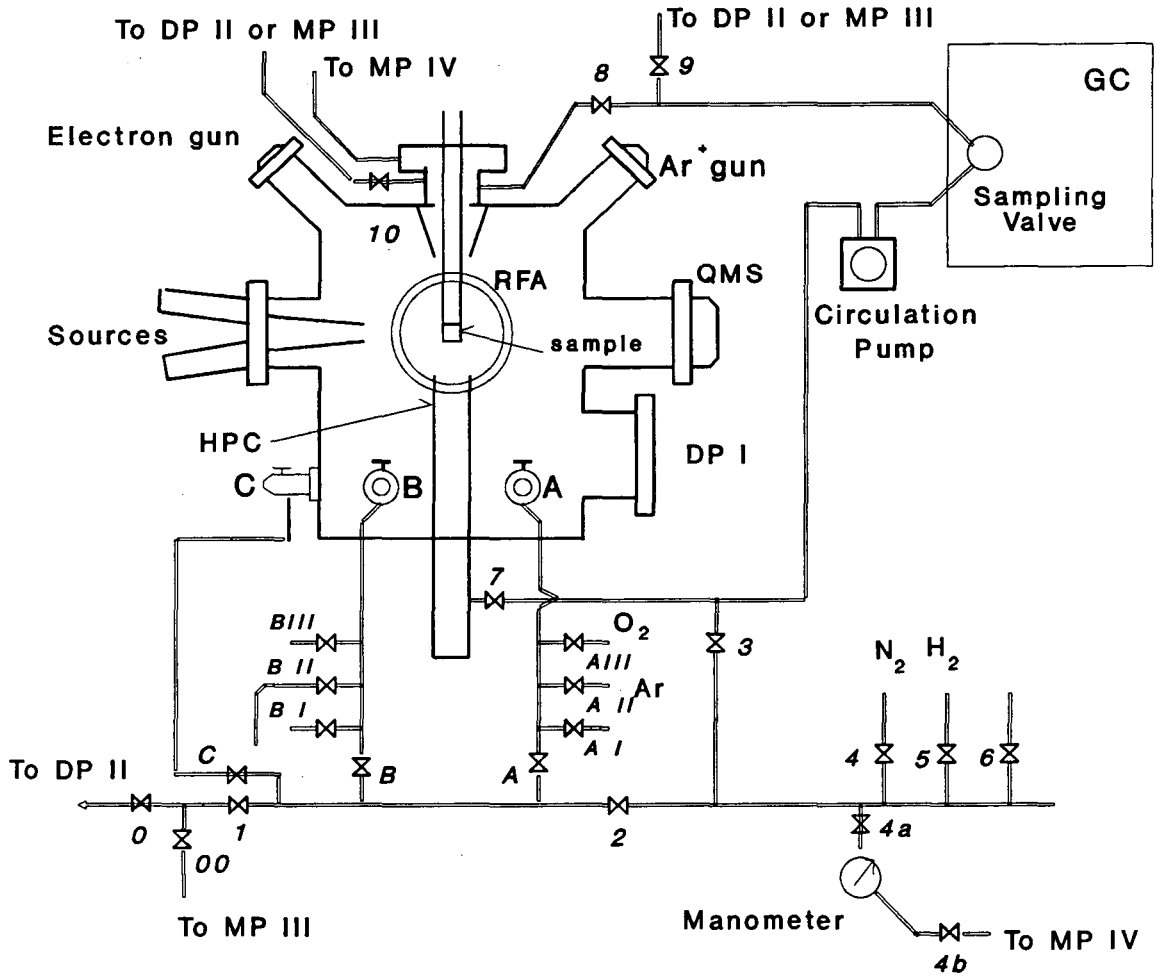

Fig. 2.1 Schematic diagram of the ultra-high vacuum - high pressure reactor cell apparatus for the combined surface science and catalysis studies. (*Italic letters* and *numbers* indicate stainless steel bellows valves (Nupro), **A**, **B** and **C**: leakvalves, DP I and DP II: Diffusion pumps for pumping the UHV system and the gas manifold, respectively, HPC: High Pressure Cell, MP III: Mechanical pump for pumping the reactor loop and the manifold, MP IV: Mechanical pump for differential pumping of the manipulator and providing the reference vacuum for the differential pressure gauge, RFA: Retarding Field Analyzer, QMS: Quadrupole Mass Spectrometer.)

sampling valve for gas chromatographic analysis (Hewlett-Packard, 5890A).

After the reaction studies, first the gases were pumped away using a mechanical pump (MP III, valve *0* closed, and valves *00, 2, 3, 7, 8, 9* and *10* open), then the loop was pumped down to $< 10^{-7}$ torr with DP II (valve *00* closed and valve

0 open). and the high pressure cell was opened (*7, 8* and *10* closed). Subsequently, the sample was characterized in UHV.

The main vacuum system consisted of a stainless steel belljar pumped by a liquid nitrogen trapped diffusion pump. The base pressure after a 40 hour bakeout (using an internal bake-out lamp and external heating tapes) was in the low 10^{-10} torr range. During continuous use, however, the it rose to $5x10^{-9}$ torr. With short overnight bake-outs we could maintain the base pressure in the high 10^{-10} range, which was adequate to prepare and characterize our model catalysts.

The ports of the UHV chamber were equipped with

- a four grid electron optics (Varian 981-0127) for the detection of the LEED pattern and for the energy analysis of the Auger electrons,
- an electron gun for Auger excitations (Varian 981-2455),
- an argon ion gun for cleaning and ion beam sputter deposition (Varian 981-2043),
- a quadrupole mass spectrometer (UTI 100C) for residual gas analysis and for temperature programmed desorption (TPD) studies
- a nude ion gauge (Varian 971-5008) to monitor the pressure
- three variable leak valves for introducing gases and vapors
- sources necessary for the preparation of model catalysts: aluminum source, alumina and zeolite targets.

In this study silicon single crystals and metal foils were used as substrates for the model catalyst. The manipulator and the reactor loop have been redesigned to decrease the adsorption capacity of the walls and to minimize the background catalytic activity. The modifications are summarized as follows:

<u>A. Manipulator</u>

- Hollow feedthroughs. So during reaction cold nitrogen or air can be used to cool them. Especially when gold foil was the substrate, it was essential that the feedthrus be cooled.

- Sample mounting: Copper support rods had a hole on the sample side (2-3 mm deep, and 0.03 mm larger in diameter than the support wire) before mounting. The gold wires holding the sample were placed inside and then this end was

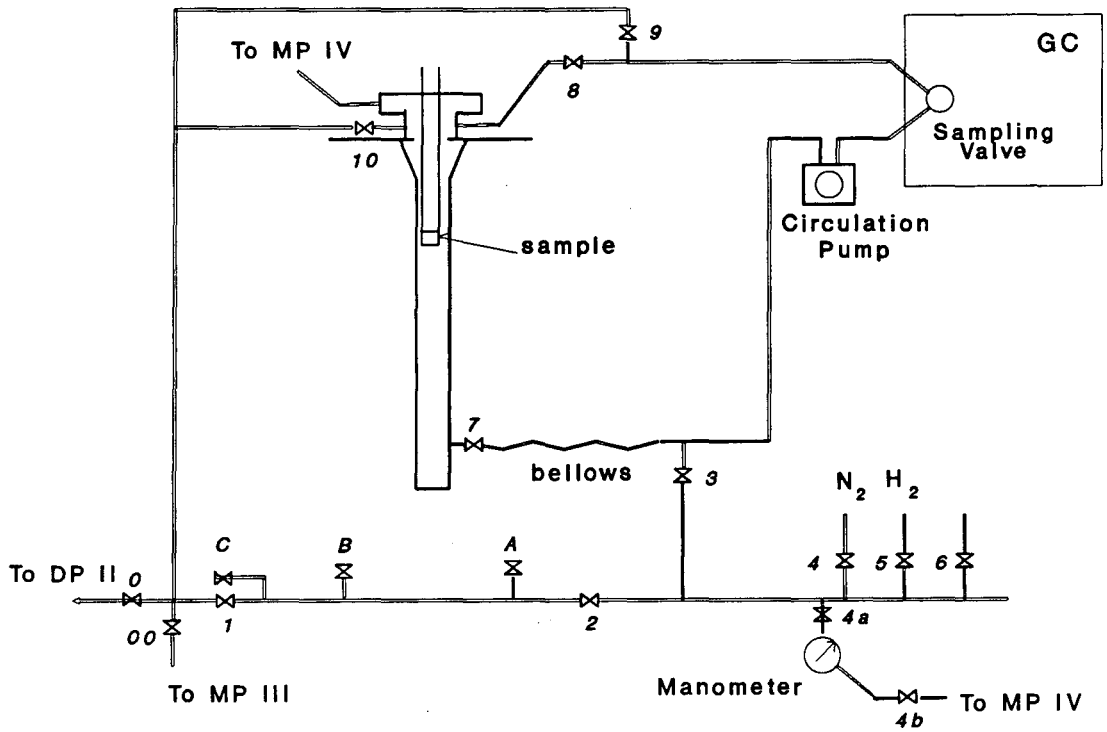

Fig. 2.2 Same as Figure 2.1, but only the reactor loop with the closed high pressure cell (HPC), and part of the gas introduction system are shown.

crimped. The other end of the rod was silver soldered to the stainless steel receptacle (Fig. 2.3). This was to minimize the resistance of metal - metal junctions and to eliminate stainless steel setscrews used in the previous design.

- Thermal breaks. One would like to minimize the heat loss from the foil to the rest of manipulator so the heat generated by the foil does not dissipate easily. The introduction of stainless steel sections having poor heat conductivity seemed to be an effective way to minimize the current necessary to heat the sample. Also, the diameter of the gold wires had to be optimized; too thick wires permitted too much heat loss, but too thin wires heated up more than the foil itself and they significantly contributed to the background catalytic activity. For UHV and catalysis studies, 0.25 mm gold wires worked the best with 0.025x10x10 mm foils. The temperature profile for this configuration, determined in air and the manipulator mounted horizontally, is indicated in Fig. 2.3.

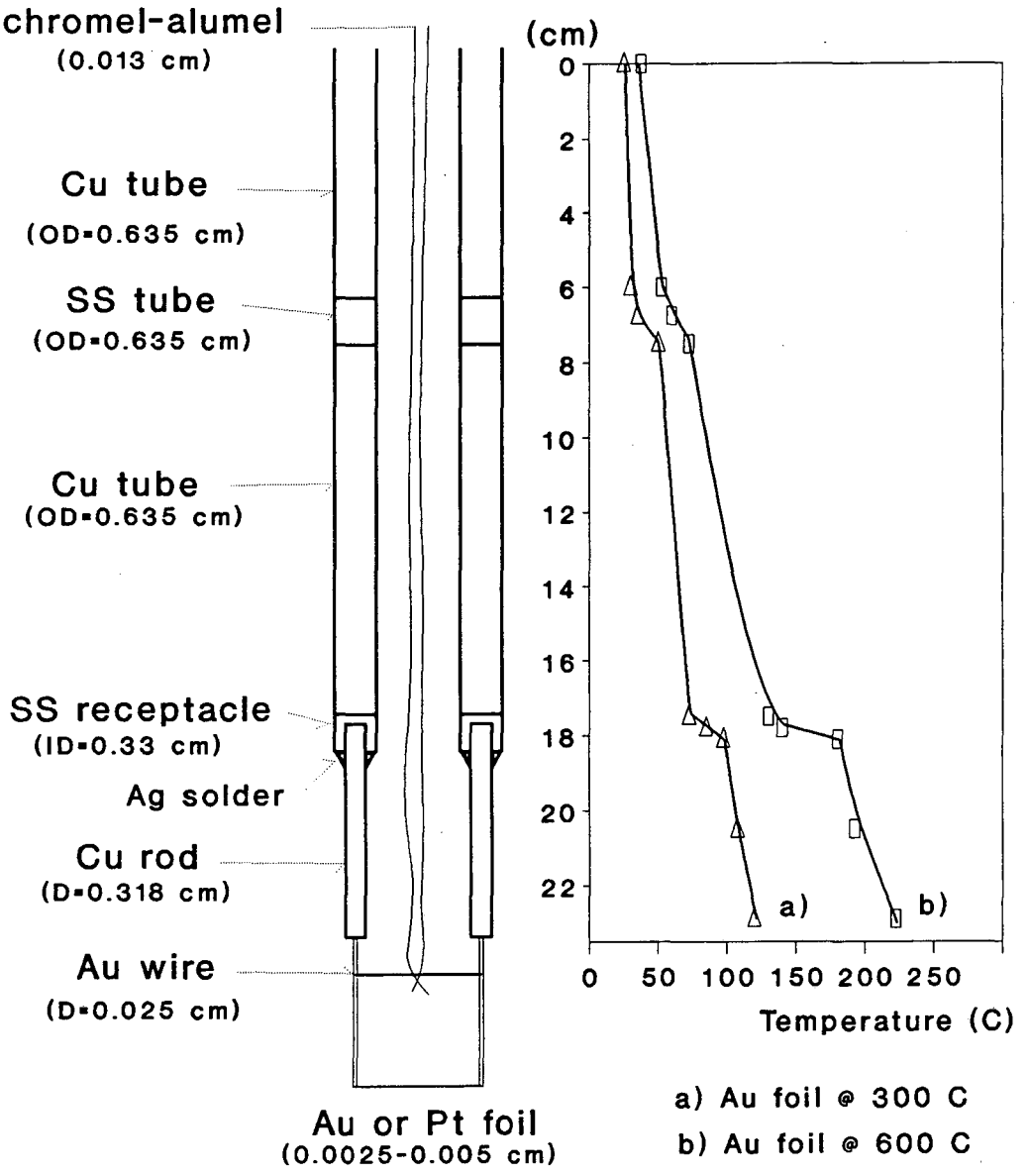

Fig. 2.3 Sample mounting. On the right we show the temperature profile when a 0.025 mm Au foil was heated to a) 300 C and b) 600 C in air.

B. Manifold, reactor loop and gas introduction system. (Fig. 2.2)

- Since Bronsted and Lewis acid sites can be interconverted by hydration - dehydration, to control the water content in the reactor and the manifold, a liquid nitrogen trapped diffusion pump (DP II) was used to pump the manifold. The pressure determined at the pump was on the order of 10^{-8} torr at the beginning of

the day, and rose to the 10^{-7}-10^{-6} torr range during the day. Valves *7, 9* or *10* (Fig. 2.1) could be opened without any increase in the pressure of the UHV chamber. We replaced all Swagelock fittings with UHV compatible VCR fittings. To minimize adsorption of reactants and products during reaction, and to facilitate the recovery of vacuum after reaction, the walls of the reactor loop and the manifold were kept at 100 C, using a heating tape.

- Wherever it was possible we substituted the stainless steel tubing with glass tubing in the reactor loop. This was necessary because we observed that significant amount of aromatic hydrocarbons adsorbed on the room temperature stainless steel parts. Since the stainless steel bellows were required to provide a flexible connection between the high pressure cell and the rest of the reactor loop, we have kept that section, but continuously heated it to 150 C. The stainless steel Nupro valves with VCR fittings were connected to the glass sections via UltraTorr unions.

- An all Teflon diaphragm pump (Cole-Parmer) was used as a circulation pump in the reactor loop, which replaced the stainless steel bellows pump used in previous studies. This modification dramatically decreased the adsorption of the products in the reactor loop. The total volume of the reactor was 260 ml.

2.2 Surface Analysis Techniques

Auger electron spectroscopy (AES), Low Energy Electron Diffraction (LEED), X-ray Photoelectron Spectroscopy (XPS), and temperature programmed desorption (TDS) were the main sources of information regarding the topmost atomic layers of our samples. Since the theory and applications of these techniques have been extensively reviewed elsewhere [3-8], only a brief discussion of these techniques will be given here.

AES, XPS and LEED are probing only the topmost layers of solids because the electrons emitted or scattered from the surface have only 10-30 Å free mean paths in the solid. The free mean path is a function of the energy, and independent

of the composition of the solid (e.g. [3]). Virtually every surface science text shows this free mean path - electron energy curve, and it is often referred to as the 'universal curve'.

The use of these techniques requires that the sample be kept clean during the measurement and that the electrons freely reach the sample (and the detector) without interaction with gas phase molecules. Thus, it is essential that ultra-high vacuum ($<10^{-9}$) is essential to be maintained during preparation and surface analysis.

A. Auger Electron Spectroscopy (AES) [3,4,6]

The Auger process involves the following steps. 1) An energetic (1-5 keV) beam of electrons or X-rays creates a core level electron hole in the atom. 2) A higher energy electron fills the hole, but instead of emitting X-rays (3) the atom ejects another electron from a third energy level with a kinetic energy characteristic of the three states involved in the process. The kinetic energy of the leaving electron is characteristic of the element, and can be used as a fingerprint of the element. The peak-to-peak height of the Auger peaks in the spectrum obtained in the derivative mode is proportional to the number of atoms on the surface. In addition to the composition, the oxidation states of certain elements can also be determined if the valence band is involved in the process (e.g. silicon and aluminum).

A four grid retarding field analyzer (RFA) was used to take the spectra. The first and the fourth grid were grounded internally and externally, respectively.
The parameters used to take the Auger spectra are as follows

Primary electron energy	1.6 keV
Modulation (peak-to-peak)	4-7 V
Scan rate	15-30 eV/min
Screen voltage	300 V

The sweep voltage was generated, and combined with the modulation by a modified power supply (Varian 981-0538). The spectra were recorded in the

derivative mode using a lock-in amplifier (EG&G Brookdeal 9503) with a time constant of 0.3 s.

Since the model catalyst preparation always included the deposition of a metal or the sputter deposition of an oxide, with time, a significant amount of metal oxide accumulated on the electron optics. In every 2-3 months the grids had to be cleaned and the screen had to be recoated. The symptom of the deposition of oxides was an ever increasing background in the Auger mode.

The cleaning procedure involved a brief (3-5 min) dipping of the grids in dilute aqua regia solution: 25 ml 70% HNO_3 + 225 ml 37% HCl + 1050 ml water. After etching, the grids were rinsed with deionized water and methanol.

B. Low Energy Electron Diffraction (LEED) [3,4,5]

In LEED, a monochromatic beam of electrons is directed at the single crystal surface and the pattern caused by constructivel interference of electrons elastically backscatted from the surface are observed on a fluorescent screen as bright spots. Although the observed pattern on the screen is characteristic of the structure of the surface layers, the structural parameters (interatomic distances and angles) cannot be determined directly from one pattern. To determine the structure, the intensity of the diffraction spots (I) has to be followed as a function of the primary electron energy (V). The theoretical I-V curves can be calculated for each proposed structure and compared with the experimental ones. The structure corresponding to the best fit is considered to be the 'solved surface structure'.

In this study the patterns were observed on the same four grid electron optics as used for AES. The sample was not exactly in the center of curvature of the LEED optics, because in order to accommodate both the electron optics and the high pressure reactor cell the LEED system had to be mounted on a spacer flange of about 1.2 cm. Photographs of the LEED patterns at different electron energies were taken by a Polaroid camera. The screen voltage and the crystal current were 5 kV and 0.5 microamperes, respectively.

C. X-ray Photoelectron Spectroscopy (XPS) [3,4,6]

X-rays of 1-2 keV energy can ionize the atoms in the solid. The kinetic energy of the electrons (E_K) leaving the solid depends on the energy of the x-ray photon (E_P) and the binding energy (E_B) of the electron: $E_B = E_P - E_K$. The binding energy of core and valence electrons is a function of the chemical environment and oxidation state of the surface atom, thus the position of the XPS lines can be used to identify different elements and different oxidation states of the same element. The integrated intensity of the XPS peaks is proportional to the surface concentration of the element.

The XPS analyses were carried out in a commercial ESCA system (Perkin-Elmer, PHI 5300) pumped with an ion pump and a titanium sublimation pump, and equipped with a magnesium X-ray source (E_P= 1253.6 eV), a hemispherical energy analyzer and a position sensitive detector.

The samples were mounted on the sample holder and transferred into the UHV chamber through a sample introduction system pumped by a turbomolecular pump. First survey spectra were taken in the 0-1100 eV binding energy range and then multiplex data was collected in the energy range of interest.

The magnesium source was operated at 400 W power (15 kV). The pass energy during survey and multiplex spectra were 44.75 eV and 17.9 eV, respectively. The angle between the surface normal and the analyzer was 45 degrees.

D. Temperature Programmed Desorption (TPD) [3,7]

The sample is exposed to a gas at low pressures at a fixed temperature. After the adsorption the temperature of the sample is heated in a linear fashion, and using a quadrupole mass spectrometer the partial pressure of the fragments desorbing from the surface is plotted against the temperature of the sample.

The desorption peak temperature (the maximum rate of desorption) is related to the activation energy of desorption, i.e., how strongly the adsorbate is attached to the surface

We take advantage of the technique in Chapter 4. where CO TPD from platinum foil is used to calculate the relative number of Pt atoms on the surface of the sample. For experimental details see Chapters 4.2.1 and 4.3.1.

References

1. Naasz, B. M., Ph. D. Thesis, University of California, Berkeley, 1986.
2. Naasz, B. M., Boszormenyi, I., and Somorjai, G. A., *J. Cat.*, **115**, 399 (1989).
3. Somorjai, G. A., "Chemistry in Two Dimensions: Surfaces," Cornell, Ithaca, 1981.
4. Ertl, G. and Kuppers, J, "Low Energy electrons and Surface Chemistry", VCH, Weinheim, 1985.
5. a) Pendry, J. B., "Low Electron Energy Diffraction", Academic Press, London, 1974.

   b) Van Hove, M. A. and Tong, S. Y., "Surface Crystallography by LEED", Springer Series in Chem. Phys., Vol. **2**, 1979.
6. Briggs, D. and Seah, M. P., Eds. "Practical Surface Analysis", Whiley, Chichester, 1984
7. Redhead, P. A., *Vacuum*, **12**, 203 (1962).

3. Model Silica-Alumina Catalysts

Our goal is to prepare thin layers of silica alumina mixtures on conductive substrates and test their acid catalytic properties. First, one has to chose a substrate, that does not have significant catalytic activity in hydrocarbon reactions. From this point of view, elemental silicon, aluminum and gold have been found to be the three most suitable substrates. One can devise a number of routes to fabricate silica-alumina layers on these three substrates. Without detailed discussion, here we list a few that may prove to be promising in future studies. * indicates the ones described in the next three chapters, and # labels the ones that were tried but with no or limited success.

<u>I. Preparation in Ultra-High Vacuum:</u>

A. Silicon substrate (single crystal - (111), (100), (110))

1.a	*	$Si_{(s)} + Al_{(v)} + O_{2(g)}/H_2O_{(g)}$	(Chapter 3.1.1)
b		$Si_{(s)} + O_{2(g)}/H_2O_{(g)} + Al_{(v)} + O_{2(g)}/H_2O_{(g)}$	
2.a		$Si_{(s)} + AlH_{3(g)} + O_{2(g)}/H_2O_{(g)}$	
b		$Si_{(s)} + Al(iPr)_{3(g)} + O_{2(g)}/H_2O_{(g)}$	
c	#	$Si_{(s)} + H_2O_{(g)} + AlH_{3(g)} + O_{2(g)}/H_2O_{(g)}$	
d	#	$Si_{(s)} + (Al(iPr)_{3(g)} + O_{2(g)}/H_2O_{(g)})$	

B. Aluminum substrate (single crystal - polycrystalline foil)

1.a		$Al_{(s)} + H_2O_{(g)} + SiH_{4(g)} (+ O_{2(g)}/H_2O_{(g)})$
b		$Al_{(s)} + (SiH_{4(g)} + O_{2(g)}/H_2O_{(g)})$
c		$Al_{(s)} + (SiH_{4-x}(iBu)_{x(g)} + O_{2(g)}/H_2O_{(g)})$

C. Gold substrate (single crystal - or polycrystalline foil)

1.a		$Au_{(s)} + Al_{(v)} + H_2O_{(g)} + SiH_{4(g)} (+ O_{2(g)}/H_2O_{(g)})$	
b	#	$Au_{(s)} + (Al_{(v)} + SiH_{4(g)} + H_2O_{(g)})$	
2.		$Au_{(s)} + (AlH_{3(g)} + SiH_{4(g)} + H_2O_{(g)})$	
3.	*	$Au_{(s)} + AlO_{x(g)} + SiO_{y(g)}$	(Chapter 3.2)

II. Preparation in solution:

A. Silicon substrate {single crystal - (111), (100), (110)}

1. # $Si_{(s)}$ + Zeolite synthesis gel
2.a * $Si_{(s)} + OH^-_{(aq)} + Al_{(s)}$ (Chapter 3.1.2)
b * $Si_{(s)} + (OH^-_{(aq)} + SiO_{2(coll.)}) + Al_{(s)}$
3. $Si_{(s)} + H_2O_{(l)} \rightarrow Si(OH)_2/Si_{(s)} + Al(OiPr)_{3(org.solv.)}$

B. Aluminum substrate (polycrystalline foil)

1. # $Al_{(s)} + OH^-_{(aq)} + Si_{(s)}$
2. $Al_{(s)} + H_2O_{(l)} \rightarrow Al(OH)_3/Al_{(s)} + SiH_{4-x}(OiBu)_{x(org.solv.)}$

C. Gold substrate (polycrystalline foil)

1. # $Au_{(s)}$ + Zeolite synthesis gel
2. # $Au_{(s)} + OH^-_{(aq)} + Al_{(s)} + SiO_{2(coll.)}$

We believe that most of these methods, with the proper set of parameters (e.g. temperature, pressure, concentration and time), could produce homogeneous silica-alumina layers or particles on the surface of the substrate. Both UHV and aqueous methods have advantages and disadvantages. For example, the advantage of the UHV preparations is that the samples can be produced in a very clean environment, and the surface analysis can be performed *in situ*. On the other hand, the species that form the silica-alumina layer in UHV are very different from the ones that form practical catalysts from aqueous solutions. In this respect, the aqueous preparations appear more attractive.

After preparation and surface characterization, one would like to find out if the low surface area model silica-alumina thin film possesses acidic properties. Unfortunately, the number of methods available to determine the acidity of low surface area samples is very limited (see Chapter 1.3.1), because none of the volumetric titrations, indicator, infrared, NMR or calorimetric methods are sensitive to 10^{11}-10^{13} acid sites. In principle, the temperature programmed desorption of a

probe molecule and the test reaction method can be useful to us. Preliminary results, however, indicated that, due to the very inhomogeneous nature of our model catalysts, ammonia and methyl amine gave very small and very broad, featureless TPD peaks.

Thus the only methodology left and probably suitable for our purposes is the testing of the model catalysts in typical acid catalyzed reactions. Having ruled out the other techniques based on their lack of sensitivity, one has to ask if it is possible at all to measure catalytic reaction rates over 1-2 cm^2 surface area silica-alumina samples.

In the UHV - high pressure catalytic reactor cell apparatus (Fig. 2.1) equipped with a gas chromatograph (GC) and designed to study metal single crystals as model catalysts, we can detect 10^{11} molecules/GCsample. With 10^3 sec between GC samples, reaction rates of 10^8 product molecules/sec can be measured, provided that the catalyst remains active for 10^3 seconds.

Nielsen *at al.* [15] studied the isomerization of 1-butene on silica-alumina catalysts. They found that the isomerization rate was on the order of 10^{11} molecules/cm^2/sec. Similar rates have been reported for other silica-alumina systems and reactions. Assuming that we can make samples of similar acid site strength and density we conclude that we should be able to detect activity of our model catalysts.

The three methods we discuss in this thesis are the following:

1) $Si(111) + Al_{(v)} + O_2(H_2O)_{(g)} \rightarrow Al_xSi_yO_z/Si(111)$
   Deposition of aluminum on Si(111) followed by oxidation with oxygen and/or water in ultra-high vacuum.
2) $Si(111) + Al_{(s)} + NaOH_{(aq)} \rightarrow Al_xSi_yO_z/Si(111)$
   $Si_{(s)} + (OH^-_{(aq)} + SiO_{2(coll.)}) + Al_{(s)} > Al_xSi_yO_z/Si(111)$
   Deposition in aqueous NaOH solution.
3) $Au_{(s)} + AlO_{x(g)} + SiO_{y(g)} \rightarrow Al_xSi_yO_z/Au_{(s)}$
   Preparation in UHV by Ar^+-ion Beam Sputter Deposition

3.1 $Al_xSi_yO_z$/Si(111)

We chose silicon (111) as substrate for our model catalysts because, thanks to the microelectronics industry, its surface structure and chemical properties have been extensively studied, and high quality crystals are available in large quantities at 8very low cost. In addition, from the point of view of surface characterization and reproducibility, the use of a well defined substrate is always preferred in surface science studies.

3.1.1 Preparation in UHV:

$$Si(111) + Al_{(v)} + O_2(H_2O)_{(g)} \longrightarrow Al_xSi_yO_z/Si(111)$$

First, we deposit aluminum metal on a clean Si (111) single crystal surface, then we expose the surface to oxygen or water. In this manner, we hope to make a few atomic layers of silicon oxide and aluminum oxide in intimate contact.

Although the fact that the clean annealed Si(111) surface is not bulk terminated, but it shows a (7x7) reconstruction has been known since 1959 [1], the real space structure that would be consistent with available LEED, transmission electron diffraction (TED), Rutherford backscattering (RBS) and scanning tunneling microscopy (STM) data was not proposed until 1985 by Takayanagi *at al.* [2]. According to this model the structure consist of two reconstructed (111) layers and 12 adatoms on top. The structure is the result of a delicate balance of forces. What makes the bulk terminated (111) face of silicon energetically unfavorable is the large density of electron pairs (dangling bonds) on the surface, one in each 1x1 unit cell. To minimize the number of dangling bonds the surface reconstructs, but at the same time the number of energetically favored tetrahedral Si-Si bonds decreases. Thus, part of the energy gained by the elimination of dangling bonds is 'spent' on the distortion of tetrahedral bonds in the top two atomic layers. The resulting structure has only 13 dangling bonds on a 7x7 area as opposed to 49 on 1x1.

Although the 7x7 structure is very stable, it is removed by contaminants or overlayers [3,4]. When aluminum is deposited on the 7x7 surface and annealed between 873 and 1173 K a r3xr3 R30 LEED pattern is observed at about a third of a monolayer coverage. (The r3xr3 R30 notation means that the length of the unit cell is square root of 3 times longer than that of the unreconstructed unit cell and it is rotated by 30 degrees with respect to the unreconstructed 1x1 cell.) Recent LEED I-V analysis and calculations [5] confirmed previous total energy calculations [6] that the aluminum atoms occupy fourfold atop (T_4) sites.

Because of its importance in the microelectronics industry, the oxidation of silicon single crystals by oxygen and water have been extensively studied. LEED investigations showed that neither oxygen nor water forms ordered overlayers on Si(111) [7]. Synchrotron radiation results indicated [8] that chemisorbed oxygen and Si-O-Si bridges coexist even at very low coverages (0.2 monolayers), thus ruling out a two step oxidation process of chemisorption followed by deeper oxidation. It is also well known that a thicker (>100 Å) thermally grown stoichiometric oxide is amorphous [9]. The interface between the oxide and the silicon is very thin, and may consist of a substoichiometric SiO_x layer [10].

The oxidation of Al/Si(111) system has not been investigated.

3.1.1.1 Experimental

The silicon was first cleaned in air before introduction to UHV by immersing the wafer in the following solvents and solutions at temperatures and for periods of time indicated below [11].

1.	Trichloro ethylene		75 C	4 min
2.	Acetone		RT	1 min
3.	Methanol		RT	1 min
4.	Rinse three times with deionized water			
5.	H_2O:NH_4OH:H_2O_2	1:1:1	80 C	5min
6.	Rinse three times with deionized water			
7.	H_2O:HF	1:1	RT	0.5 min

8.	Rinse three times with deionized water			
9.	H_2O:H_2O_2:HCl	5:1:1	80 C	5 min
10.	Rinse three times with deionized water			
11.	H_2O:HF	1:1	RT	0.5 min
12.	H_2O:H_2O_2:HCl	1:1:3	95 C	10 min

After this treatment the 0.8x1.2x0.05 cm silicon wafer was mounted on the manipulator as shown in Fig. 3.1. The thermocouple was mounted on the gold foil. Using an optical and an infrared pyrometer, we found that in UHV the temperature difference between the gold foil and the silicon wafer was < 25 C.

The surface oxide that developed during the above cleaning procedure could be removed in UHV by heating the sample to 1370 K for 3-5 minutes. If necessary, Ar^+ ion bombardment was also used to remove carbon and oxygen. The cleanliness of the sample was monitored by AES. Annealing of the clean Si(111) at 1270-1370 K yielded the characteristic 7x7 LEED pattern. Aluminum was vapor deposited on the Si(111) surface in UHV ($p < 8x10^{-10}$ torr) at room temperature from a 3 mm internal diameter high purity alumina crucible heated to ca. 950 K by a coiled tantalum wire (d=0.127 mm). The aluminum source was preheated before deposition for 20 minutes at 950 K with the sample turned away, and during depositions it was moved within 1.5 cm of the silicon sample. The deposition was monitored by AES.

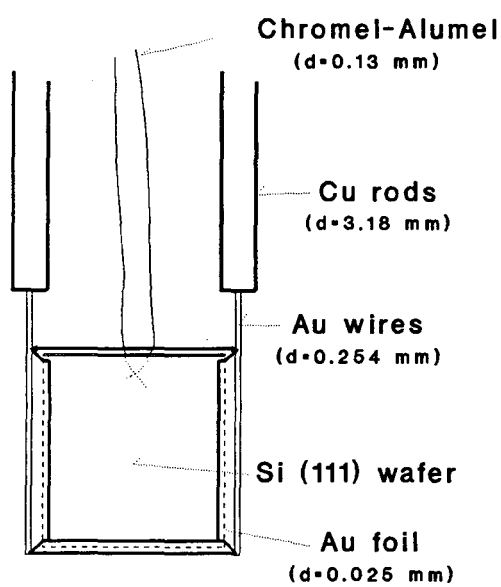

Fig. 3.1

The aluminum could be easily removed by heating the silicon wafer to 1250 K. Temperature programmed desorption of aluminum was carried out by heating the sample to 1300 K using a linear temperature controller. The heating rate was approximately 10 K/s. We chose this low rate to minimize the temperature

difference between the gold foil an the Si sample. We estimate that during TPD runs the temperature of the sample was lagging behind by no more than 50 K.

Following the deposition the Al/Si(111) surface was oxidized by exposing it to 1-100 L oxygen or water (1 L = 10^{-6} torr.sec) at various temperatures. The oxidation was followed by AES and the change in the LEED images was noted.

Materials: The silicon samples were cut from 76 mm diameter and 0.5 mm thick boron doped (111) single crystal wafers (Siltec, Co., 5-50 ohm.cm). The high purity alumina crucible was filled with aluminum pieces (99.999%) and heated to 940 K in a vacuum furnace prior to mounting in the UHV chamber.

3.1.1.2 Results And Discussion

Fig. 3.2 a) shows the aluminum uptake curves. The deposition of the aluminum was not sequential, i.e. after deposition of a certain amount, the Auger spectrum was taken and the sample was cleaned by flashing to 1300 K. Both Al and Si curves exhibit a break at around 32 second deposition time indicating that in the first stages of the growth the layer grows in a 'layer by layer' fashion up to one monolayer. After the monolayer break, the curves change exponentially, implying a three dimensional growth mode [12]. In contrast with the literature [3,4], after deposition of 1/3 of a monolayer of aluminum followed by annealing at 1100 K, the r3xr3 R30 LEED pattern could not be observed. After annealing the surface, the aluminum concentration dramatically decreased, and the 7x7 LEED pattern was observed. To determine if the Al diffuses into the bulk or desorbs during annealing we performed TPD measurements.

Aluminum desorbs from Si(111) in one single peak at around 1200 K and the desorption temperature is independent of Al coverage. In Fig. 3.2c, we show the area of the aluminum desorption peak as a function of coverage. Clearly, there is hardly any desorption taking place at low (< 0.75 monolayer) coverages. In this regime the aluminum mainly diffuses into the bulk of Si(111). According to the

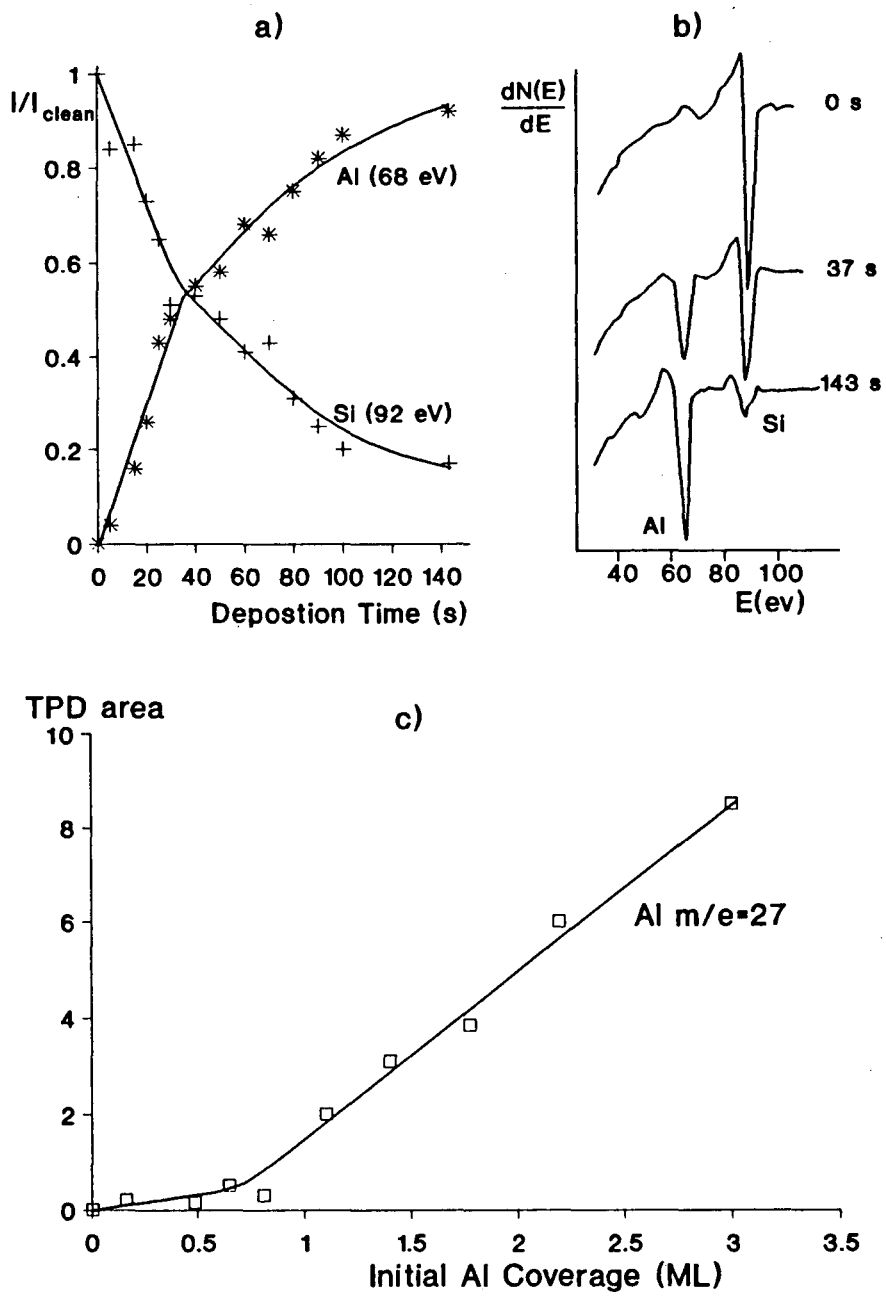

Fig. 3.2 a) The relative Auger peak intensity of the Al and Si Auger lines as a function of deposition time. b) Three examples of Auger spectra in the 20-110 eV region taken after 0, 37 and 143 s of deposition. c) Area of Al TPD peak as a function of aluminum coverage.

phase diagram, aluminum does not form silicide, and has a limited solubility in silicon [13]. As to why the Al TPD peak area starts to increase after the deposition of approximately 0.75 monolayer equivalent of aluminum, we can only speculate that the near surface region has to be saturated first with aluminum before appreciable desorption can be detected. This is supported by the observation that the r3xr3 R30 LEED pattern can be obtained only after 1) several 1/3 monolayer equivalent Al doses and annealing cycles or 2) deposition of 2 monolayer equivalent of aluminum followed by annealing. The fact that more than 1/3 of a monolayer (ML) of aluminum is necessary to form the '1/3 ML coverage' r3xr3 R30 Al-Si(111) implies that the presence of aluminum atoms in the second or third layer might be required to stabilize the structure. This possibility has been considered in LEED crystallography calculations [5], but because of lack of sensitivity to the substitution of silicon by aluminum, the results have not been conclusive.

Fig. 3.3 shows the two characteristic patterns obtained in this study: 7x7 Si (111) and r3xr3 R30 Al/Si(111).

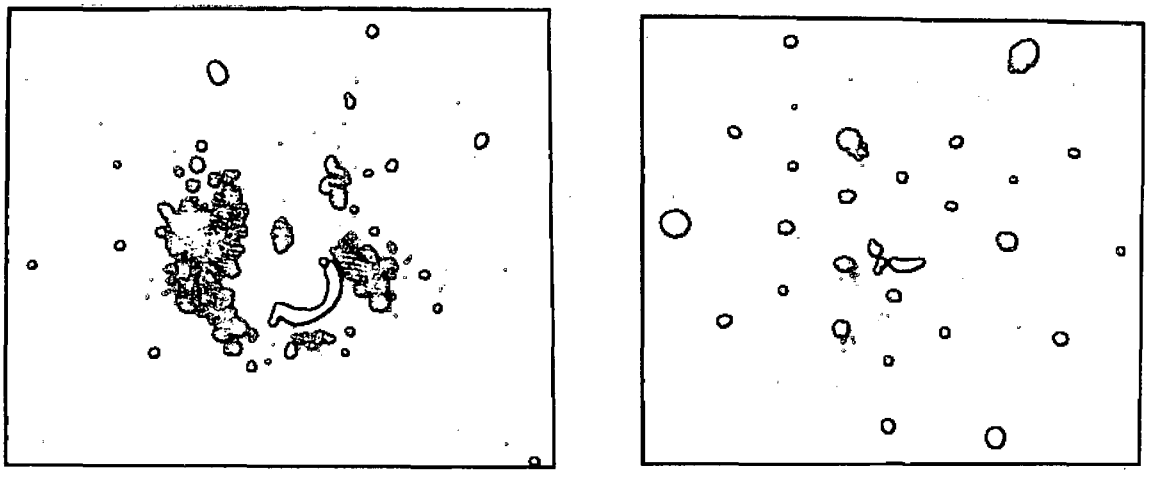

a) b)

Fig. 3.3 LEED patterns of a) clean silicon (111) showing the 7x7 reconstruction and b) r3xr3 R30 Al-Si(111). (E_p = 122 eV)

3.1.1.2 $Al_xSi_yO_z$/Si(111) - Results and Discussion

To prepare a mixture of silica and alumina we exposed the r3xr3 R30 Al-Si(111) structure to 4 L of oxygen at 570 K. Fig. 3.4 shows the Auger spectra before and after oxidation. The low energy Al and Si Auger transitions are LVV transitions, the position and the shape of the Auger lines are different for the elements and for the oxides. Since the line shapes can change due to slight changes in the density of states also, it is difficult to quantify how much of the surface is oxidized. From Fig. 3.4 we learn that after this oxidation treatment the aluminum is fully oxidized, and the appearance of the peak at 84 eV indicates the formation of oxidized silicon as well.

For both clean aluminum and silicon samples we observed that the intensity of the peaks for the oxides is always smaller than that of the non oxidized form. We note that the AlO_x peak in Fig. 3.4 is larger than the initial Al^o peak, which probably indicates that the aluminum atoms that diffused into the near surface region of silicon during the preparation of the r3xr3 R30 Al-Si(111) structure, now diffuse back to the surface.

The 7x7 structure reacts with oxygen and Si-O-Si bridges are formed. The chemisorption of oxygen and the oxidation process occurs concurrently [8] even at room temperature. Considering that aluminum in the r3xr3 R30 structure occupies the same kind of adatom positions as the adatoms in the 7x7 structure [2,5] and that aluminum is chemically more reactive then silicon we can assume, that in this oxidation process AlO_x and SiO_y species are forming in the vicinity of each other. We noted that the disappearance of the r3xr3 R30 pattern was much more rapid than that of the 7x7 pattern when the samples were exposed to oxygen.

The question is if any ordered structures can be observed after this oxidation procedure. It would be extremely advantageous to find ordered Si-Al-O structures, because then, the same way as metal single crystals are used to model metal catalysts, we could use these structures as model acid catalysts. For this reason we spent considerable amount of time looking for conditions to prepare such structures.

Less than one Langmuir exposure of the r3xr3 R30 structure to oxygen or to water at room temperature is enough to increase the background intensity and

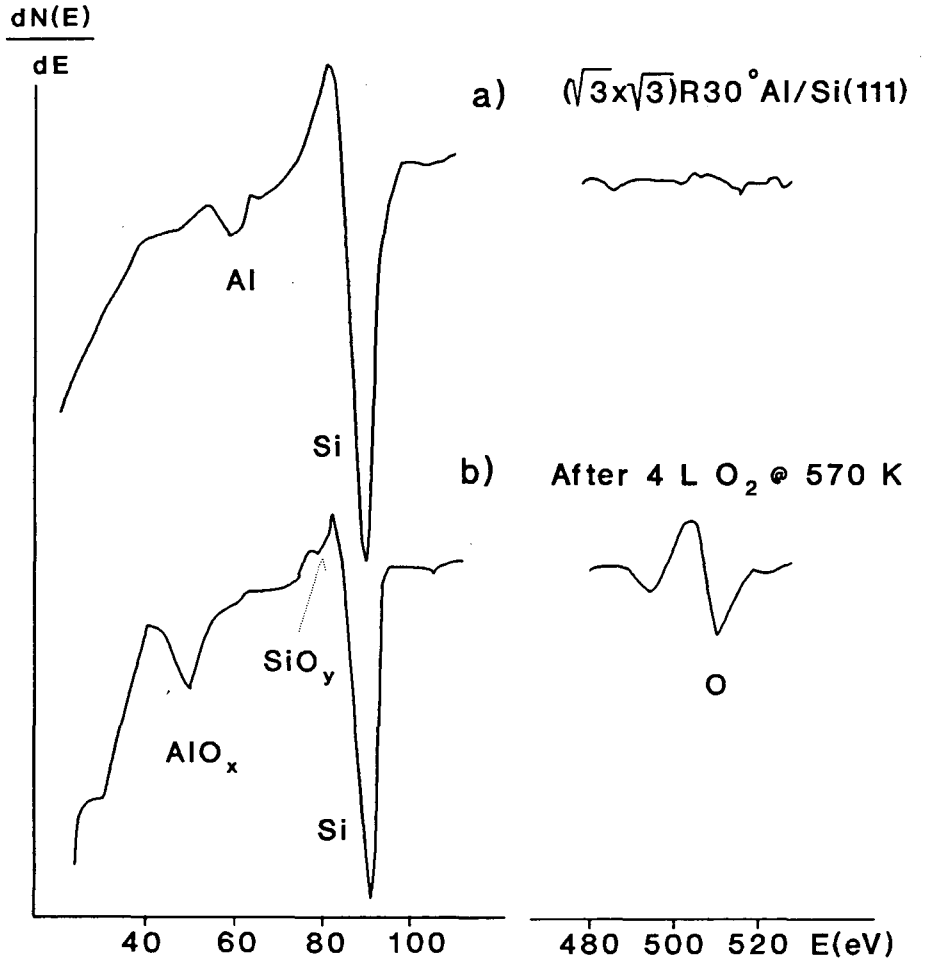

Fig. 3.4 Auger spectrum of the r3xr3 R30 Al-Si(111) structure before oxidation (a) and after 4 L oxygen exposure at 570 K (b).

decrease the spot intensity of the LEED pattern. More than 10 L exposure completely removes the r3xr3 R30 structure. At higher temperatures (> 470 K), the pattern turns into a 1x1 (Fig. 3.5) with a somewhat higher background than observed for the r3xr3 R30 . This 1x1 pattern was the best we could do in the quest of an ordered silica-alumina layer on Si(111). This pattern can be due to 1) an unreconstructed silicon (a) under a thin layer of amorphous silica-alumina or (b) between islands of silica-alumina or perhaps 2) to a partially ordered silica-alumina layer.

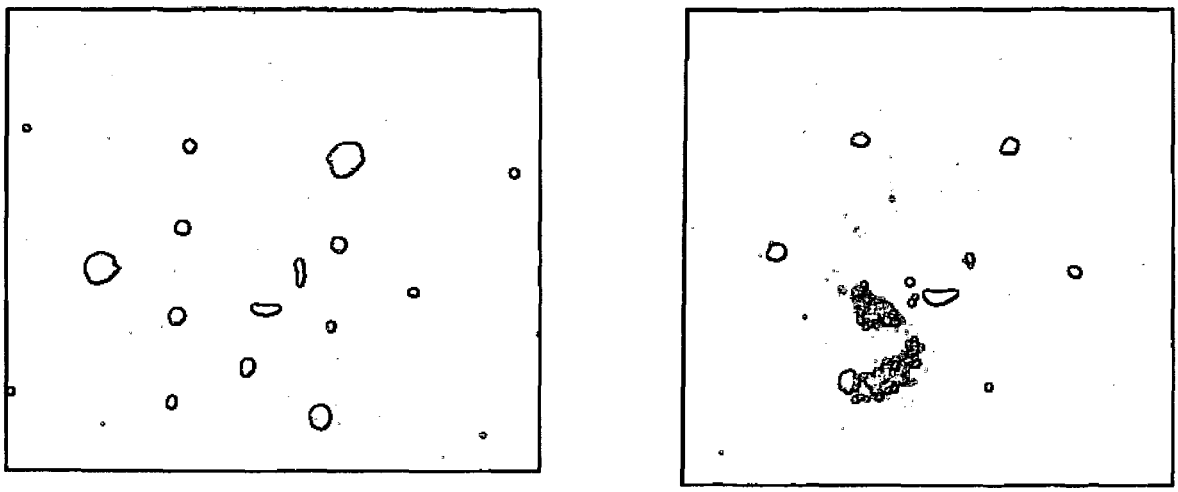

a) b)

Fig. 3.5 LEED patterns before (a) and after (b) 4 L oxygen exposure of r3xr3 R30 Al/Si(111) at 570 K. (E_p=66eV)

Careful I-V analysis could suggest which of these is more likely. Qualitatively, if the pattern is due to unreconstructed silicon between patches of an oxide layer the I-V curves should be the same as the 1x1 Si(111) curves. On the other hand, if a new structure was present the features (especially the position of the intensity maxima) would be rather different. Because the manipulator used in this study allowed only rotation we could not carry out a rigorous analysis, but we attempted to collect some qualitative data anyway.

The sample turned away from normal incidence by 8-10 degrees, using a spot photometer, we measured the intensity of the (0,0) beam as a function of electron energy. The results are shown in Fig. 3.6. The intensities are not normalized to constant beam current and probably that is why the curves are sloping. In the literature it has been reported that the I-V curves for the (0,0) beam are very similar for the r3xr3 R30 Al-Si(111), 1x1 Si(111) and for the 7x7 Si(111) structures [5,14]. Our crude curves are in accordance with those results.

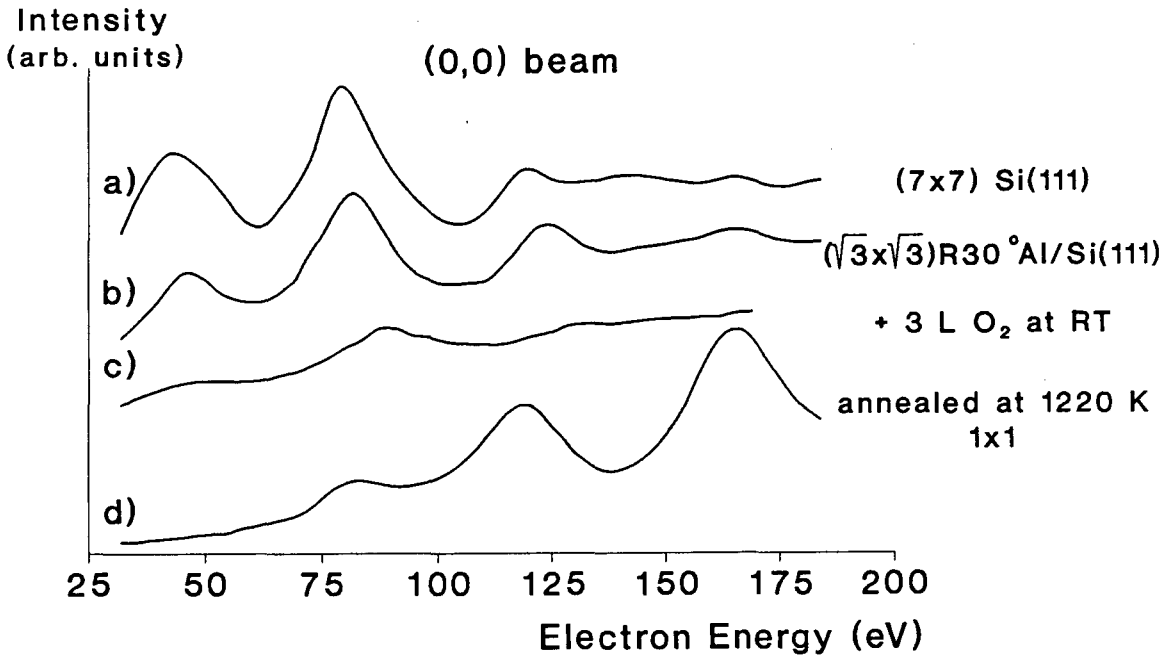

Fig. 3.6 The intensity of the (0,0) beam of the LEED pattern obtained for the four samples as a function of the electron energy. (Raw data, not normalized to constant beam current!)

When we expose the r3xr3 R30 structure to 3 L oxygen at room temperature, the intensity of the spots dramatically decreases, and the background increases, as indicated by an almost featureless curve. When the same sample is annealed at 1220 K, however, a very sharp 1x1 pattern can be observed, and the I-V curve for the (0,0) beam is shown in Fig. 3.6. Although the relative intensities of the maxima are very different from that of the clean silicon or the r3xr3 R30 pattern, the peak positions which are more characteristic of the structure are very close in all four curves.

Based on this rough analysis of one single beam it would be premature to draw a conclusion. If anything, it can be said, however, that the formation of a partially ordered silica-alumina layer is less likely, because in that case very different features would be expected in the I-V curves. And it is more probable that amorphous silica-alumina islands cover a partially oxidized 1x1 Si (111) surface. We have to add, however, that the 1x1 structure is certainly different from that of an

unreconstructed Si(111), because the LEED pattern has a sixfold symmetry in a wide primary electron energy range. (The unreconstructed 1x1 Si(111) has threefold symmetry.)

We were interested in seeing how a thicker aluminum layer oxidizes. After deposition of ca. 2 monolayer equivalent aluminum, the sample was exposed to 30 O_2. Before and after the deposition no sign of LEED pattern can be seen. But subsequent annealing at 1270 K produced a sharp 1x1 LEED pattern with high background. By slightly moving the electron beam across the sample, the quality of the 1x1 pattern changed rather drastically (Fig 3.7). To determine the surface

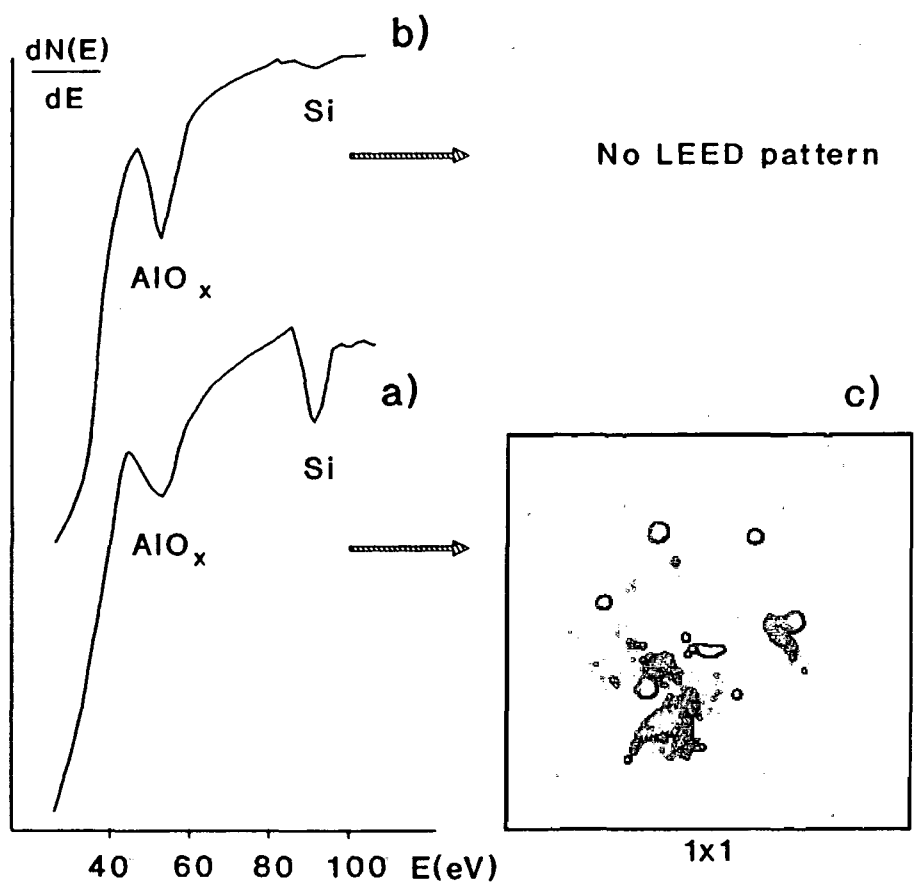

3.7 AES spectra obtained using the LEED electron gun after the oxidation of 2 ML Al/Si(111) at two different areas on the sample. a) an area that exhibit a 1x1 LEED pattern shown in c) and , b) another area of the same sample showing no ordering by LEED. (E_p = 122 eV)

composition at different degrees of ordering, we took Auger spectra using the LEED electron gun at the same electron beam positions used for the LEED analysis. The results clearly indicate that the more AlO_x present the less order can be detected by LEED.

The oxidation of both the r3xr3 R30 Al-Si(111) and 2 ML Al on silicon by water produced similar LEED patterns. The only difference we noticed was that water oxidized somewhat faster than oxygen.

Thin uniform layers of $AlO_x + SiO_y$ could be produced on silicon (111) by oxidation of an ordered r3xr3 R30 Al-Si(111) structure. Since the low energy Si^0 LVV transition is still clearly detectable, based on the mean free path of the emerging electron, we estimate that the thickness of this layer is not more than 10 Å. Although before the oxidation step the Si/Al ratio in the r3xr3 R30 Al-Si(111) is most likely 2:1, after oxidation it is smaller, because of migration of aluminum atoms from the near surface region to the surface. The resulting layer is most likely amorphous, and can be produced by oxidation using oxygen or water vapor. The oxidation of higher coverage Al/Si(111) results in the formation of larger AlO_x islands.

To test if this silica-alumina layer had acid catalytic properties we carried out a series of typical acid catalyzed reactions described in Chapter 3.1.3.

3.1.2 Preparation in Aqueous Media:

$Si(111) + Al_{(s)} + NaOH_{(aq)} \longrightarrow Al_xSi_yO_z/Si(111)$

Practical acid catalysts are precipitated or crystallized from highly basic aqueous solutions [16,17]. The role of the cation in the solution is essential in directing the structure of the forming crystalline alumino silicate. Common cations used are sodium, potassium and alkyl ammonium (e.g. tetrabuthyl ammonium) ions. The next step in the preparation is the exchange of these ions with ammonium ions.

The ammonium salts are not stable at high temperatures, and decompose leaving behind highly acidic OH groups.

Our attempts at producing thin layers of crystalline alumino silicates have also failed on substrates such as gold foil, silicon or mica. We have developed, however, a simple method to deposit amorphous silica-alumina thin films on silicon single crystals in aqueous media.

This method utilizes the amphoteric nature of silicon and aluminum. It is known from elementary inorganic chemistry that both silicon and aluminum dissolve in basic solutions and produce hydrogen gas. This caustic etching process has been extensively used and studied in the microelectronics industry, especially for silicon.

Silicon, having the higher electronegativity, dissolves less readily than aluminum. Palik and co-workers [18] studied the species formed in the etching process. Using Raman spectroscopy they determined that the species present in the solution is exclusively $SiO_2(OH)_2^{2-}$. The reaction equation is likely the following [19]:

$$Si_{(s)} + 2OH^-_{(aq)} + 2H_2O_{(l)} \rightarrow SiO_2(OH)_2^{2-}{}_{(aq)} + 2H_{2(g)} \quad (1)$$

The chemistry of silicate ions in aqueous solutions has been thoroughly investigated, because it plays an important role in synthesis of crystalline alumino silicates, zeolites. ^{29}Si NMR studies revealed that depending upon the Na/Si ratio of the solution dimers, trimers, and oligomers of linear and cyclic geometry can be present. In dilute solutions (Na/Si ratio of about 40) only the monomer species can be detected. At higher silica concentrations (Na/Si ratio of 15-20) dimers and cyclic trimers appear [20].

The rate of caustic etching of silicon depends on the orientation of the single crystal, the OH^- concentration, and temperature. In concentrated solutions (8 M) the rate depends on the H_2O concentration [21]:

$$r = k[H_2O]^4[OH^-]^{1/4}$$

In low concentration solutions, the rate, in general, can be expressed as

$$r_{Si} = k_{Si} A_{Si} [OH^-]^a \qquad (2)$$

where A_{Si} is the surface area of the clean silicon exposed to the basic solution.

As the reaction proceeds, the solution slowly becomes saturated in silicate ions and another reaction, analogous to the dimerization, can take place on a substrate having OH groups:

$$SiO_2(OH)_2^{2-}{}_{(aq)} + 2\text{-}OH_{(s)} \leftrightarrow O_2SiO_2^{2-}{}_{(s)} + 2H_2O_{(l)} \qquad (3a)$$

$$SiO_2(OH)_2^{2-}{}_{(aq)} + 2\text{-}O^-{}_{(s)} \leftrightarrow O_2SiO_2^{2-}{}_{(s)} + 2OH^-{}_{(aq)} \qquad (3b)$$

(3b) regenerates the OH^- ions, and the whole process can be viewed as oh catalyzed oxidation of silicon. The rate of formation of the silica deposits on a surface can be described by

$$r_{SiOx} = k_1 A_{OH} [SiO_2(OH)_2^{2-}] - k_2 A_{OH} [OH^-]^c \qquad (4)$$

where k_1 and k_2 are the rate constants in reaction *(3)* from left to right and right to left, respectively, A_{OH} is the surface area covered with OH groups, and c is the order of reaction with respect to OH^- concentration.

The chemical reaction on aluminum single crystals has not been studied. Similarly to the silicate ions, aluminate ions can also form oligomers. The degree of polymerization is pH dependent. Infrared, Raman and ^{27}Al NMR studies [22] indicated that at pH < 13 $Al(OH)_4^-$ ions are present, and only concentrations above 1.5 M can a dimer exist.

Analogously to equations and reactions *(1-4)*, we can express the rate of formation of alumina like deposits. First of all, the formation of aluminate ions can be written as

$$Al_{(s)} + OH^-{}_{(aq)} + 3H_2O_{(l)} \rightarrow Al(OH)_4^-{}_{(aq)} + 1.5H_{2(g)} \qquad t(5)$$

and the rate expression

$$r_{Al}=k_{Al}A_{Al}[OH^-]^d \qquad (6)$$

For the deposition (or precipitation) process:

$$Al(OH)_4^-{}_{(aq)} + -OH^-{}_{(s)} \leftrightarrow OAl(OH)_3^-{}_{(s)} + H_2O_{(l)} \qquad (7a)$$

$$Al(OH)_4^-{}_{(aq)} + 2\text{-}OH^-{}_{(s)} \leftrightarrow O_2Al(OH)_2^-{}_{(s)} + 2H_2O_{(l)} \qquad (7b)$$

$$Al(OH)_4^-{}_{(aq)} + 3\text{-}OH^-{}_{(s)} \leftrightarrow O_3Al(OH)^-{}_{(s)} + 3H_2O_{(l)} \qquad (7c)$$

e.g. $$Al(OH)_4^-{}_{(aq)} + 2\text{-}O^-{}_{(s)} \leftrightarrow O_2Al(OH)_2^-{}_{(s)} + 2OH^-{}_{(aq)} \qquad (7d)$$

and

$$r_{AlOy}= k_3A_{OH}[Al(OH)_4^-] - k_4A_{OH}[OH^-]^e. \qquad (8)$$

where k_2 and k_3 are the rate constants in reaction *(7a)* from left to right and right to left, respectively and A_{OH} is the surface area covered with OH groups.

If both silicon and aluminum are present in a basic solution, all of the above processes will take place simultaneously. The deposition of alumina and silica can take place on walls of the reactor vessel and on the surfaces of the silicon and aluminum as well. Depending on pH, surface area of exposed elemental silicon and aluminum, volume of the solution, reaction time and temperature one can envision a process that deposits a mixture of silica and alumina on the surface of the silica covered silicon single crystal. For example:

$$Al(OH)_4^-{}_{(aq)} + \{(OH)_2SiO_2\}/Si(111) \leftrightarrow \{O_2SiO_2Al(OH)_2\}^-/Si(111) + 2H_2O_{(l)}$$
$$Al(OH)_4^-{}_{(aq)} + \{O_2SiO_2\}^{2-}/Si(111) \leftrightarrow \{O_2SiO_2Al(OH)_2\}^-/Si(111) + 2OH^-{}_{(aq)}$$

Since no data is available on the kinetic parameters for the reaction system described above, we carried out an exploratory study to find a set of conditions that produce thin (< 100 Å) silica-alumina layers on Si(111).

3.1.2.1 Experimental

The simple experimental setup for the preparation of thin silica-alumina films on Si(111) is shown in Fig. 3.8. Commercial Si(111) wafer was cut to 0.8x1.2 cm rectangular pieces. The deposition procedure involves many parameters: pH, volume of solution (V), surface area of both aluminum and silicon (A_{Al} and A_{Si}), temperature (T) and deposition time (t). The ranges we varied these parameters are the following: $11 < pH < 14$, $5\ ml < V < 25\ ml$, $2\ cm^2 < A_{Al} < 6\ cm^2$, $298\ K < T < 360\ K$, deposition time $0.5\ h < t < 22\ h$. After finding promising values for the volume of the liquid phase (20 ml), temperature (298 K), the surface area of the aluminum, we kept those constant and varied only the remaining parameters. The Si (111) sample and the aluminum wire (0.2 cm diameter, 10 cm long) were hung from a 0.025cm diameter gold wire. The NaOH solutions used varied in concentration between 0.05 M and 1 M.

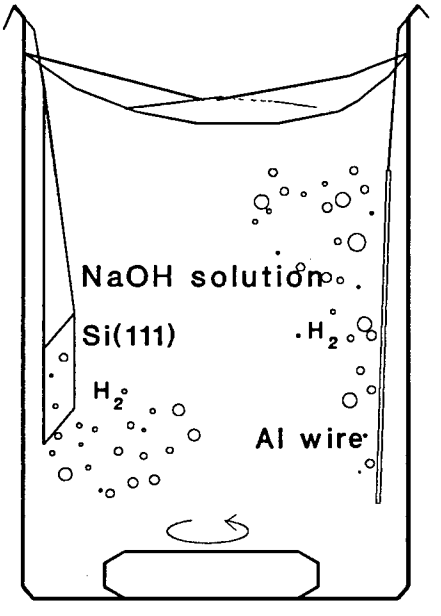

Fig. 3.8

The deposition was carried out for 0.5-22 hours at room temperature. After a certain amount of time, the Si(111) samples were removed from the solution, washed with deionized water and dried at room temperature. The surface was analyzed by XPS, SEM and SAM. During XPS analysis charging can develop on the sample surfaces since the oxide layers are insulators. This charging causes the spectrum to shift to higher binding energies, making the determination of the absolute binding energies difficult. In this study we used carbon 1s referencing (see ref. 49 in Chapter 1.); the binding energy of the adventitious carbon 1s line was fixed

at 284.6 eV. Depending on the thickness of the layers, charging of 0.2-2 eV was observed.

Samples that did not have macroscopic (> 1 micrometer) depositions of alumina, underwent a Na^+ > NH_4^+ ion exchange. The wafer was placed in a 10 ml solution of 6N ammonium hydroxide solution heated to 330 K for 5-10 minutes.

We also developed a modified method. According to this procedure the aluminum and the silicon was placed in a basic colloidal silica solution. The dissolution of silica in a basic solution can be described by the following equation [23] :

$$SiO_{2(s)} + 2OH^-_{(aq)} \rightarrow SiO_2(OH)_2^{2-}{}_{(aq)} \qquad (9)$$

This reaction produces the same ion as the dissolution of silicon and it is the same as *(3b)* right to left. The etching rate of silica is a linear function of the OH^- concentration [23].

The modified method is as follows. First, a colloidal solution was prepared by adding 300 mg Cab-O-Sil (colloidal amorphous silica, Cab-O-Sil L-90, Cabot, Co) to 100 ml 0.1 M NaOH solution. Approximately 10 hours later, 80 mg NaOH was dissolved in 15 ml of this solution, and then the Si wafer and the Al wire was placed into the beaker.

After preparation of the thin film the sodium ions were exchanged with ammonium ions. Ten milliliter of 6N ammonium nitrate solution was heated to 330 K in a beaker and the silicon wafer with the thin silica alumina layer was added. After 5-10 minutes the samples were removed and washed with 330 K deionized water three times.

The samples were dried in air and introduced in the ESCA system. The ammonium salt of the surface acid was thermally decomposed under vacuum (20 mtorr) in a small glass tube heated to 660 K.

3.1.2.2 Results and Discussion

First we summarize the qualitative findings of our preliminary studies.

A. If the concentration of the sodium hydroxide solutions was larger than 1 M only etching could be observed, and no deposition took place.

B. If the initial OH concentration was < 0.2-0.3 M, initially no significant deposition took place, but later (> 4 hours) macroscopic amounts of white precipitate formed on the surface. This white precipitate was exclusively alumina, determined by XPS.

C. Above room temperatures the etching process was more dominant than the deposition.

D. If several pieces of silicon were placed in the same solution, after 2-3 hours, the H_2 evolution on the aluminum stopped. XPS results indicated the aluminum surface was covered with a silica layer.

Based on these observations and the chemical reactions presented earlier we developed a kinetic model (shown in Fig. 3.9) that would qualitatively describe this complex reaction system.

According to this scheme, a high OH^- concentration (>1M, see **A.** above) results in high etching rates (*I* and *IV*), and because of the second terms in *II, III, V* and *VI*, the deposition of SiO_x and AlO_y is very slow. The rates are also determined by the ratio of surface areas (**D**). A large Si/Al surface area ratio at medium OH concentrations can result in high silicate ion concentrations in the solution (*I*), and, thus, a high deposition rate on the aluminum (*V*) can be expected.

We are not aware of any kinetic data published in the literature for this system. It was not our intention at this stage to determine the kinetic parameters, but we would like to point out two qualitative relationships between various constants in this scheme.

- Literature data showed [21] that the etching rate of SiO_2 is a linear function of KOH concentration, therefore under our conditions, exponents b and e in *II* and *V*,

$$\frac{d[SiO_2(OH)_2^{2-}]}{dt} = k_{Si}[OH^-]^a(1 - \Theta_{Si}^{SiOx} - \Theta_{Si}^{AlOy})A_{Si} \qquad (I)$$

$$\frac{d\Theta_{Si}^{SiOx}}{dt} = \overrightarrow{k_{Si}^{SiOx}}[SiO_2(OH)_2^{2-}] - \overleftarrow{k_{Si}^{SiOx}}\Theta_{Si}^{SiOx}[OH^-]^b \qquad (II)$$

$$\frac{d\Theta_{Si}^{AlOy}}{dt} = \overrightarrow{k_{Si}^{AlOy}}[Al(OH)_4^-] - \overleftarrow{k_{Si}^{AlOy}}\Theta_{Si}^{AlOy}[OH^-]^c \qquad (III)$$

$$\frac{d[Al(OH)_4^-]}{dt} = k_{Al}[OH^-]^d(1 - \Theta_{Al}^{SiOx} - \Theta_{Al}^{AlOy})A_{Al} \qquad (IV)$$

$$\frac{d\Theta_{Al}^{SiOx}}{dt} = \overrightarrow{k_{Al}^{SiOx}}[SiO_2(OH)_2^{2-}] - \overleftarrow{k_{Al}^{SiOx}}\Theta_{Si}^{SiOx}[OH^-]^e \qquad (V)$$

$$\frac{d\Theta_{Al}^{AlOy}}{dt} = \overrightarrow{k_{Al}^{AlOy}}[Al(OH)_4^-] - \overleftarrow{k_{Al}^{AlOy}}\Theta_{Si}^{AlOy}[OH^-]^f \qquad (VI)$$

$$[OH^-]_0 = [OH^-] + [Al(OH)_4^-] + [SiO_2(OH)_2^{2-}] \qquad (VII)$$

[ ] concentrations

Θ_{Si}^{SiOx} Θ_{Si}^{AlOy} SiOx and AlOy coverages on Si

Θ_{Al}^{SiOx} Θ_{Al}^{AlOy} SiOx and AlOy coverages on Al

A_{Al} and A_{Si} surface areas

Fig. 3.9 Kinetic equations to describe the rate of chemical reactions taking place when a silicon single crystal and a piece of aluminum is immersed in sodium hydroxide solution. See corresponding chemical reactions in text: *(I)* - *(1)*, *(II)* and *(V)* - *(3)*, *(III)* and *(VI)* - *7* and *(IV)* - *5*.

respectively, are likely to be unity.

- From the work of Seidel *at al.* [21] we estimate that the k_{Si}^{Siox}/k_{Si} ratio can be as low as 10^{-2} - 10^{-3}.

Now we turn our attention to the deposited films. In Fig. 3.10, a series of characteristic XPS spectra obtained in this study are shown. The major disadvantage of this deposition method is immediately clear from the survey spectrum in Fig. 3.10 a). Since the deposition takes place outside a clean UHV

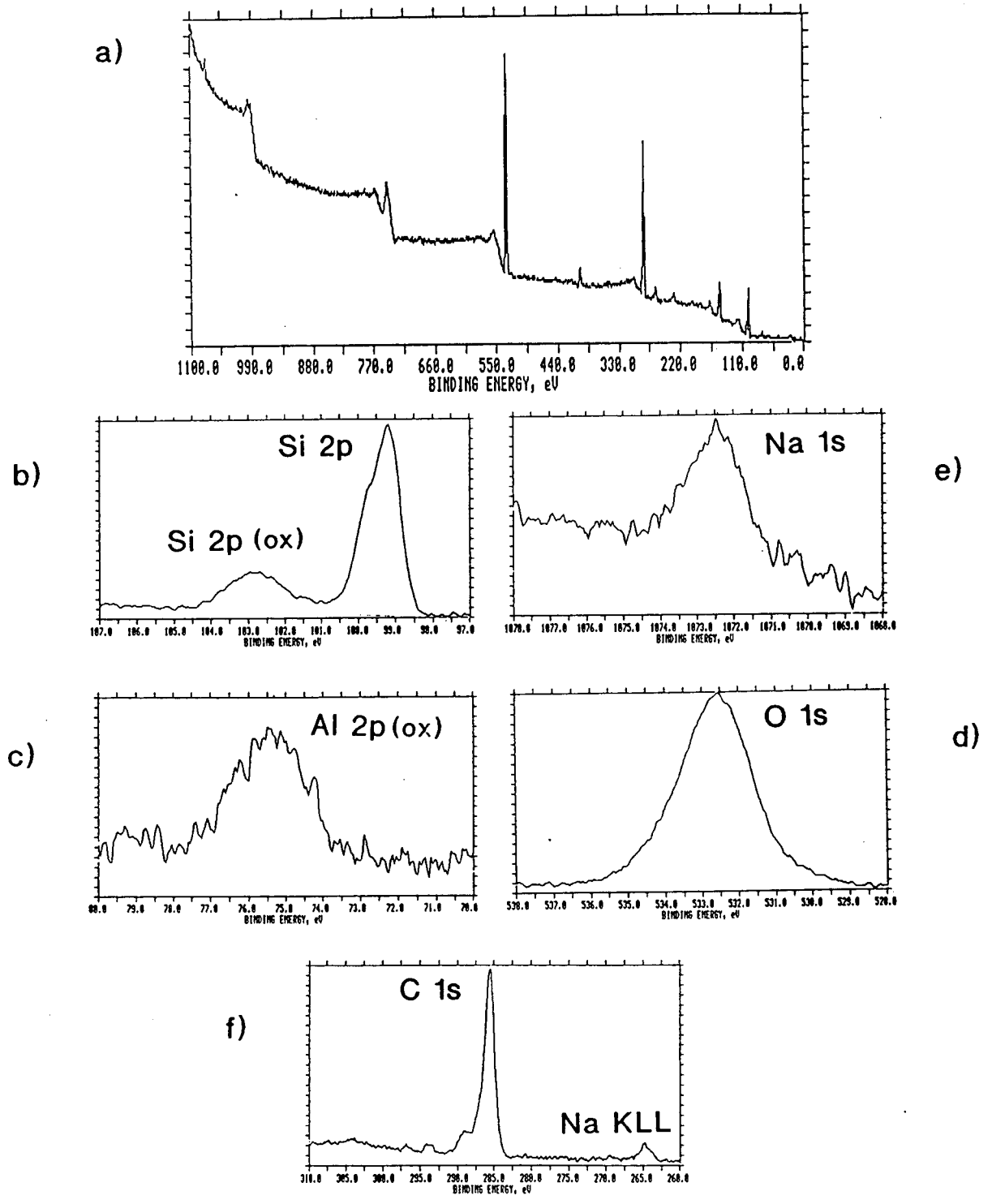

Fig. 3.10 XPS spectra obtained from a thin film deposited in 0.5 M NaOH solution at room temperature. The deposition time was 5 hours. a) survey spectrum, b) the silicon 2p, c) aluminum 2p, d) oxygen 1s, e) sodium 1s, and f) carbon 1s lines and sodium KLL Auger transition. The spectra are not charge corrected.

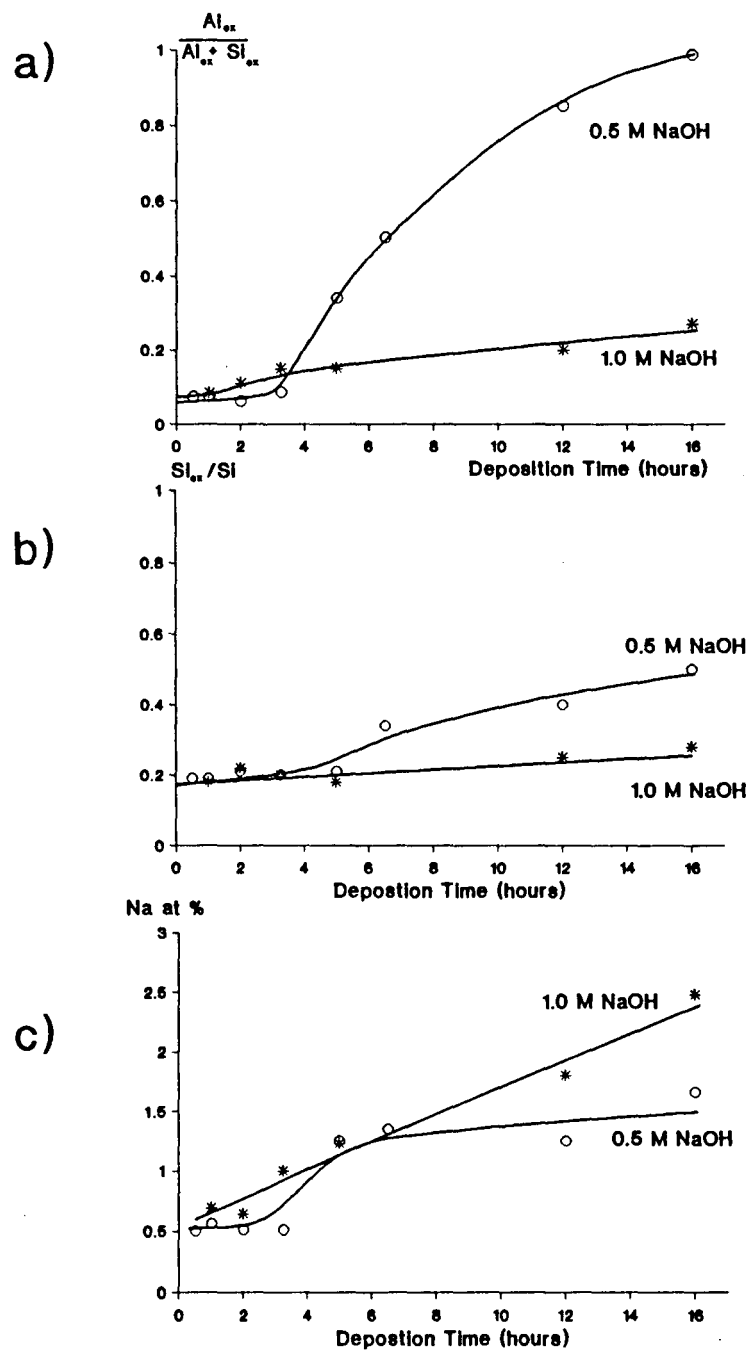

Fig. 3.11 a) The $Al_{ox}/(Al_{ox}+Si_{ox})$, b) Si_{ox}/Si ratios and c) the concentration of sodium ions in the surface layers as a function of deposition time for two sets of experiments using 0.5 and 1.M NaOH solutions.

environment, the surface contains not only Si, Al, O and Na as it would be desirable, but contaminants such as carbon and occasionally nitrogen as well. The carbon contamination can be, at least partially, removed in ultra-high vacuum by heating the sample to 770 K in the presence of $5x10^{-8}$ torr of water or oxygen. During this treatment, however, further oxidation of the silicon substrate takes place.

Using atomic sensitivity factors the concentrations of the elements in the surface layer can be calculated. In Fig. 3.11, the concentrations and atomic ratios for two sets of experiments (for 0.5 M and 1.0 M NaOH solutions) are plotted as a function of time. In both cases, there is an induction period with no deposition.

Initially, when the more dilute NaOH solution is used, hydrogen evolution can be observed on both silicon and aluminum. As the deposition of alumina starts, however, the evolution of hydrogen on the Si(111) surface diminishes, while on the aluminum it continues vigorously. During the induction period the concentration of both silicate and aluminate ions increases, and when a saturation concentration is reached the deposition starts. The length of this induction period depends on the OH^- concentration, temperature and the volume of the liquid phase. For example, if 10 ml aqueous solution was used, instead of the usual 20 ml, the length of the induction period decreased to 0.3-1 hour. We find that the deposition rate of aluminum is higher in a more dilute solution and the formation of the silicon oxide layer is slower at higher OH^- concentration (Fig. 3.11b).

It is interesting that the sodium concentration of the surface layers increases steadily when the deposition is very slow and the alumina content of the film is low (Fig. 3.11c). Once the deposition of the alumina started the surface sodium content does not change significantly in the more dilute solution. In the 1 M solution the sodium ion concentration steadily increases.

We would like to form a homogeneous well mixed silica-alumina layer on our silicon substrate. At the initial stages of deposition the solution is clear and the surface of the Si(111) sample is shiny. Later the surface becomes first uniformly hazy, but in the final stages (>5-10 hours), macroscopic deposits start to develop.

Scanning electron microscopy (SEM) and scanning Auger microscopy (SAM) of these thick layers revealed that these macroscopic deposits consist of oxidized aluminum, oxygen and sodium and no silicon is present. Between the deposits only silica covered silicon could be observed. Thus it seems that in order to obtain thin homogeneous films long deposition times should be avoided.

Using XPS, one can obtain information on the chemical environment of the elements on the surface. In Fig. 3.12, the charge corrected binding energies of the O 1s, Si 2p, Al 2p and Na 1s electrons are shown. In the figure we also indicate the binding energies for the same core electrons in relevant compounds (see reference [49] in Chapter 1). Since the reported values of binding energies scatter considerably, it is impossible to unequivocally assign a peak positions to one compound.

The oxygen 1s and silicon 2p binding energies indicate that the oxidized silicon formed is not quartz, but more closely related to alumino silicates. However, since XPS is not directly structure sensitive, by no means do we imply that any structural similarity exists between our films and crystalline alumino silicates. Based on these XPS results we can only say that there is an interaction between the silica and alumina species. The Na 1s binding energies shift with increasing oxide coverage, and converge to values characteristic for sodium silicates. The binding energy of the Al 2p electrons does not vary significantly in Al-O(-Si) compounds (ref. [49] in Chapter 1). With increasing film thickness the values are approaching the values reported for aluminum oxides. In agreement with this, SEM and SAM studies of these films revealed the formation of alumina islands after long depositions (> 6 hours).

The disadvantage of this method is that the only source of silicate ions is the silicon surface itself onto which we wish to deposit the layer. Thus, with increasing silica-alumina coverage, the silicate/aluminate ion ratio decreases in the solution, and as a result, the silica/alumina ratio on the surface also decreases. This change in composition with time translates into change in composition perpendicular to the surface.

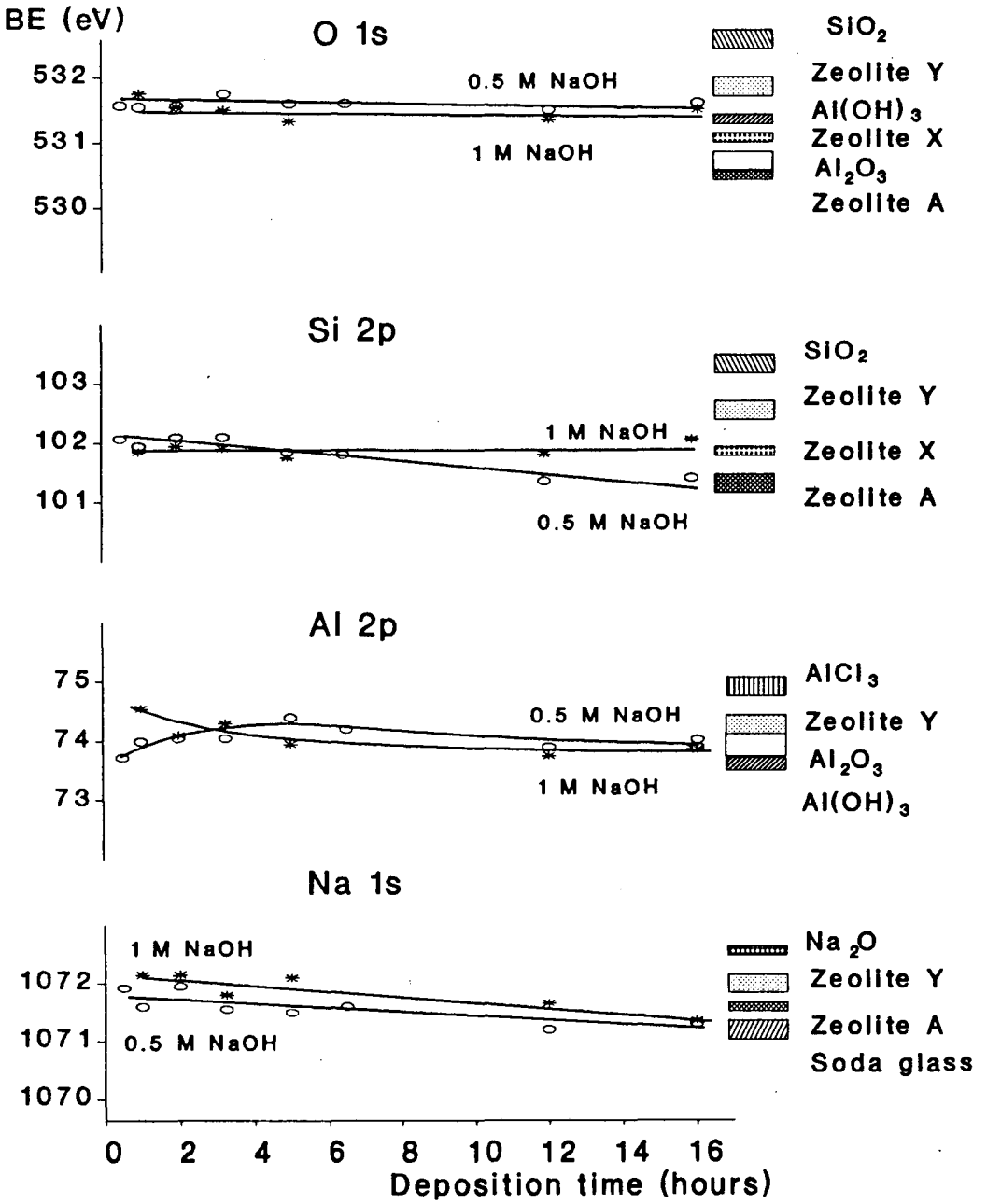

Fig. 3.12 Charge corrected binding energies for the O 1s, Si 2p, Al 2p and Na 1s lines, obtained from thin films prepared using 0.5 M and 1.0 M NaOH solutions. The literature values for the Si, O, Al and Na containing solids are also given, as reported by Wagner *at al.* and Barr *at al.* [49a and 49b in Chapter 1.]

In order to deposit silica alumina layers with a constant Si/A ratio, the deposition method has to be modified such that a silicate source is also present in the solution. According to our modified method a basic colloidal silica solution was used instead of the sodium hydroxide solution. The driving force of this deposition process is the irreversible dissolution of aluminum. As the aluminate ions reach saturation concentration in the solution which already contains silicate ions the alumina starts to precipitate along with some silica. The presence of solid SiO_2 ensures that silicate ion concentration is maintained, provided that dissolution of silica can keep up with the disappearance of silicate ions due to the precipitation. In Table I. we report the binding energies and the composition of silica-alumina layers prepared according to this modified method.

After 12 hours of deposition the sample was still shiny, even though in the solution a large amount of white precipitate has formed. After 21 hours the surface became hazy and macroscopic features, similar to the ones observed for the previous (without colloid) samples, could be detected by SEM.

Table I.

Time (h)	SiO_y/Si	Al/(Al+Si)[a)]	Na at%	Si 2p (eV)	Al 2p (eV)	O 1s (eV)	Na 1s (eV)
5.8	4.8	0.63	1.5	101.5	73.9	531.4	1071.4
12.0	4.4	0.52	0.6	101.9	73.9	531.6	1071.4
21.0	4.2	0.54	0.1	101.9	74.1	531.8	1071.8

a) Oxidized aluminum and silicon only: $AlO_x/(AlO_x+SiO_x)$.
Deposition was carried out according to the following recipe:
Ten hours before deposition a colloid solution was prepared by adding 300 mg Cab-O-Sil (amorphous silica) to 100 ml 0.1 M NaOH solution. Then 80 mg NaOH was dissolved in 15 ml of this solution, and the Si wafer and the Al wire was placed into the beaker.

An SEM image obtained from a sample after 21 hours of deposition, and the corresponding AES spectra from three characteristic area are shown in Figs. 3.13

Fig. 3.13 SEM image of a thin layer on silicon (111). After 21 hours of deposition according to the modified method described in the Experimental section. The scale in the bottom right corner corresponds to 10 micrometer. Auger spectra from areas 1, 2 and 3 were taken and are shown in Fig. 3.14.

and 3.14, respectively. It is clear that the cracked island deposit is aluminum oxide covering a mixture of oxidized aluminum and silicon. Note that sodium is present on the flat region only where both alumina and silica are present.

To characterize how homogeneous the film is perpendicular to the surface we performed a depth profile analysis of the flat area away from deposits. The results are shown in Fig. 3.15. As expected from our model, the surface is richer in sodium compared to deeper layers. The sodium ions are compensating the negative charge due to silicate ions attached to the surface. The reaction of these ions with aluminate ions arriving from the solution produces the silica-alumina layer and regenerates the OH^- ions (eq. 7d). The Al_{Ox}/Si_{Ox} ratio is somewhat larger in the near surface region than in deeper layers which implies that the AlO_x deposition rate is smaller at the early stages of the deposition when the aluminate ion concentration is low. Perhaps a more uniform Al/Si ratio could have been achieved

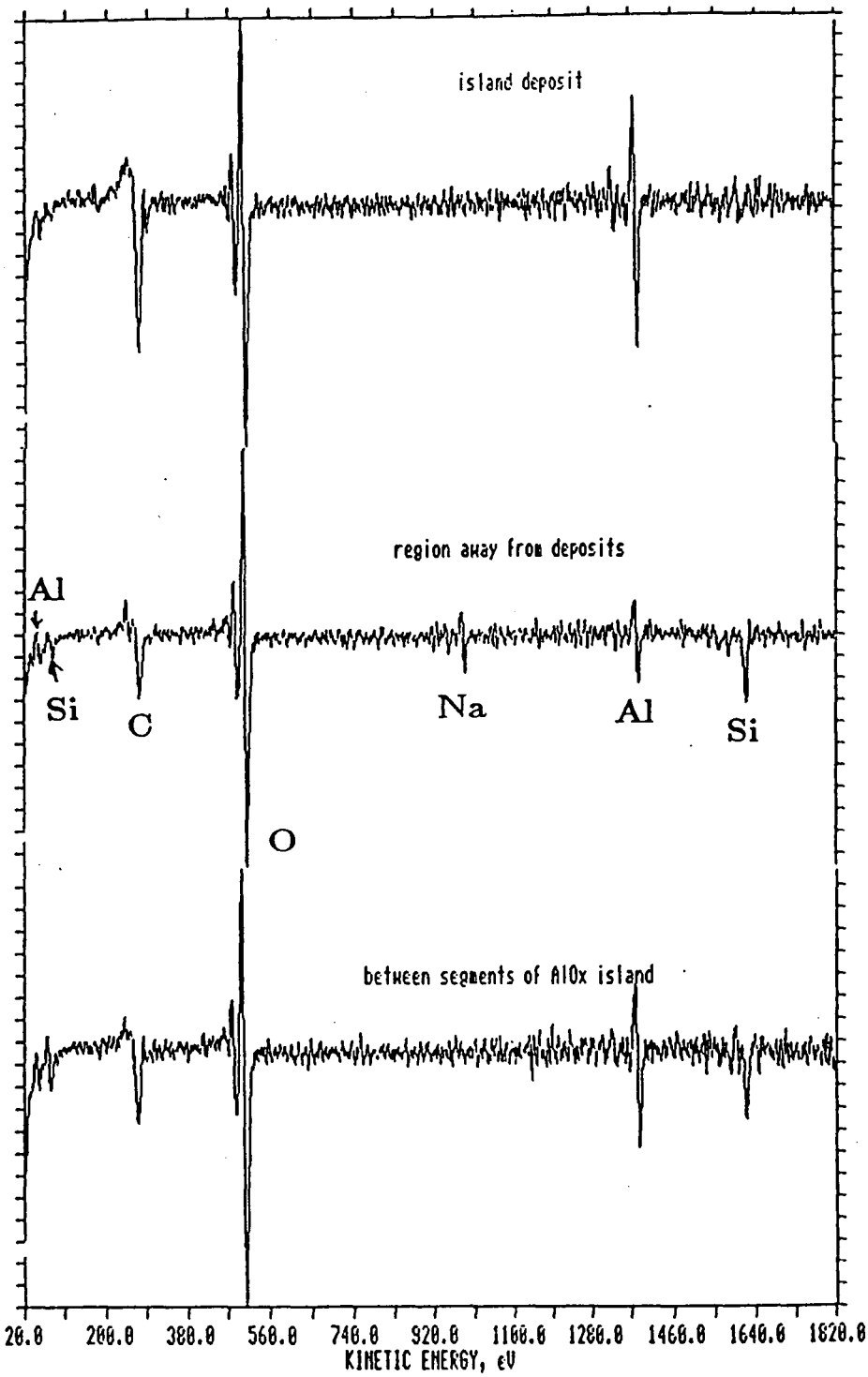

Fig.3.14 Auger spectra obtained from areas 1, 2 and 3 in Fig. 3.13.

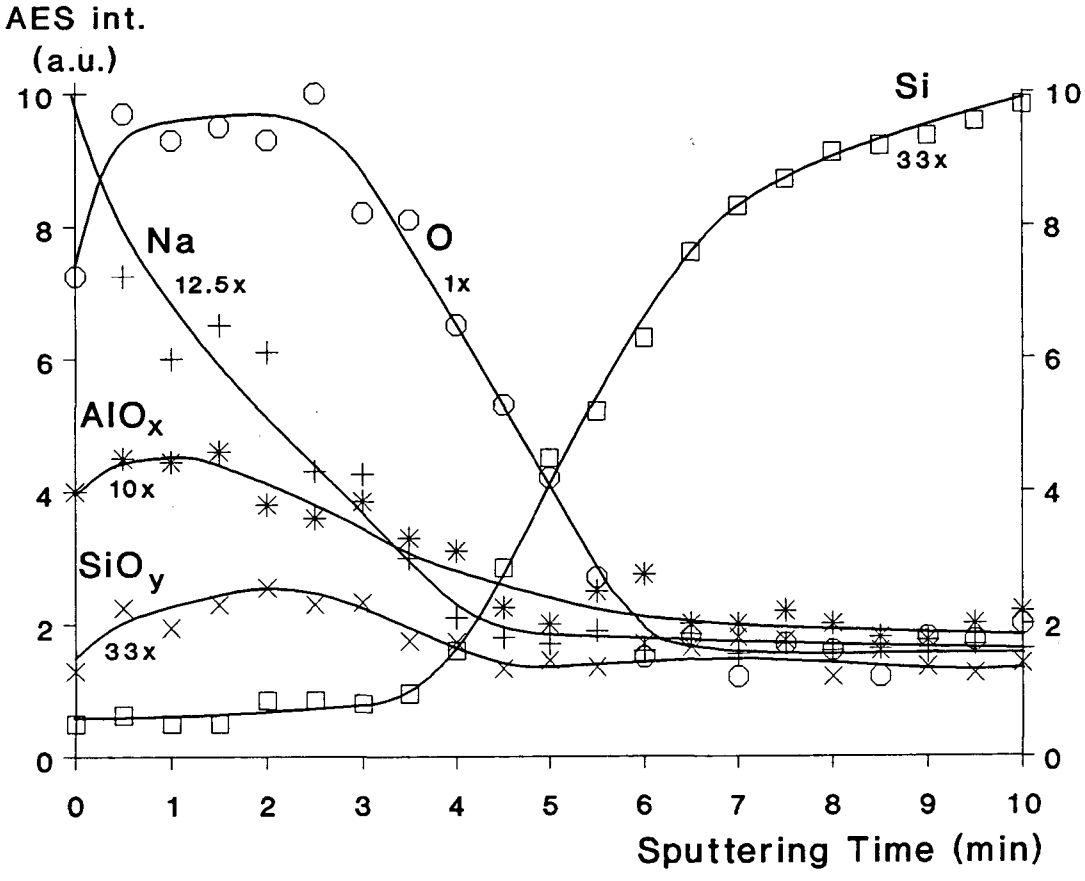

Fig. 3.15 The intensity of the O (512 eV), Al (1396 eV), Si (92 eV) and SiO_y (80 eV) peaks was determined after repeated argon ion bombardment of a 1x1 mm selected area away from deposits (see Fig. 3.13). The beam energy was 0.5 kV and the pressure was 14 mPa (PHI 660), measured in the differentially pumped raster ion gun.

if the Si wafer had been placed in the solution after the solution became saturated with aluminate ions.

Using this modified method, after one to three hours of deposition we could prepare homogeneous films; using SEM we were unable to detect any features up to 4,000x magnification. The Auger spectra indicated that the surface composition was homogeneous across the sample and similar to the flat region shown in Fig. 3.13; silicon, aluminum, oxygen and sodium were all present. From the fact that the

substrate silicon is still detectable by both AES and XPS we estimate that the thickness of these layers is <30 Å.

The surface sodium ions can be exchanged with ammonium ions. Fig. 3.16 shows that the exchange is complete 5-10 minutes at 330 K using a 6 N ammonium

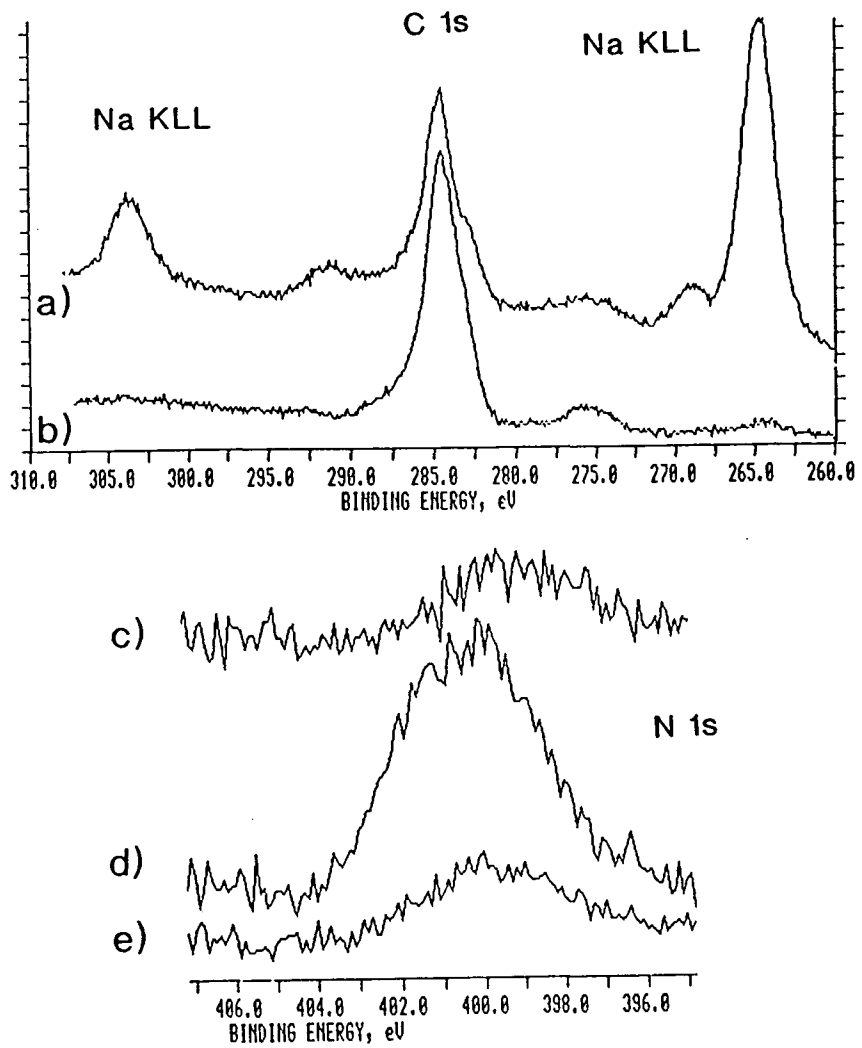

Fig. 3.16 Sodium KLL Auger lines before (a) and after (b) Na^+ > NH_4^+ ion exchange and the nitrogen 1s region before ion exchange (c), after ion exchange (d) and after thermal decomposition at 660 K (e).

nitrate solution. Nitrogen in ammonium and nitrate ions can be readily distinguished based on their chemical shifts. The presence of a single peak characteristic of ammonium salts indicates that exchange has been successful. The ammonium salt can be easily decomposed at 620 K as demonstrated by Fig. 3.16d and 3.16e.

Using this modified method we have been able to produce a homogeneous mixture of silica and alumina on silicon (111) single crystal surfaces. The thickness of these layers, estimated from the electron mean free path of the Si 2p electrons, is less than 30 Å. After characterization the samples were transferred to the apparatus described in Chapter 2.1 to study the catalytic properties. In the following chapter we will summarize these results.

3.1.3 Reactivity of Model $Al_xSi_yO_z$/Si(111) Catalysts

In the Introduction we mentioned the problems associated with the low concentration of active sites on heterogeneous acid catalysts. We have to choose the model acid catalytic reaction very carefully, because we want to probe only the acidic surfaces and want to minimize the background reactions taking place on the reactor walls and on the manipulator.

In Table III. of Chapter 1.3.1 we listed a few typical acid catalyzed reactions. Now we briefly evaluate those reactions as potential probes for acidic sites on our model catalysts. Reactions that can be carried out at lower temperatures, such as double bond shifts or isomerizations of olefins (ref. [20] in Chapter 1) would be preferable because the reactor walls and the manipulator can be colder. The disadvantage is that these reactions are not very specific to acid catalysis, and can take place readily on metals too.

The dehydration of alcohols (ref. [21] in Chapter 1) looked promising at first, but there are three reasons why we eventually abandoned this reaction: 1) it can take place thermally on almost any surface or in the vapor phase at sufficiently high

temperatures, 2) because of the batch type reactor, water accumulates in the system causing unpredictable results by adsorbing or readsorbing on walls and on the catalyst itself, and finally 3) both reactants and products have very high sticking probabilities on metals which makes the handling of these vapors impractical in UHV.

The cracking of alkyl aromatics (ref. [23] in Chapter 1) requires stronger acid sites and higher reactions temperatures than the previous reactions. Cumene (*i*-propyl benzene) cracking has been the most studied reaction:

$$C_6H_5\text{-}C_3H_7 \longrightarrow C_6H_6 + C_3H_6 \qquad (10)$$

i-propyl benzene $\longrightarrow$ benzene + propylene

Corma and Wojciechowski (ref. [23a] in Chapter 1) pointed out that in addition to this main reaction other primary and secondary reactions can take place on acidic oxides. Monomolecular side reactions can produce *n*-propyl benzene and ethyl toluene, while the reaction of two cumene molecules can result in butenes, ethyl benzene, cymene, diisopropyl benzene and benzene. On highly acidic Y zeolites, the selectivity toward the main reaction *(10)* increases with increasing temperature and it reaches 94 % at 820 K. At lower temperatures (630 K), however, the initial selectivity for diisopropyl benzenes can be as high as 19 %.

An important aspect of the reaction is that the catalysts poison rather quickly. Thus, in kinetic models describing the reaction, this poisoning always has to be included unless initial rates and product distributions are studied. The poisoning is due to the deposition of coke which blocks active sites (ref. [23a]. in Chapter 1). In the case of porous materials, the kinetic model also has to include terms to describe the diffusion of reactants and products in the pores.

If non porous model silica-alumina layers, such as the ones described in the previous chapters, could be used as model catalysts the kinetic model could be greatly simplified.

3.1.3.1 Experimental

After preparation in aqueous solution the surface sodium ions were exchanged with ammonium ions and the sample was mounted on the manipulator as shown in Fig. 3.1. After pumping down, and baking out the system, the surface of catalyst had a substantial amount of carbon. To remove this carbon and to decompose the ammonium salts the sample was exposed to 50 L O_2 or H_2O (both were effective) at 570-620 K. Auger electron spectroscopy confirmed the removal of carbon.

The oxidation of the r3xr3 R30 Al-Si(111) followed by annealing in UHV produced a clean mixture of silicon oxide and aluminum oxide, thus further cleaning was not necessary.

In preliminary catalytic studies we tried several reactions listed in Table III. of Chapter 1.3.1. The general procedure is given in Chapter 2.1. No significant difference in the reaction rates between the model catalysts and the background was found for the 1-butene double bond shift reaction, the dehydration of *i*-propanol and the dehydration of methanol at 373, 420 and 470 K. (Blank reactions were carried out on gold foil without silicon wafers). Very low activity could be detected in 1-hexene and 2-methyl-pentane isomerization and again, the rates and product distributions were within experimental error for the model catalysts and blank runs.

Cumene cracking was performed at 570-670 K on both catalytic systems, prepared in UHV and in aqueous media. The sample prepared in UHV by the oxidation of r3xr3 R30 Al/Si(111) had very low activity. The aqueous method appeared to produce a slightly more active material, but background activity (gold foil without the silicon sample) was close to the activity of the thin layer. To find out if this low activity on samples prepared in aqueous solution was due to the lack of sufficient number of sites we prepared samples of higher surface area according to the following procedure.

A 7.6 cm diameter Si(111) wafer was crushed in a porcelain mortar to increase the specific surface area. Using the BET method we determined that the

small particles had about 0.43 m^2 surface area per gram. Silica-alumina was deposited on these particles for one hour according to the modified method described in Chapter 3.1.2.1.. Along with the silicon particles we placed a 0.8x1.2x0.05 cm wafer in the solution and used this sample for surface characterization. After the deposition the silicon pieces were filtered washed, dried and underwent ion exchange.

The reactor loop shown in Fig. 2.2 was modified such that the high pressure cell was by-passed and a small horizontal section of the glass reactor loop was replaced with quartz section (reactor). The glass section with 0.85 g catalyst (silica-alumina on silicon particles) was heated using a nichrome wire from the outside. The temperature was measured by a chromel-alumel thermocouple taped to the reactor. First a 15 minute oxygen treatment at 570 K was used to remove carbon, then the reactor was heated to 650 K in vacuum to activate the catalyst. The reactor loop (ca. 100 ml) was then filled with 1 atm of dry nitrogen, and 0.2-1 microliter cumene was injected.

3.1.3.2 Results and Discussion

The product accumulation curves for cumene cracking is shown in Fig. 3.17 for a 1 cm^2 model catalyst prepared in aqueous solution (according to the modified method the deposition time was 3 hours, see Chapter 3.1.2.1 for details). The activity of the model catalyst is only about 50% higher than that of the blank. Although the rates have been reproducible within 15-20%, based on these results only, we hesitate to conclude that the silica-alumina layer is active in cumene cracking. Model catalysts prepared in UHV by the oxidation of r3xr3 R30 Al-Si(111) showed even lower activities.

In order to determine if the thin silica-alumina films area active we have to either decrease the background activity or increase the surface area of our samples. The background activity shown in Fig. 3.17 is the lowest we could achieve. We have

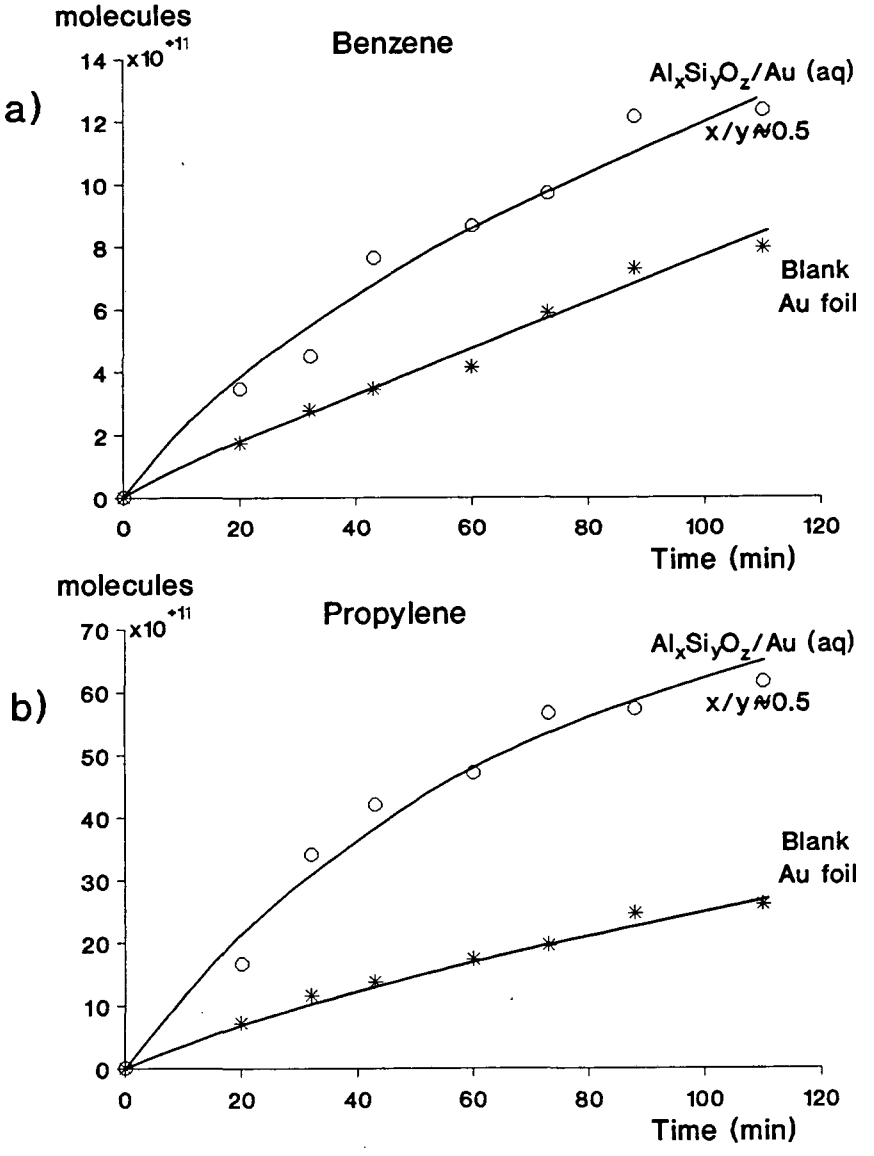

Fig. 3.17 Benzene (a) and propylene (b) accumulation curves for a 1 cm^2 surface area silica-alumina layer prepared on Si(111). Silica-alumina layer was deposited in aqueous media according to the modified method described in Chapter 3.1.2.1.

to increase the total activity by at least one order of magnitude, i.e. at least ten times higher surface area is needed.

Clearly, UHV preparations do not allow this. But as we described in the Experimental, we could prepare silica-alumina layers on higher specific surface area silicon particles. Table II. shows the reaction rates for this model catalyst prepared in aqueous NaOH solution according to the modified method. The surface area of the catalyst is 3500 cm^2. The background activity was two orders of magnitude lower than the reaction rates over the model catalyst.

Table II.

	$x10^6$ molec./cm^2/s	
	589 K	638 K
Benzene	1.3	5.4
Propylene	1.3	4.0

The activation energy calculated from these two points (21 kcal/mol)compares well with literature values of 20-25kcal/mol [23].

The thin silica-alumina film prepared in aqueous solution on silicon particles is active in cumene cracking, but its activity is much lower than anticipated from literature data on practical silica-alumina catalysts. Clearly activity of this magnitude cannot be measured in a standard UHV - high pressure cell apparatus developed for the study of single crystal metal catalysts.

References

1. Schlier, R. E. and Fransworth, H. E., *J.Chem. Phys.*, **30**, 917 (1959).
2. Takyanagi,K, Tanishiro, Y., Takahashi, S., and Takahashi, M., *Surf. Sci.*, **164**, 367-392 (1985).
3. Yang, W. S., Wu, S. C., and Jona, F, *Surf. Sci.*, **169**, 383-393 (1986).
4. Lander, J. J. and Morrison, J., *Surf. Sci.*, **2**, 553-565 (1964).
5. Huang, H., Tong, S. Y., Yang, W. S., Shih, H. D., Jona, F., *Phys. Rev. B.*, **47**,7483 (1990).
6. Northrop, J. E., *Phys. Rev. Lett.*, **53(7)**, 683-686 (1984).
7. a) Nishijima, M., Edamoto, K., Kubota, Y, Tanaka, S., and Onchi, M., *J. Chem. Phys.*, **84(11)**, 6458-6465 (1986).
   b) Lander, J. J. and Morrison, J., *J. Appl. Phys.*, **33**, 2089 (1962).
8. Hollinger, G., Morar, J. F., Himpsel, F. J., Hughes, G., and Jordan, J. L., *Surf. Sci.*, **168**, 609-616 (1986).
9. e.g. Krivanek, O. L. and Mazur, J. H., *Apll. Phys. Lett.*, **137(4)**, 392-394 (1980).
10. Renaud, G., Fuoss, P. H., Ourmazd, A., Bevk, J., Freer, B. S., Hahn, P. O., *Appl. Phys. Lett.*, **58(10)**, 1044-1046 (1991).
11. From Prof. Brian Bent, now at Columbia University, New York.
12. Argile, C., and Rhead, G. E., *Surf. Sci. Rep.*, **10**, 277-356 (1989).
13. Murray, J. L., and McAlister, A. J., *Bull. Alloy Phase Diagrams*, **5(1)**, 74-84 (1984).
14. a) Jepsen, D. W., Shih, H. D., Jona, F., and Marcus, P. M., *Phys. Rev. B*, **22(2)**, 814-824 (1980).
    b) Miller, D. J.and Haneman, D., *J. Vac. Sci. Technol.*, **16(5)**, 1270-1285 (1979).
15. Nilsen, B. P., Onuferko, J. H., and Gates, B. C., *Ind. Eng. Chem. Fundam.*, **25**,337-343 (1986).
16. Ryland, L. L. B., Tamele, M. W., and Wilson, J. N., "Cracking Catalysts," in

Catalysis, **7** (Emmett, P. H., Ed.), Reinhold, New York, 1960.

17. Breck, D. W., "Zeolite Molecular Sieves, Structure Chemistry and Use", Chapter 4, Wiley, New York, 1974.
18. Palik, E. D., Gray, H. F., and Klein, P. B., *J. Electrochem. Soc.*, **130**, 956 (1983).
19. Palik, E. D., Bermudez, V. M., and Glemboczki, O. J., *J. Electrochem. Soc.*, **132**, 871 (1985).
20. Engelhardt, G., Zeigan, D., Jancke, H., Hoebbel, D., and Wieker, W., *Anorg. Allg. Chem.*, **418**, 17 (1975).
21. Seidel, H., Csepregi, L., Heuberger, A., and Baumgartel, H., *J. Electrochemical. Soc.* **137(11)**, 3612-3626 (1990).
22. Moolenaar, R. J., Evans, J. C., and McKeever, L. D., *J. Phys. Chem.*, **74(20)**, 3629-3636 (1970).
23. Kern, W. and Puotinen, D. A., *RCA Rev.*, **31**, 187 (1970).

3.2 $Al_xSi_yO_z$/Au Preparation in UHV by Ar^+ ion Beam Deposition

Ion beam sputter deposition seemed to be an attractive method to prepare homogeneous mixtures of silica and alumina because secondary ion mass spectroscopy (SIMS) and fast atom bombardment mass spectroscopy (FABMS) results had indicated [1,2] that the major species sputtered off surfaces of silica and alumina, as well as from zeolites, are atomic Si, Al and O species. In the spectra, dimers like charged SiOSi, SiOAl and AlOAl are also present, but they are much less abundant. The mass distribution of the largest fraction of the sputtered species, i.e. the neutral ones, is not known.

In this chapter we report the deposition of thin, homogeneous silica-alumina films on polycrystalline gold foils using zeolite targets. After deposition the samples were characterized by X-ray Photoelectron Spectroscopy (XPS), Scanning Auger Electron Microscopy (SAM), Scanning Electron Microscopy (SEM), and X-ray Diffraction (XRD). The catalytic properties were tested in cumene cracking.

3.2.1 Experimental

A. Preparation of sputter deposited thin films on gold foil

We used two ultra-high vacuum deposition systems. 1) One to study the deposition process and the surface properties of the films, and 2) another more efficient one to prepare samples for the catalytic work.

1) The deposition was carried out in a sample preparation chamber attached to a commercial ESCA (Electron Spectroscopy for Chemical Analysis) system (Perkin-Elmer, PHI 5300). In the preparation chamber a 2 kV Ar^+-ion beam of about 0.8 cm^2 cross section bombarded a 1.8 cm diameter Y zeolite disc at about

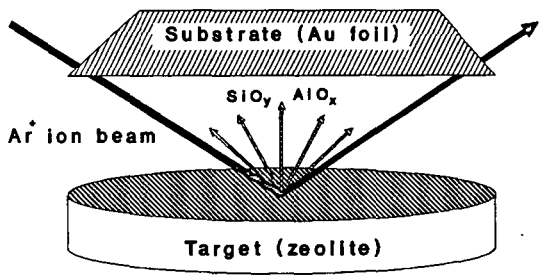

Fig. 3.18

50-60 degrees off from the surface normal (Fig 3.18). The room temperature polycrystalline gold substrate was positioned at 1-1.5 cm from the target in the direction of the surface normal. The ion gun (Varian 981-2043) was operated at 20 mA emission and at $1x10^{-4}$ torr argon pressure. After deposition, the specimen could be transferred to the XPS analyzing chamber without exposing it to the atmosphere. Utilizing a Mg source (15 kV, 300 W), survey spectra in the 0-1100 eV region and multiplex spectra for the Si 2p, Al 2p, Au 4f, O1s, O KVV and C 1s regions were recorded.

To determine the surface composition of zeolites used in this study, before mounting the target disc in the deposition chamber, we deposited some gold on it and introduced it in the ESCA analyzing chamber. Survey and multiplex spectra were taken with the same parameters as for the thin films.

In the case of the sputter deposited films we used Au 4f (83.8 eV) referencing to determine the absolute binding energies. (A small piece of gold foil was placed in the vicinity of the target zeolite so a small amount of gold always sputtered with the silica and alumina fragments.) For the 'bulk' zeolite samples, since adventitious carbon was always present, we could use both the C 1s (284.6 ev) and the Au 4f (83.8 ev) lines to correct for charging [1,7].

2) Samples for the catalytic studies were prepared in an ion beam micro sputterer system of Varian Group, Inc. (Model 705). To obtain homogeneous films and increase the deposition rate, the geometry of the micro sputterer was modified such that the substrate was parallel with the target and the distance between them was approximately 1 cm. The argon pressure was 3×10^{-4} Pa. The beam voltage and the emission current were 5 kV and 4 A, respectively.

Films were deposited on both sides of 1x1x0.0025 cm foils for 1-1 hour. To determine the deposition rate and to find out if the films show any sign of crystallinity, we carried out the deposition for 100 hours. The thickness of this film was estimated to be one micron using SEM. XRD results indicated that it was amorphous.

The target materials were HY zeolites: HY-82 (Si/Al=1.3) and HY-62 (Si/Al=2.1) from Union Carbide, dealuminated HY from Dow Chemicals, amorphous SiO_2 (Cab-O-Sil L-90, Cabot, Co) and amorphous Al_2O_3 (Aluminium Oxid C, Degussa), pressed into 1.8 cm diameter discs by a hydraulic press. The substrate was gold foil of 99.99% purity.

B. Catalytic studies

First, cumene cracking was carried out in the UHV - high prerssure reactor cell apparatus described in Chapter 2.1. Similarly to the films deposited in aqueous media, the activity of the thin layers of 1-2 cm^2 geometric surface area was very low and it was only slightly higher than that of the background. We increased the surface area to find out if the sputter deposited material is active at all.

Instead of one 1-2 cm^2 foil, in these studies, we used ten pieces prepared under the same deposition conditions. Cumene cracking on these foils was performed in a closed Pyrex grass system that could be pumped down to 10^{-8} torr using a diffusion pump prior to the catalytic runs. The samples were transferred from the micro sputterer through air and heated in air, then in vacuum at 723 K and $2x10^{-8}$ torr for 10 hours. After this pretreatment the reactor was filled with dry nitrogen (1 atm), the sample was heated to reaction temperature (570 K) and $2x10^{-3}$ ml liquid cumene was injected. The reaction mixture was circulated in the glass system using an all Teflon diaphragm pump (Cole-Parmer). The total volume of the system was about 200 ml. Samples were taken with a six port sampling valve incorporated in the reactor loop, and introduced into the gas chromatograph (Hewlett-Packard, 5790A, column: 0.1% SP 1000 on 80/100 Carbopack C).

The cumene (Aldrich) contained 0.3% ethyl and 0.1% n-propyl benzene as contaminants determined by GC-MS analysis.

3.2.2 Characterization of sputter deposited silica-alumina thin films

The deposition process was followed by XPS. The prepared films were very clean and since the targets where decationized, only Au, Si, Al, and O peaks were present in the spectra.

In Fig. 3.19a and 3.19b, we plot the integrated XPS areas for the Au 4f, O 1s, Si 2p and Al 2p peaks as a function of sputter deposition time in the experiment when Y-62 was used as target. (Very similar trends in the uptake curves were observed for the Y-82 and the dealuminated zeolite Y targets.) The curves can be described by simple exponential functions characteristic of three dimensional film growth. This growth mode requires that the surface species have no mobility [3]. According to SIMS and FABMS results by Dwyer *at al.* [1,2a], the majority of fragments leaving zeolite samples are atomic Si, Al and O species, some AlOH and SiOH, along with some dimers. It is expected that these species, after landing on the surface, do not have appreciable mobility at room temperature. They stay where they arrived and form three dimensional islands. This also implies that the developing film is most likely amorphous.

The atomic concentrations in the topmost atomic layers can be calculated based on the sensitivity factors (Perkin Elmer handbook, $S_{Si}/S_{Al}=1.48$). Figures 3.20a and 3.20b show that while the O/Si atomic ratio is constant during the entire course of deposition, the Si/Al ratio initially changes rather dramatically.

This can be due to one or more of the following three factors: 1) - higher silica concentration on the surface of the target, 2) - preferential sputtering of Si(-O) species, and 3) - lower initial sticking probability of the Al(-O) species on the substrate.

In Fig. 3.20b we indicated the surface composition of the target zeolite as well as the bulk composition. In agreement with Barr and Lishka [4], we found that the surface of the zeolite samples was richer in silica. On the other hand Suib *at al.* [2b] reported that surface and bulk compositions were identical. They pointed out

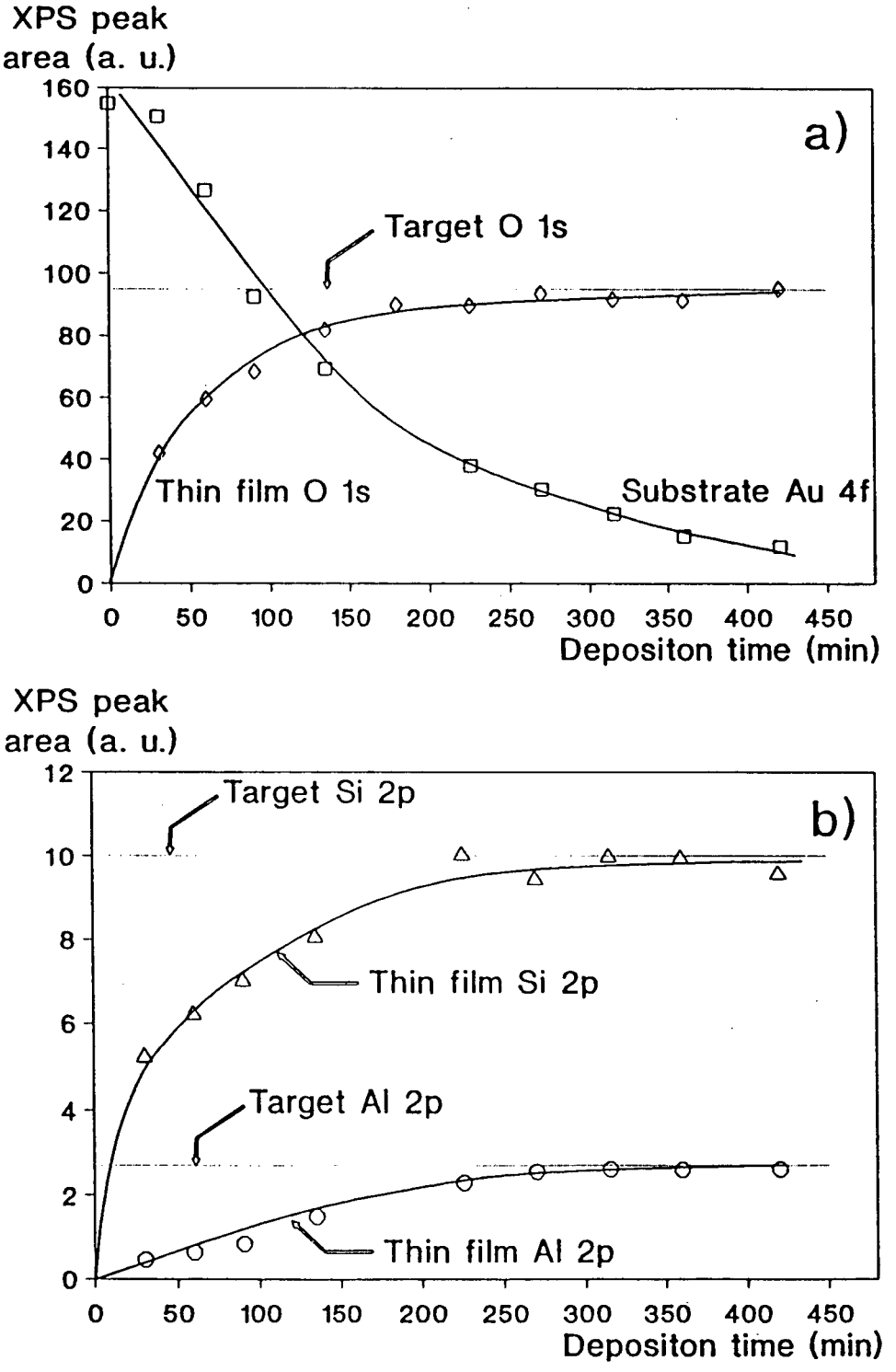

Fig. 3.19 Ion beam sputter deposition of silica-alumina on gold foil using Y zeolite (Y-62) as target. Integrated XPS peak intensities are plotted as a function of deposition time. a) O 1s and Au 4f peak areas, and b) Si 2p and Al 2p peak areas.

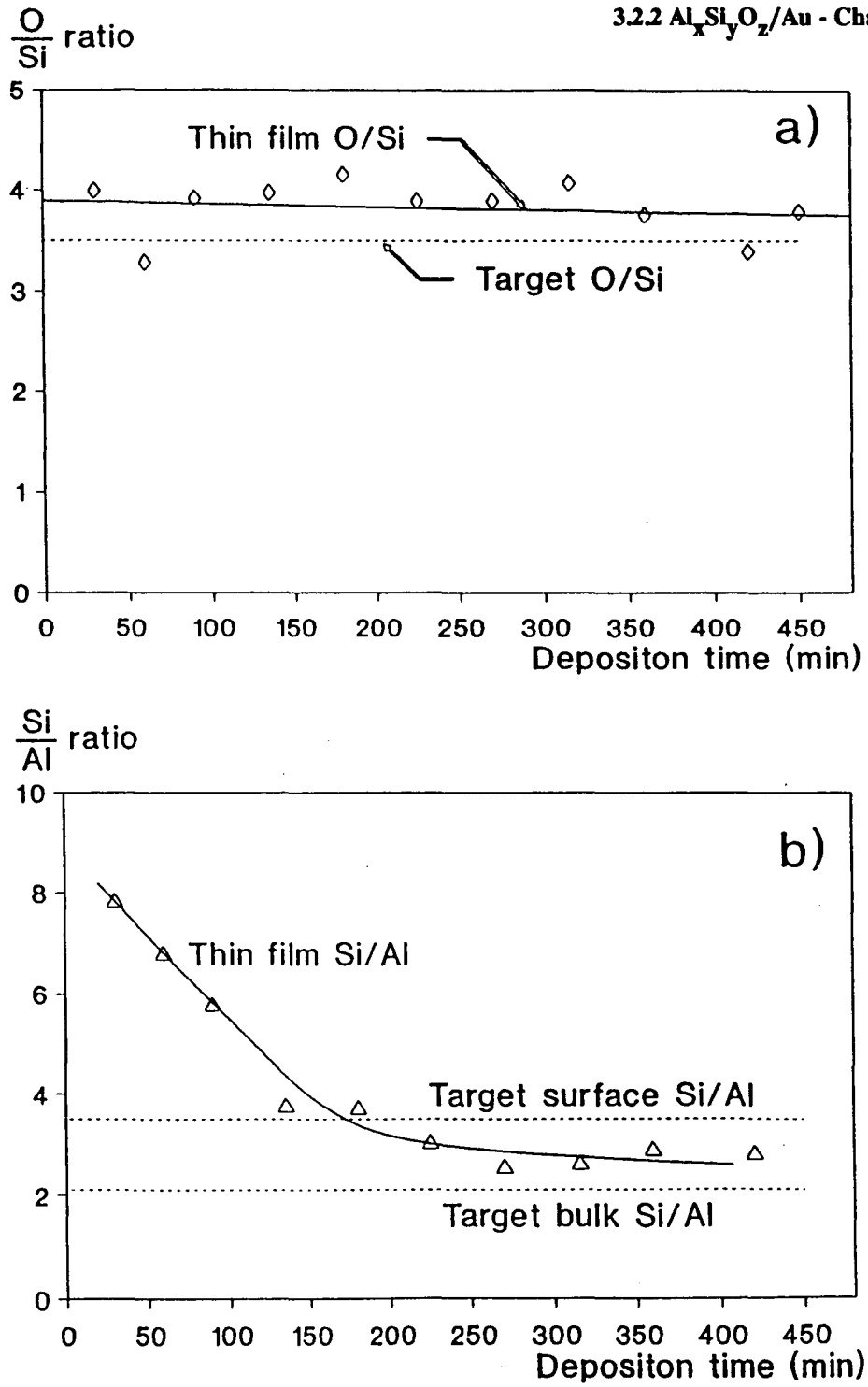

Fig. 3.20 Ion beam sputter deposition of silica-alumina on gold foil using Y zeolite (Y-62). Atomic concentration ratios as a function of deposition time; a) O/Si atomic ratio, and b) Si/Al atomic ratio. Horizontal lines indicate values calculated for the target.

that the history and the preparation of the sample is probably more important than the type of zeolite under investigation.

Quantitatively, however, the higher Si concentration on the target cannot explain why we have a higher silica concentration in our sputter deposited films initially. The Si/Al ratio in the films is 3-4 times higher than the ratio determined for the surface of the zeolite sample.

Ar^+ ion sputtering is a common surface science method to clean surfaces. If more than one component is present on the surface it is possible that one element can sputter more readily than the others. In the literature extensive experimental and theoretical efforts have been made to understand the phenomenon of preferential sputtering [5]. In general, similar atomic weight species sputter with similar rate unless they have different chemical bonding on the surface [5b]. Since silicon and aluminum are neighbors in the periodic table it is not expected that based on the atomic weight one should sputter faster than the other. From this point of view it would be interesting to investigate the role of the zeolitic structure of the target material in preferential sputtering of Si(-O) species.

It is interesting that, although Ni and Cu are also next to each other in the periodic table and have very similar atomic weights, Ni sputters preferentially from a 50% Ni - 50% Cu alloy. Shimizu *at al.*[6] found that the composition of the sputter deposited Ni-Cu films, using this alloy as target, initially changes with the target composition, but after prolonged sputtering (deposition) the composition of the film was identical to that of the bulk alloy. Because of conservation of mass, this should be true for any material after long sputtering. The film composition has to be equal to the bulk composition unless the target is non isotropic or some species sputter in certain directions more readily.

Finally, we cannot rule out the possibly that the sticking probability of the AlO_x and/or SiO_y species changes with the composition of the film. This would mean that either the sticking probability of the AlO_x ($0<x<4$) species is smaller on or the sticking probability of SiO_y ($0<y<4$) species is higher on silica rich films. We

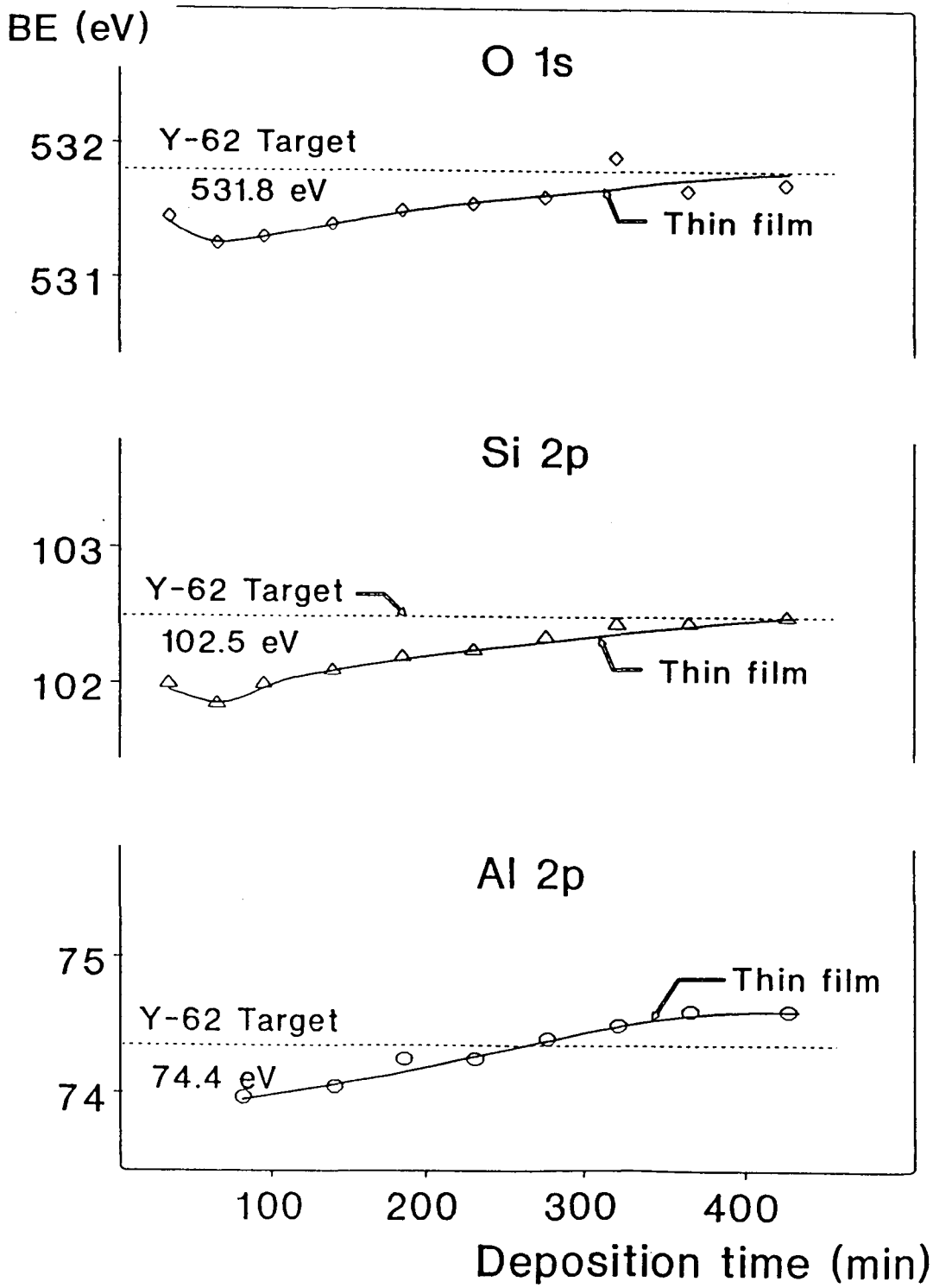

Fig. 3.21 Binding energies of the O 1s, Si 2p and Al 2p electrons in the sputter deposited silica-alumina film as a function of deposition time.

cannot rule out this possibility because the Si/Al ratio is always higher initially if one starts with a clean gold substrate no matter how many times the target had been used. Thus, the changing ratio has to be the property of the substrate and/or that of the film. Neither preferential sputtering nor initially rich silica surface could explain this.

Fig. 3.21 shows the binding energies of Si 2p, Al 2p and O 1s electrons as a function of deposition time. The Si 2p and O 1s binding energies behave similarly. Initially, they are lower than the ones for the bulk material, but with increasing deposition time they approach bulk values. As we saw in Fig. 3.20a, the oxygen to silicon ratio is unchanged during the entire deposition. Thus the deviation from the bulk binding energy of the O 1s and Si 2p is probably associated with the absence of alumina. The binding energy of the Al 2p follows a slightly different trend. It increases with increasing film thickness, but it does not approach the value obtained for bulk HY-62. All binding energies reported here are well within the range of binding energies published for Y zeolites [4,7].

An interesting feature of the oxygen Auger line in the XPS spectra is that it can provide some structural information. Wagner *at al.* [7], based on slight differences in the line shape, classified the O KVV transitions in Al-Si-O compounds into three groups: I. aluminum oxides and hydroxides, and silicates, II. uncharged silica networks having Si-O-Si bonds only, and III. compounds with high concentration of tetrahedral aluminum ions in molecular sieves (see Fig. 3.22). We wanted to see if this classification can be useful in extracting some structural information from the spectra.

A few typical O KVV Auger lines obtained in this work are shown in Figures 3.23 and 3.24. Spectrum a) in fig. 3.23 is from a dealuminated Y zeolite which belongs to group II. of the above classification and shows a well defined shoulder on the lower electron kinetic energy side of the peak maximum, as expected.

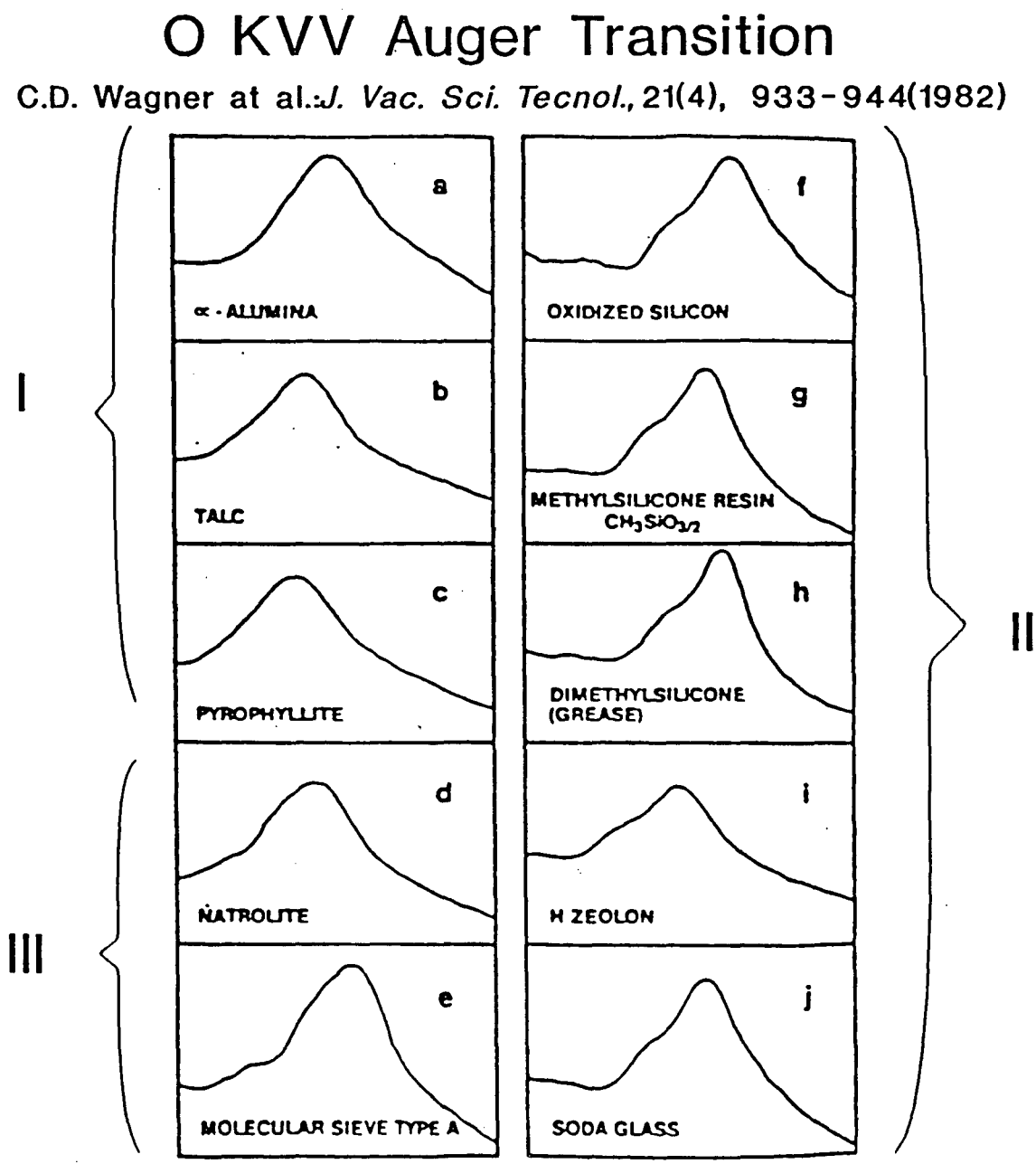

Fig. 3.22 Characteristic O KVV Auger transitions in different Al-Si-O compounds [7]. I. Aluminum oxides, hydroxides and silicates. II. Uncharged silica network and silicones. III. Oxygen in AlO_4^- tetrahedra such as in zeolites.

This feature is also present in the spectrum obtained from the sputter deposited film (Fig. 3.23b).

In fig. 3.24a we show the O KVV line for the Y-82 target (Si/Al = 1.3). The line is rather sharp and no shoulder at lower electron kinetic energy is visible, only one at the higher electron kinetic energy side of the maximum. This line shape does not fit in any categories of the classification developed by Wagner [7]. Fig. 3.24b shows the oxygen Auger peak from the same Y-82 sample after thermal decomposition at 1470 K for 10 hours in helium. As confirmed by XRD, this

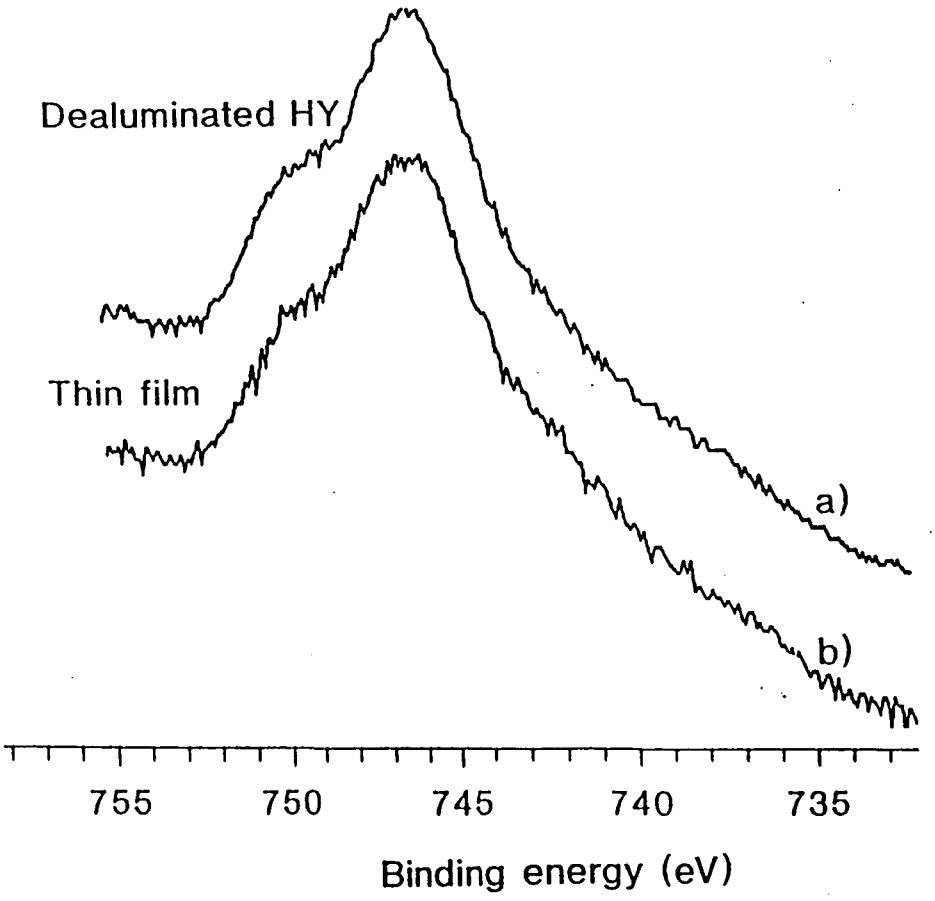

Fig. 3.23 Oxygen O KVV Auger transitions: a) dealuminated Y zeolite target b) sputter deposited thin film using dealuminated Y zeolite.
(Electron kinetic energy = 1253.6 eV - Binding energy).

treatment eliminates the zeolitic structure and the sample turns into an amorphous mixture of silica and alumina. As a result, the shoulder characteristic of uncharged Si-O-Si units appears on the oxygen Auger line (Fig. 3.24). It is interesting that this shoulder is absent if the target has been zeolite Y or a mechanical mixture of silica and alumina. Note, that the other shoulder at about 740 eV binding energy (Mg X-ray source) is still present after the loss of crystallinity. Although these differences appear minor they can be used as structural fingerprints. Especially in the future if line shapes for more Si-O-Al compounds become available.

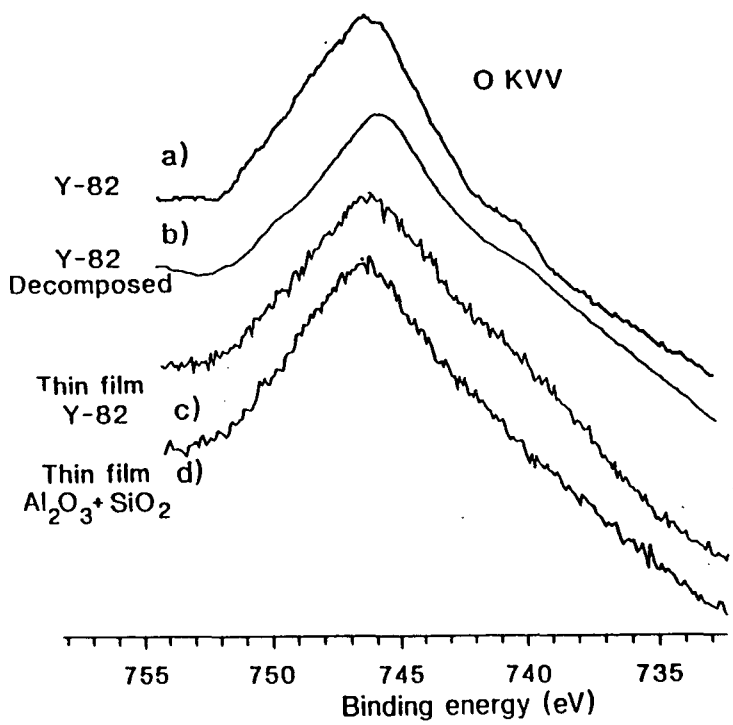

3.24 Oxygen O KVV Auger transitions: a) Y-82 target, b) thermally decomposed Y-82 (1470 K, 10 hours), c) sputter deposited silica alumina film on gold foil using Y-82 as target, and d) sputter deposited silica alumina film on gold foil using a mechanical mixture of SiO_2 and Al_2O_3.
(Electron kinetic energy = 1253.6 eV - Binding energy.)

From the XPS results we conclude that the films deposited by argon ion beam sputtering are silica-alumina mixtures having very similar composition to the

Y zeolite used as target. XPS results revealed that the silicon, aluminum and oxygen environments are also very similar to those of the target.

3.2.3 Reactivity in Cumene Cracking

To investigate the catalytic properties of the sputter deposited silica-alumina layers on gold, first we tried to use a traditional ultra-high vacuum - high pressure catalytic reactor system, now routinely used in model metal catalysis studies. We prepared a silica-alumina thin film on both sides of a 1x1x0.0025 cm gold foil in ultra-high vacuum. The deposition process was followed by Auger electron spectroscopy and the intensity of the gold and oxygen Auger peaks showed the same exponential change with deposition time as the XPS signals. After deposition the sample was introduced into the high pressure cell, and we attempted to run several typical acid catalytic reactions: 1-butene double bond shift, dehydration iso-propanol and cumene cracking.

The activity of a 2 cm^2 sputter deposited film in any of these reactions was only 10-50% higher than that of the gold substrate without the film. All our attempts at decreasing the background activity or increasing the activity of the film by at least an order of magnitude, have failed.

In order to investigate if the sputter deposited film is active at all in a typical acid catalyzed reaction, we increased the macroscopic surface area of our samples to 20 cm^2 by simply using ten pieces of gold foil, 2 cm^2 each. Instead of stainless steel high pressure reactor cell, at this time, we used an all glass system with a Teflon circulation pump.

The silica-alumina films were prepared from zeolite Y-82 and from a mechanical mixture of silica and alumina. Also, we prepared separate silica and alumina thin films and compared their activity to the silica-alumina samples. Blank experiments on gold foils (20 cm^2) showed some activity. We could detect the formation of diisopropyl benzenes, benzene, propene and iso-butene at 570 K. The

reaction rate was very low, in the order of 10^{10} molecules/min. We found that the adsorption rate of the aromatic products on the glass walls of the reactor was within the same order of magnitude. Since propene did not adsorb on the walls, we chose its rate of formation as the measure of catalytic activity. This choice was further supported by the reaction network developed by Wojciechowski [8],because propene is produced only in one primary reaction: the cracking of isopropyl benzene.

In Fig. 3.25 typical product accumulation curves obtained in this study are

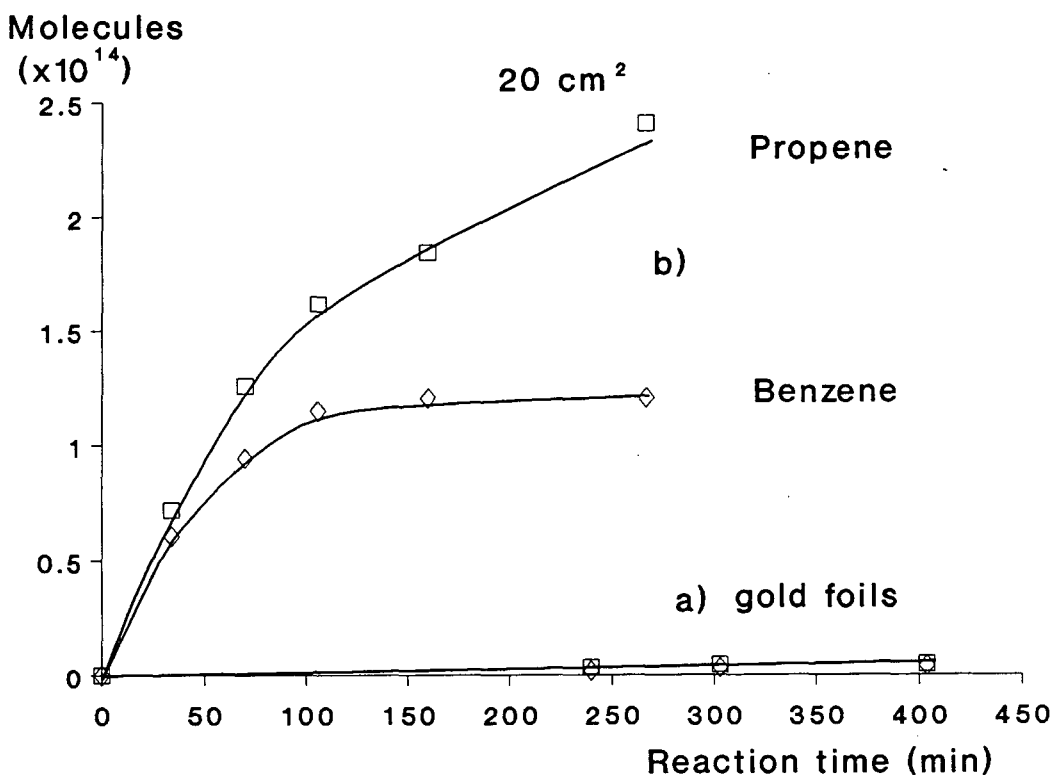

Fig. 3.25 Product accumulation curves for cumene cracking reaction at 570 K over blank reactor (a) and over sputter deposited silica-alumina layers (b) deposited on gold foil using zeolite Y-82 as target.

shown for the glass reactor system. The activity of the sputter deposited silica-alumina layer was two orders of magnitude larger than that of the background when

zeolite Y-82 was used as target. This proves that the sputter deposited films have acidic properties.

In Fig. 3.26 we report the initial reaction rates for both the sputter deposited films and the targets themselves. The high surface area catalysts show the expected trend. The zeolite sample is 6-7 orders of magnitude more active than alumina or silica. When thermally decomposed, its activity drops as the zeolitic structure collapses. The relative initial rates for the sputter deposited films are also shown in Fig. 3.26. The activities are low, but clearly measurable. The initial rate of cumene cracking on alumina, silica and silica-alumina thin films deposited from high surface

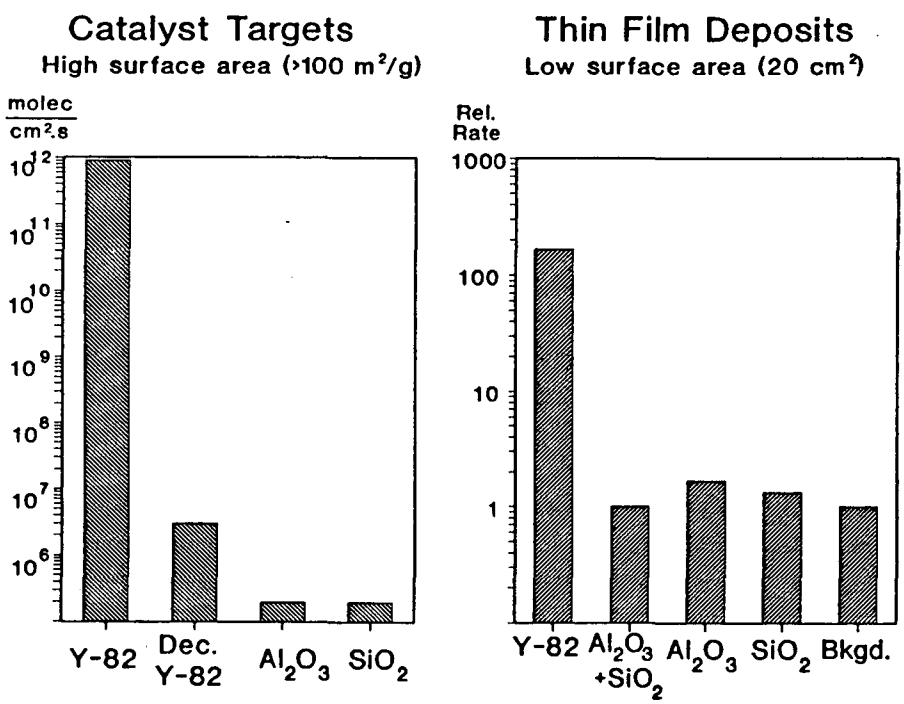

Fig. 3.26 Initial rate of cumene cracking at 570 K a) for high surface area catalysts: zeolite Y-82, decomposed zeolite Y-82 (in He at 1470 K for 10 hrs), alumina and silica, and b) for sputter deposited thin films using Y-82, a mixture of alumina and silica, alumina, silica as targets and the initial rate for the background reactions as well.

area targets could hardly be distinguished from the rate measured on gold foils. There is a two order of magnitude higher activity, however, on films deposited using a zeolite target. This implies that the sputter deposited film has some chemical

memory of the parent material. It would be early to speculate if this effect is due to similar local structures in the amorphous thin film and in the target zeolite. Further studies using a series of zeolite targets could settle this question.

References

1. Dwyer, J., Fitch, F. R., Machado, F., Qin, G., Smyth, S.M., and Vickerman, J. C., *J. Chem. Soc., Chem. Comm.*, **1981**, 422.
2. a) Dwyer, J., Elliott, I. S., Fitch, F. R., van den Berg, J.A., and Vickerman, J. C., *Zeolites*, **3**, 97-98 (1983).

   b) Suib, S. L., Coughlin, D. F., Otter, F. A. and Conopask, L. F., *J. Cat.*, **84**, 410-422 (1983).
3. Argile, C., and Rhead, G. E., *Surf. Sci. Rep.*, **10**, 277-356 (1989).
4. a) Barr, T. L., and Lishka, M. A., *J. Am. Chem. Soc.*, **108**, 3178-3186 (1986).
5. a) Malherbe, J. B., Hofmann, S., and Sanz, J. M., *Appl. Surf. Sci.*, **27**, 355-365 (1986),

   b) Kelly, R., *Surf. Sci.*, **100**, 85-107 (1980), and c) Kelly, R., *Nucl. Inst. Meth.*, **149**, 553-558 (1978).
6. Shimizu, R. and Saki, N., *Surf. Sci.*, **62(2)**, 751-755 (1977).
7. Wagner, C. D., Passoja, D. E., Hillery, H. F., Kinisky, T. G., Six, H. A., Jansen, W. T., and Taylor, J. A., *J. Vac. Sci. Tech.*, **21(4)**, 933-944 (1982).
8. a) Corma, A. and Wojciechowski, B.W., *Catal. Rev. Sci. Eng.*, **24(1)**, 1-65 (1982).

   b) Best, D.A. and Wojciechowski, B.W., *J. Catal.*, **47**, 343 (1977).

3.3 Summary

We have developed three methods to prepare silica-alumina thin films on Si(111) and on gold substrates. We tested if these layers can serve as model catalysts in a combined surface science and catalysis study.

The oxidation of r3xr3 R30 Al-Si(111) by oxygen or water leads to the formation of a thin (< 15 Å) layer consisting of silica and alumina. After annealing the a sharp 1x1 LEED pattern is observed on a high background. The ordering is probably due to exposed silicon and not an ordered Si-Al-O layer. We have not been able to show that this silica alumina on a 1 cm^2 Si(111) is catalytically more active than the blank stainless steel reactor in a series of typical acid catalyzed reactions.

Thin, homogeneous silica-alumina films can also be prepared on Si(111) in aqueous sodium hydroxide - sodium silicate colloidal solution. According to this method the silicon sample is placed in the basic solution which also contains a piece of aluminum. The deposition rate of the alumina depends on the pH, temperature, the volume of the solution and the surface area of the silicon and the aluminum. The deposited silica-alumina film is homogeneous by SEM and SAM. The surface sodium can be exchanged with ammonium ions and the ammonium salt can be decomposed to form OH groups on the surface. XPS results indicated that the chemical environments of the surface aluminum, silicon and oxygen atoms are in the same range for high surface area alumino silicate samples.

Catalytic studies of small surface area (1-2 cm^2) samples have failed to clearly demonstrate a significant cumene cracking activity. Larger surface area (3500 cm^2) samples prepared using the same deposition methods on silicon particles undoubtedly showed that the films exhibit acid catalytic properties.

Using argon ion beam sputter deposition, homogeneous and amorphous thin silica-alumina layers can be prepared on gold foil using zeolite targets. Although the Si/Al ratio of the films initially is larger than the ratio for the target it approaches that of the target with increasing thickness. XPS results indicate that the O 1s, Al 2p and Si 2p peak positions and the line shape of the O KVV Auger transition are very similar to ones obtained from the target zeolites. This method seems to be a promising new tool to prepare model catalysts from high surface area practical catalysts.

We have shown that the sputter deposited thin silica-alumina films are active in cumene cracking, but one needs at least 20 cm^2 total geometric surface area to detect it. We have also found that the films deposited using zeolite targets are more active than the ones deposited from a mechanical mixture of silica and alumina.

These studies clearly demonstrate that a combined surface science and catalysis approach to acidic oxides requires the modification of the ultra-high vacuum - high pressure reactor cell design used in metal single crystal investigations. These modifications have to be aimed at minimizing the background activity due to manipulator parts and reactor walls and at minimizing the adsorption of reactants and/or products on the walls of the reactor loop. (A few idea to improve the reactor system: coat stainless steel parts with nonporous glass, increase the distance between the reactor walls and the sample, use a molecular beam directed at the surface and detect the products by a mass spectrometer.)

We have also demonstrated that increasing the surface area of the model catalyst is another effective way to raise the activity above the background. The approach we used can be generalized as follows. One develops a method that is suitable to deposit a thin layer of a model catalyst on both high and low surface area substrates. After the deposition under the same conditions the low surface area sample is introduced into a UHV - high pressure cell apparatus for surface analysis, and the high surface area portion of the material is introduced into a catalytic

reactor for the catalysis study. The low surface area sample can be treated in UHV or in the high pressure cell with same reactants under the same conditions as the high surface area sample. Thus the surface properties and the effects of reactants on the composition and surface properties can be studies. But the catalytic studies have to be carried out on a higher surface area portion of the model catalyst. To be able to correlate the results obtained in the two studies, one has to ensure that the high and the low surface area samples can undergo exactly the same treatments. Which means that ultra-high vacuum is a basic requirement not only for the surface analysis chamber but for the catalytic reactor as well.

This methodology, although not as elegant as the metal single crystal approach, can be an interim solution to the problems associated with low catalytic activity of low surface area model catalysts. An interim solution, until new reactor designs become available.

When dealing with multicomponent model catalysts one has to realize that, although they are called models, they are not necessarily any simpler than their practical counterparts. This especially true for the Pt-Al-O-Cl(-Au) model system described in the next chapter.

4. Model Pt-Cl-Al_2O_3 Catalysts

In the previous chapters we demonstrated that the combined ultra-high vacuum - high pressure catalytic reactor cell system in its present form is not suitable to study low catalytic activity oxides using the same strategy as for model metal catalysts. These reactor systems, however, have been proved to be appropriate to investigate the interactions between metals and metal oxides [1].

These interactions are of great importance in the chemical industry, because most metal catalysts are supported on a high surface area oxides, and the interaction can dramatically influence both chemical and physical properties of metal particles.

According to this approach first an 'inverse' supported catalyst is prepared by the deposition of an ultra thin layer of $metal_1$ oxide on $metal_2$. Then the surface properties of the metal oxide - metal system is studied using surface science tools and finally the sample is introduced into the reactor for the catalytic studies. The postreaction surface is also characterized and the catalytic properties are correlated with the surface composition and structure. Here the assumption is that the interface properties are independent of the configuration, e.i. which component is supported on the other. From experimental point of view the 'inverse' system has many advantages over the 'real' catalyst system. Problems with mounting and heating of a high surface area material in a UHV chamber, for example, can be avoided. In addition, the samples are prepared in a clean UHV environment.

Here we report on the preparation and characterization of two model platinum-alumina catalysts and their catalytic properties in methyl cyclopentane (MCP) hydrogenolysis. We have been interested in comparing the 'inverse' system (alumina-on-platinum) with a model supported metal system (platinum-on-alumina). And since industrial alumina supported catalysts contain chlorine we incorporate it in our model catalysts as well.

4.1 Introduction

Platinum is an essential component of supported catalysts used in petroleum refining and in naphtha reforming, two large scale petrochemical processes to produce high octane number gasoline. In general, the preparation of supported platinum catalysts for laboratory use involves the following steps [3]: 1. a high surface area (70-400 m^2/g) support material (e.g. alumina, silica or titania) is impregnated with an aqueous solution of a platinum salt such as ammonium haxachloro platinate, $(NH_4)_2PtCl_6$, 2. the water is removed by rotary evaporation at 340 K, 3. the material is ground and dried in an air oven at 393 K, 4. the catalyst is then calcined in flowing oxygen at 673 K, and finally 5. the catalyst is reduced at temperatures ranging from 570 to 770 K. The result of this procedure is high dispersion platinum particles supported on the oxide.

The activity of Pt/Al_2O_3 gradually decreases during catalytic reaction, and this deactivation is attributed to the deposition of carbon (coke formation) [4] on the metal and to the decrease of platinum surface area (sintering) [5]. It has been known for several years, that deactivated supported platinum catalysts can be fully regenerated [6] in an oxygen treatment at 770 K. Although most papers agree that during this procedure the carbon deposits are burned off and the platinum particle size decreases, the details of this redispersion is not understood. It has been difficult to confirm if the redispersion actually takes place or not on industrial samples [7], because chemisorption and TEM methods provided contradictory results. Recently Beck and Carr [8a] reported for example that no redispersion could be observed after oxygen treatment and they could not detect sintering in hydrogen either. Using transmission electron microscopy (TEM) and model Pt/Al_2O_3 $(10\underline{1}0)$ samples, Rickard *at al.* [8b] found that the oxygen treatment produces a bimodal particle size distribution.

And there are contradictory results regarding the role of chlorine, a common component of reforming catalysts, in the redispersion process; although

Dautzenberg *at al.* [9] suggest that chlorine is not necessary for redispersion, Lieske *at al.* [10] claim that the redispersing oxidation of crystalline Pt is impossible in the absence of chlorine.

The interaction of platinum particles and the support plays an important role in this redispersion process, and it can influence the catalytic properties of the metal as well. More than 60 years ago Schwab and Pietsch [11] suggested that the active sites for certain catalytic reactions are located at interface between the metal particles and the oxide support. Since 1987, when Tauster *at al.* [12] first described the phenomenon of strong metal support interaction (SMSI), the interface (boundary) between the metal and the oxide support has become the target of intense research [13]. The SMSI effect was defined as a reduced hydrogen and CO adsorption capacity of transition metal particles supported on reducible oxides, such as titania, after a high temperature hydrogen treatment. In parallel with the decreased adsorption capacity, dramatic changes in the catalytic properties develop, and the catalyst is said to be in the 'SMSI state'.

For example the selectivity pattern of the hydrogenolysis of methyl cyclopentane (MCP) over titania platinum catalysts is characteristically different from silica supported platinum catalysts [3] after low and high temperature reduction. In most cases the selectivity of this reaction depends on the temperature, hydrogen pressure, metal particle size, and the nature of the support [14]. And even on alumina, which is not classified as an SMSI support, the product distribution changes with metal loading.

Based on a large number experimental data on different particle size catalysts, three distinct mechanisms have been suggested for the MCP ring opening. The three mechanisms result in three distinct distributions of the primary ring opening products [17]: 2-methyl-pentane (2-MP), 3-methyl-pentane (3-MP) and n-hexane (nHx).

Mechanism A; nonselective or statistical ring opening. This mechanism occurs on fine platinum particles and produces 40% nHx, 40% 2-MP and 20% 3-MP.

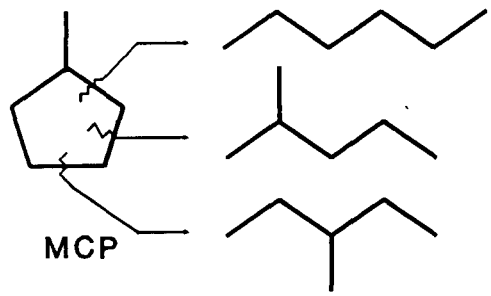

	selective	statistical
nHx	0	40
2MP	67	40
3MP	33	20

Fig. 4.1 Methyl cyclopentane ring opening selectivities [17].

Mechanism B; selective ring opening. This mechanism which yields 67% 2-MP , 33% 3MP and no nHx, is predominant on large platinum particles.

Mechanism C; intermediate or 'partially selective' mechanism. On low dispersion platinum particles, consecutive isomerization of the acyclic products can result in product distributions which are not linear combinations of mechanism A and B.

The change of selectivity with the metal loading was observed by Gault and co-workers [15]. First, the particle size effect was attributed to the geometry of the platinum particles [17], but more recently Kramer and Zuegg [16], recalling the concept of adlineation proposed by Schwab and Pietsch [11], attributed the shift in selectivity to special sites at the boundary of the metal particles and the support. They believe that the selective mechanism occurs on the platinum particles while the statistical ring opening takes place at the boundary. So the enhancement of the non-selective mechanism at high dispersions is the result of the larger number of platinum atoms at the boundary between the particles and the support.

In order to investigate both the redispersion properties and the role of the interface we prepared two model Pt-Al_2O_3 systems and studied their physical and catalytic properties as a function of preparation conditions and pretreatments in the presence and in the absence of chlorine:

- Alumina-on-platinum:

$$Pt_{(s,foil)} + AlO_{x(g)} \rightarrow AlO_x/Pt_{(s,foil)}$$

- Platinum-on-alumina:

$$Au_{(s,foil)} + Al_{(v)} + O_{2(g)} \rightarrow AlO_x/Au + Pt_{(v)} \rightarrow Pt(/Cl)/AlO_x/Au_{(s,foil)}$$

4.2 AlO_x/Pt and AlO_x/Cl/Pt

We have prepared this model system by depositing alumina on an atomically clean platinum foil to form submonolayers of AlO_x. By systematically varying the coverage, e. i. the length of the Pt-AlO_x boundary we hope to reveal the role of the interface in MCP hydrogenolysis. Also, the regeneration of used catalysts have been studied in the presence and in the absence of chlorine.

4.2.1 Experimental

A 0.051 mm thick platinum foil was mounted on the manipulator described in Chapter 2.1. The supports between the sample and the copper rod were 0.51 mm diameter gold wires (see Fig. 2.3). (Initially we used platinum wires as it had been the standard practice [18], but later when we discovered that approximately 5% of the activity was due to reactions taking place on the supports, we switched to gold.)

The surface of the platinum foil (99.99%) was cleaned in UHV by cycles of oxygen treatment at 770 K ($p=10^{-5}$ torr, for 10 min) and 10 min Ar^+-ion sputtering at room temperature ($p = 5x10^{-5}$ torr, $E_b = 2$ kV) until the characteristic platinum Auger peaks were present only. Carbon, silicon and calcium were common contaminants on the surface, but 10-15 cycles were sufficient to remove them. After the cleaning procedure the foil was annealed at 1270 K for 5-10 minutes. Once the silicon and calcium is removed, carbon that deposits in UHV or in the high pressure cell can be easily removed by heating the sample in oxygen (6,000 L, at 770 K).

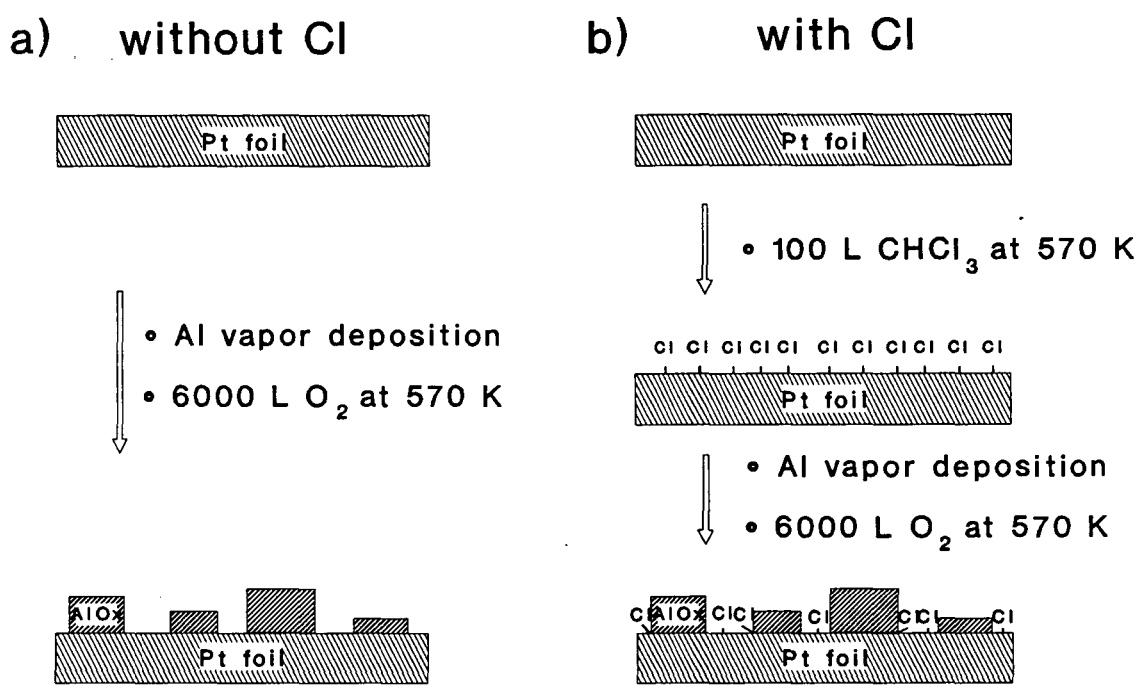

Fig. 4.2 Preparation of model catalysts a) AlO_x/Pt (**A**) and b) AlO_x/Cl/Pt (**B**).

To investigate how the rate and selectivity of MCP hydrogenolysis change with the AlO_x coverage in the absence (**A**) and in the presence (**B**) of chlorine the following deposition cycles were repeated (see Fig 4.2).

A. - without chlorine : aluminum was deposited on the clean platinum foil by vapor deposition from a small high purity alumina crucible heated to 960-970 K which was followed by an oxidative treatment at 570 K (p_{O2}=1x10^{-5} torr, 10 min). The sample was characterized by AES and CO TPD, and introduced in the high pressure cell. After the reaction, the sample was analyzed again, the carbon was burned off using an oxygen treatment at 770 K (p_{O2}=1x10^{-5} torr, 10 min). AES

spectra were recorded, and surface was exposed to the next dose of aluminum, followed by oxidation etc.

B. - with chlorine: the cycle was exactly the same as described under **A.**, but here, before the deposition of the aluminum, the sample was exposed to 100 L of $CHCl_3$ at 570 K. According to AES this method produced a saturation chlorine coverage and did not deposit carbon on the surface. We noted that the uptake of chlorine was proportional to the exposed platinum, and if the surfaces was fully covered with AlO_x no chlorine could be deposited.

In the CO TPD experiments, the sample was exposed to 60 L of carbon monoxide at room temperature. The sample was then heated to 1170 K at a rate of 40 K/s.

The catalytic reaction was carried out according to the general procedure described in Chapter 2.1. The hydrogen to MCP molar ratio was about 230, and the total pressure was 1 atmosphere. The reactions were carried out at 620K according to the procedure described in Chapter 2.1.

4.2.2 Results and Discussion

We would like to model the redispersion properties of Pt/Al_2O_3 using an 'inverse' catalytic system prepared by depositing alumina of platinum foil in the presence and in the absence of chlorine. Lieske and co-workers [10] developed a comprehensive scheme to explain the redispersion process and claim that the presence of chlorine is essential for the redispersion to take place. Our system is rather different from the industrial one, but if the properties of the alumina-platinum interface is influenced by the presence of chlorine we should be able to detect differences between the chlorine free and the chlorine containing samples.

Typical Auger spectra obtained in this study are shown in Fig. 4.3. The top spectrum was obtained after several cycles of AlO_x deposition - MCP hydrogenolysis - regeneration. The characteristic platinum and oxygen transitions are present only.

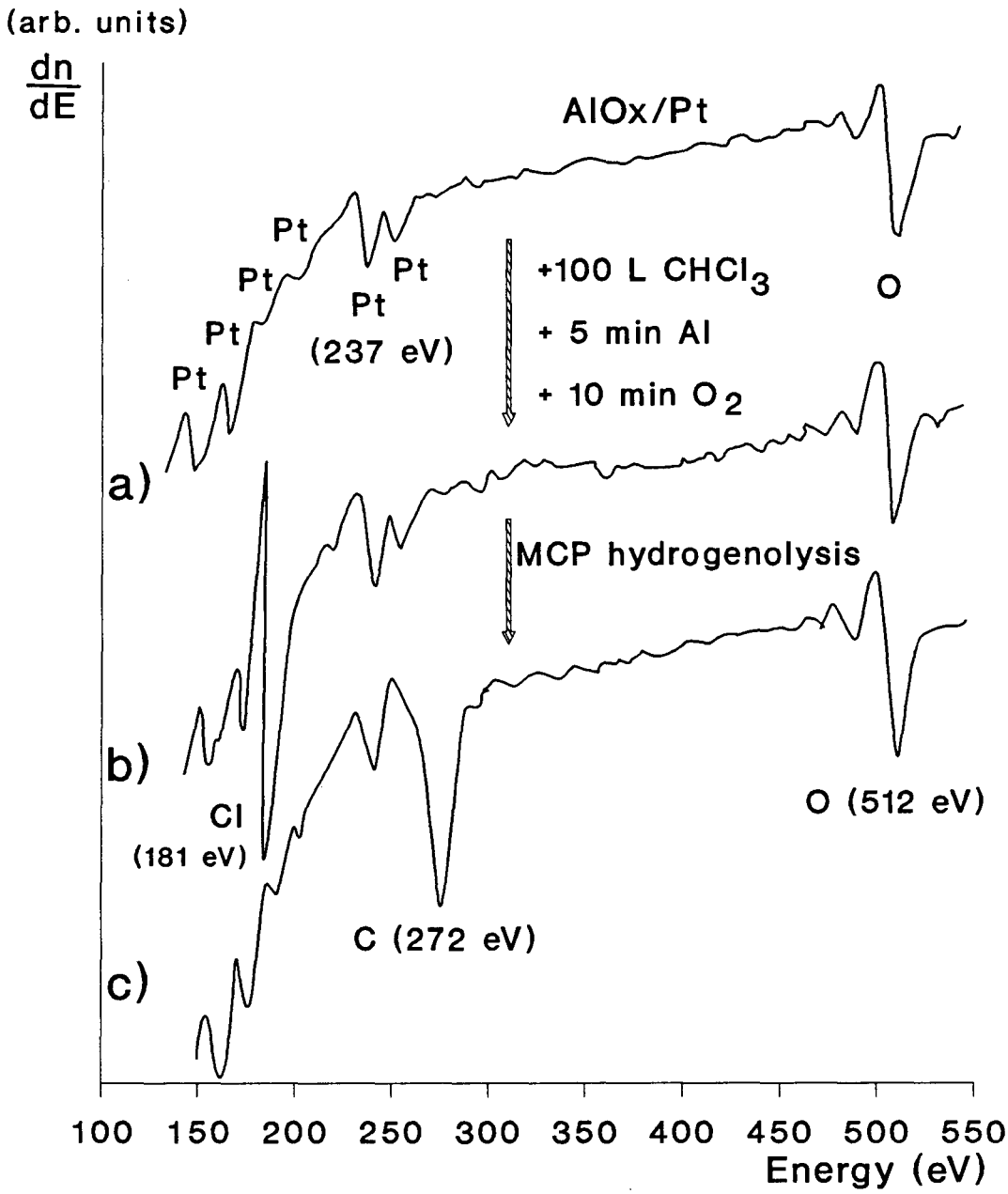

Fig 4.3 Characteristic Auger spectra. a) After accumulative deposition of 30 min AlO_x on platinum foil, b) after chlorine deposition, and c) after MCP hydrogenolysis.

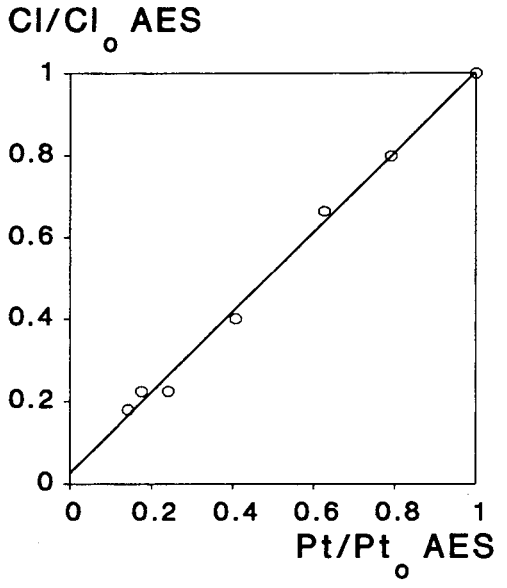

Fig. 4.4 Relative intensity of the chlorine Auger peak (181 eV) as a function of the platinum Auger peak (237 eV) intensity. Pt_o and Cl_o are the intensity of the platinum and chlorine Auger peaks before deposition of AlO_x, respectively.

After chloroform treatment only chlorine appears on the surface and no carbon can be detected (see Fig. 4.3 b).

The next question is if the chlorine is attached to the platinum or to the alumina or perhaps both. In Fig. 4.4 we show how the relative intensity of the chlorine Auger peak changes with that of the platinum Auger peak. From this and the fact that a completely covered platinum sample could not be chlorinated we conclude that the chlorine is attached to the platinum only.

This is rather surprising. Chlorinated hydrocarbons are often used in the chemical industry to increase the acidity of aluminas [19]. In a separate experiment we deposited AlO_x on a gold foil (as described in Chapter 4.3.1) and tried to chlorinate the surface with chloroform under higher pressures and temperatures ($<$100 torr $CHCl_3$ and 650 K), but without success.

The surface chlorine is removed after very short (5-10 min) hydrogenolysis (Fig. 4.3c), which further supports that the chlorine is attached to the exposed platinum. The chlorine content of real life Pt-Al_2O_3-Cl catalysts, however, does not

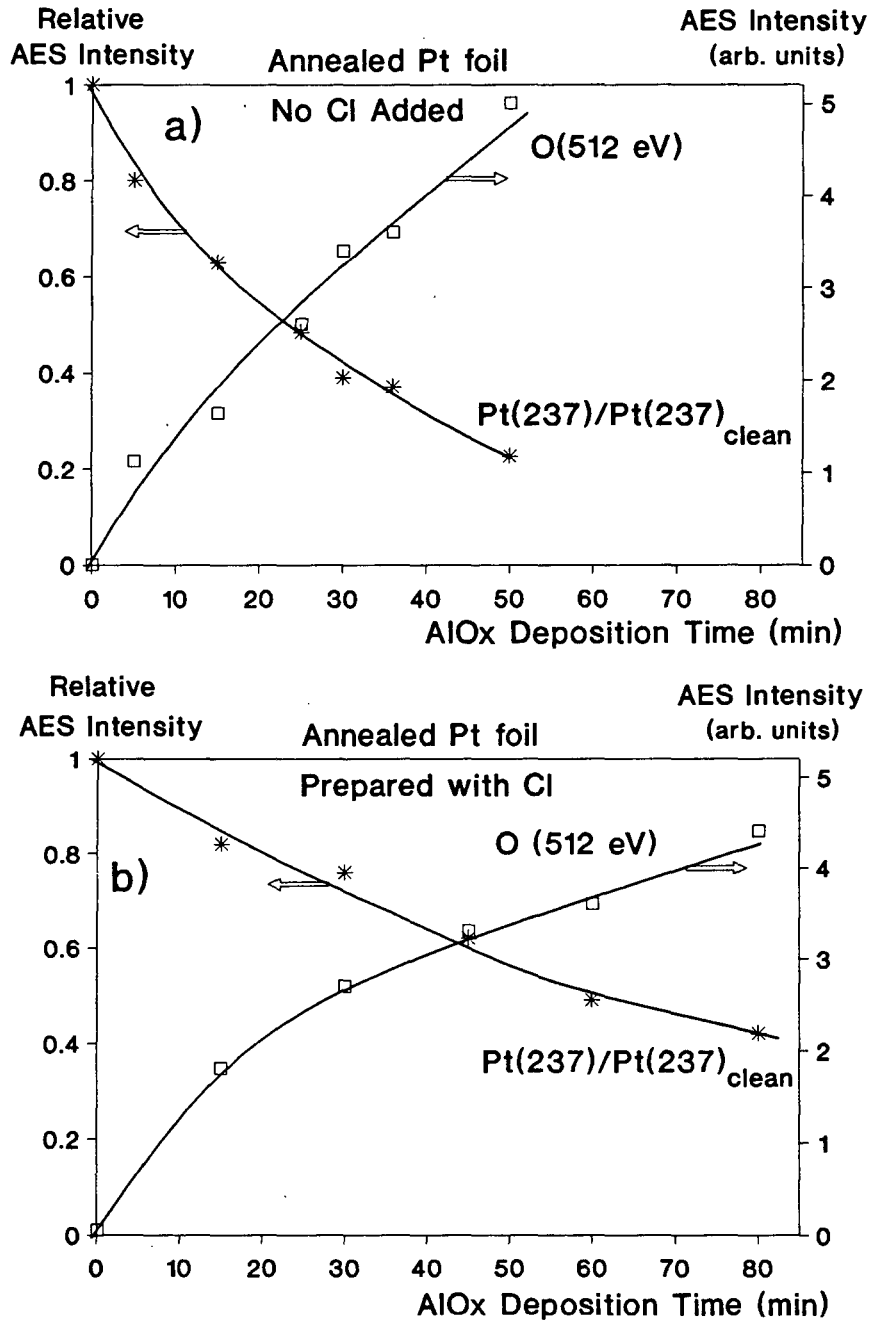

Fig. 4.5 Auger uptake curves for annealed platinum foil a) in the absence and b) in the presence of chlorine.

change during reaction or hydrogen reduction [20]. This is a major difference between our model systems and the industrial catalysts.

In Fig. 4.5, the uptake curves are shown for an annealed foil in the presence and in the absence of chlorine. Using the same deposition conditions we can assume that the deposition time is proportional to the amount of alumina deposited. We find that the surface concentration of platinum at a given deposition time is higher if the preparation of the model catalysts involved the chlorination step. We do not have enough data points to classify the growth mode. But it is most likely three dimensional as opposed to layer by layer based on qualitative comparison of these curves with ones published in the literature for a large number of systems [21].

In order to determine the fraction of the platinum surface still exposed we performed CO TPD experiments. The desorption of the CO molecules produced one peak at 495 K with a shoulder at around 430 K. In Fig. 4.6 the total area under the CO TPD curve is shown relative to the clean platinum foil as a function

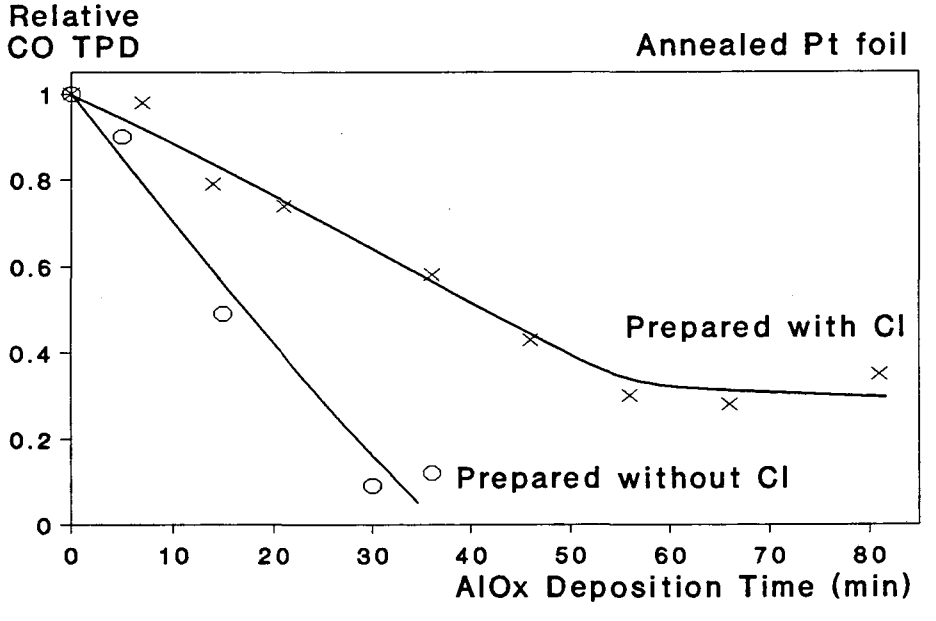

Fig. 4.6 Relative CO TPD areas as a function of AlO_x deposition time for annealed platinum foil.

deposition time. If AlO_x is deposited on chlorine free platinum the surface can be covered in 30-40 minutes. On the other hand, when a saturation coverage of chlorine was present on the platinum, even after 70-80 minutes of deposition, 30-40% of platinum is still available for adsorption. This is in qualitative agreement with the AES data that showed a higher concentration of platinum when the catalyst was prepared in the presence of chlorine. After a given amount of AlO_x deposition the chlorine containing catalysts always expose more platinum.

After deposition the catalysts were introduced in the high pressure cell (HPC) and the MCP hydrogenolysis was carried out. The relative rate and the relative CO adsorption capacity as a function AlO_x deposition time is shown in Fig. 4.7. Since both the activity and the CO TPD area are the measure of the number of

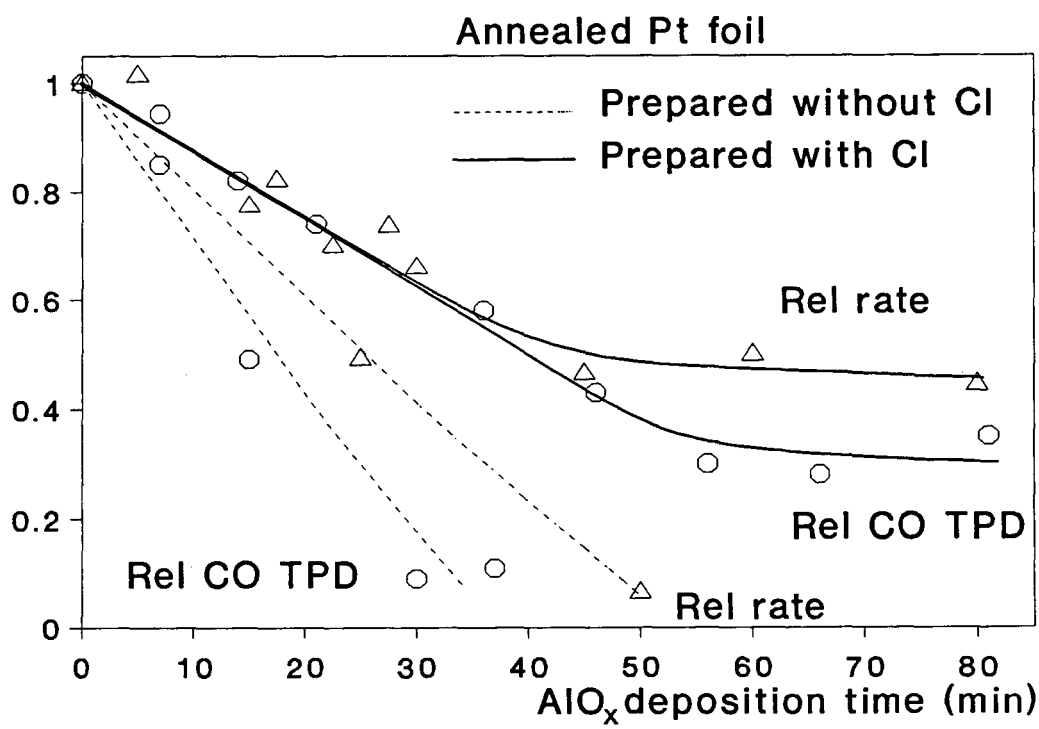

Fig. 4.7 Relative MCP hydrogenolysis rate and relative CO TPD area as a function of AlO_x deposition time for samples prepared with and without chlorine deposition on an annealed platinum foil. Initial rate on the clean foil was approximately 0.2 MCP molec/Pt/sec. ($T=620K$, $p_{H2}=1$ atm, $H_2/MCP=240$)

exposed platinum atoms, the two curves for the chlorine free and chlorine containing samples show similar trends.

In the absence of chlorine, after 30-40 minutes of deposition, only a very small fraction of the platinum surface is available for CO adsorption and methyl cyclopentane hydrogenolysis. But in the presence of chlorine, even after twice as long deposition, both the activity and the CO adsorption capacity are about 30-40% of that of the clean platinum foil. And both become independent of the amount of alumina deposited. This happens only after the deposition of the amount AlO_x necessary to fully cover the platinum surface in the chlorine free experiments. The initial slope of the two curves is identical and smaller than in the chlorine free case. In other words, at a given amount of AlO_x deposition, more platinum is present on the surface if it was saturated with chlorine.

The two most likely mechanisms responsible for the higher platinum surface area are depicted in Fig. 4.8. In the presence of chlorine on the platinum surface, 1) the alumina islands contract exposing more platinum or 2) atoms or small clusters of

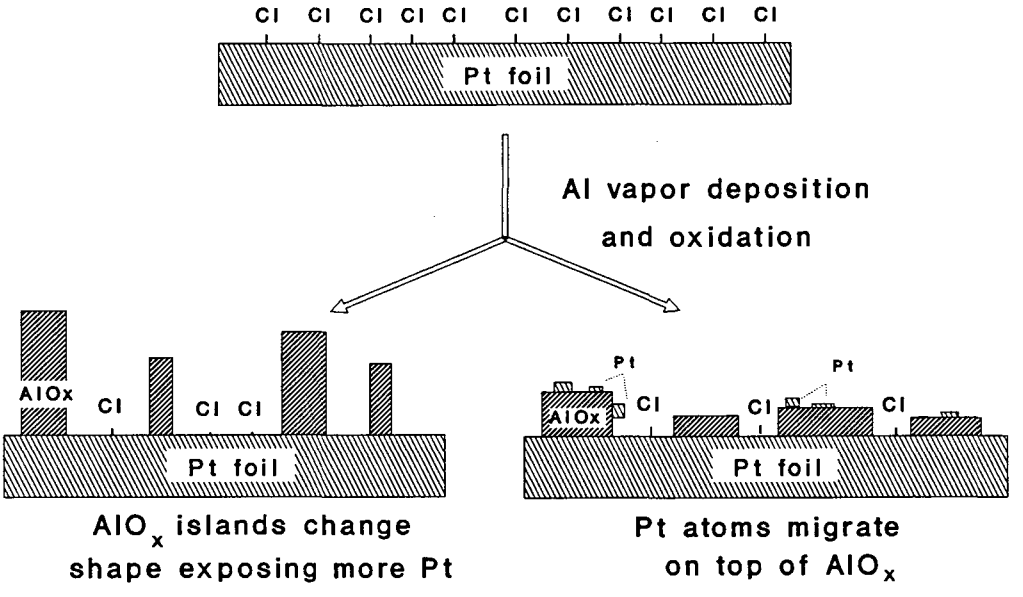

Fig. 4.8 Two possible mechanisms to explain the larger platinum surface area when the catalysts were prepared in the presence of chlorine.

platinum migrate on top of the aluminum oxide islands. It is not easy to distinguish these two mechanisms, and it is also possible that they occur simultaneously.

Lieske *at al.* [10], using temperature programmed reduction (TPR), hydrogen adsorption spectroscopy and uv-vis spectroscopy, identified $Pt^{IV}O_xCl_y$ as the mobile species in the redispersion process. According to them the chlorine assisted redispersion involves the following steps. 1) In an oxidizing atmosphere, platinum atoms are attacked by chlorine ions coming from the support and form $Pt^{IV}O_xCl_y$, 2) These mobile species migrate on the alumina surface and get trapped on certain alumina sites. 3) In a reducing environment, the chlorine is transferred back to the alumina.

What we find in our model system is somewhat different. According to our observation the chlorine, if attached to platinum, is removed instantaneously by hydrogen at 570 K, and no exchange of chlorine between the platinum and the AlO_x takes place. Yet, we find that the platinum surface area is larger if chlorine was present during the preparation.

Foger and Jaeger [22] studied the effect of chlorine treatment on the redispersion of platinum particles supported on alumina and silica using XRD, TEM, TPR and uv-diffuse reflectance spectroscopy. Their experimental conditions are perhaps closer to ours. Alumina and silica supported platinum particles were exposed to chlorine gas in an inert atmosphere. On silica, where the metal - support interaction is believed to be weaker, chlorination converted the platinum particles into crystalline platinum halides and the gas phase transfer of these volatile halides was found to be the main mechanism for the redispersion. On alumina, on the other hand, they postulate the formation of a stable and mobile $[Pt^{IV}Cl_x]$ species which is responsible for the redispersion. The role of the chlorine attached to the alumina was not discussed.

In our systems, the vapor transport of chlorinated platinum or chlorinated aluminum species can be undoubtedly excluded from the discussion because the probability of readsorption of gaseous species under vacuum conditions is extremely low. The mechanism, thus, has to involve the formation of mobile surface species.

If the alumina islands grew taller (Fig. 4.8) in the presence of chlorine these species could be mobile $AlCl_x$ or perhaps AlO_xCl_y species. On the other hand, if platinum particles migrate on top of AlO_x islands it is more likely that chlorinated platinum species similar to the ones postulated by Lieske *at al.* [10] are responsible for the observed trends.

We tend to believe that chlorine (and oxygen) aided transport of platinum atoms is responsible for the higher platinum surface area. We have shown that if chlorine is present on the platinum surface (Figs. 4.6 and 4.7), after the deposition of the amount of AlO_x sufficient to block a chlorine free platinum foil, the fraction of the accessible platinum surface does not change anymore. This can be easily explained by the platinum migration model. As we are depositing the alumina more and more platinum covers the alumina as well, but as soon as the alumina layer is completed no more chlorine can adsorb on the surface, and there is no more platinum available for transport. It would be difficult to explain why the alumina islands grew taller while occupying the same surface area after 40-50 minutes of deposition (Figs. 4.6 and 4.7).

If the platinum migration model is correct, one would think that the platinum surface area could be increased at any AlO_x coverage, as long as platinum atoms area available on the substrate. But it is not the case. If we stop the deposition, say, at 30 minutes and try to 'redisperse' the catalyst by $CHCl_3$ + O_2 treatments after reaction, the maximum surface area we can get is the initial one. This observation implies that the number of platinum atoms on the substrate available for transport is limited and/or the partially oxidized aluminum species that arrive on the chlorinated platinum during the preparation procedure also play a role in the transport of platinum atoms.

If chlorine really helps to spread the platinum atoms from an annealed foil, on which the number of available platinum atoms is limited, one would expect that a sputtered foil behaves differently. And we can assume that mobile chlorine containing species would form more readily on a rough surface.

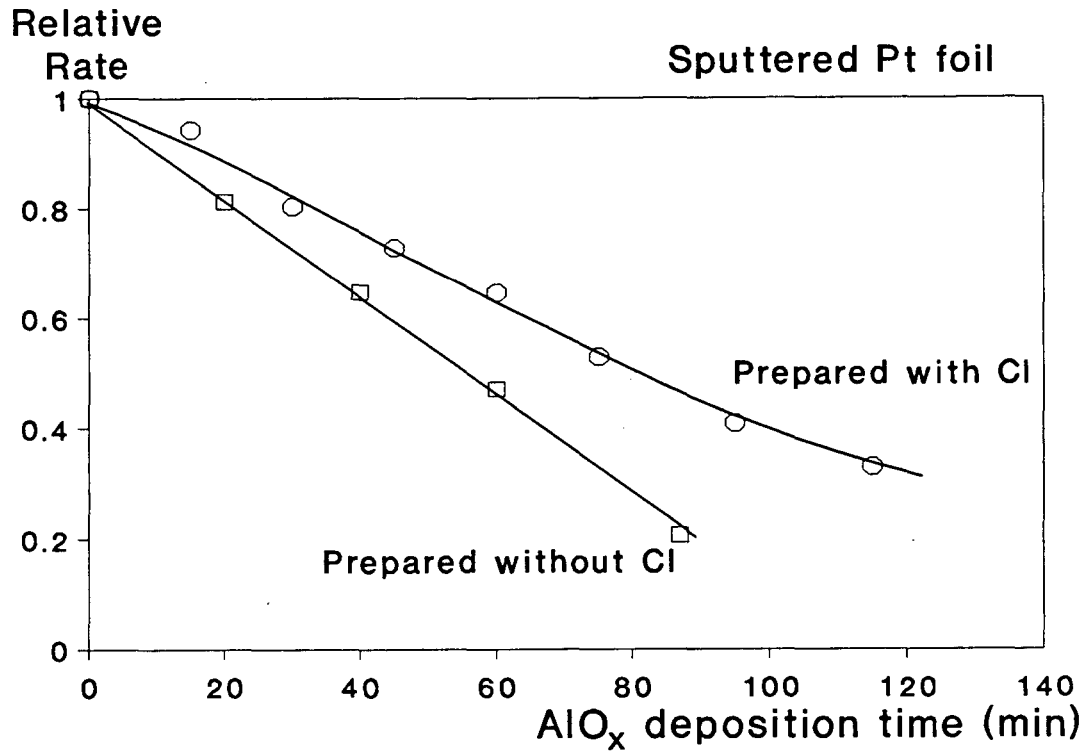

Fig. 4.9 The relative rate of MCP hydrogenolysis as a function of AlO_x deposition time for argon ion beam sputtered platinum substrate.

In Fig. 4.9 we show the relative rates for an initially sputtered platinum foil. Argon ion sputtering increases the surface roughness, and, based on CO TPD and the initial MCP hydrogenolysis rate, 40% more platinum is exposed than on the annealed clean foil. As we increase the amount of alumina on the chlorine free platinum surface, the activity decreases as expected (Fig. 4.9). Due to the higher initial platinum surface area, the initial slope is not as steep as for the annealed platinum foil (Fig. 4.7); at a given amount of alumina deposition, a smaller fraction of the surface gets covered. Similarly to the annealed platinum substrates, we find that presence of chlorine during the deposition influences the platinum surface area.

To determine if the chlorine is more effective redispersing agent on an annealed or on a sputtered platinum foil, let us consider the following simple model (Fig. 4.10). Let us assume that the Pt coverage on the AlO_x, at the early stages of

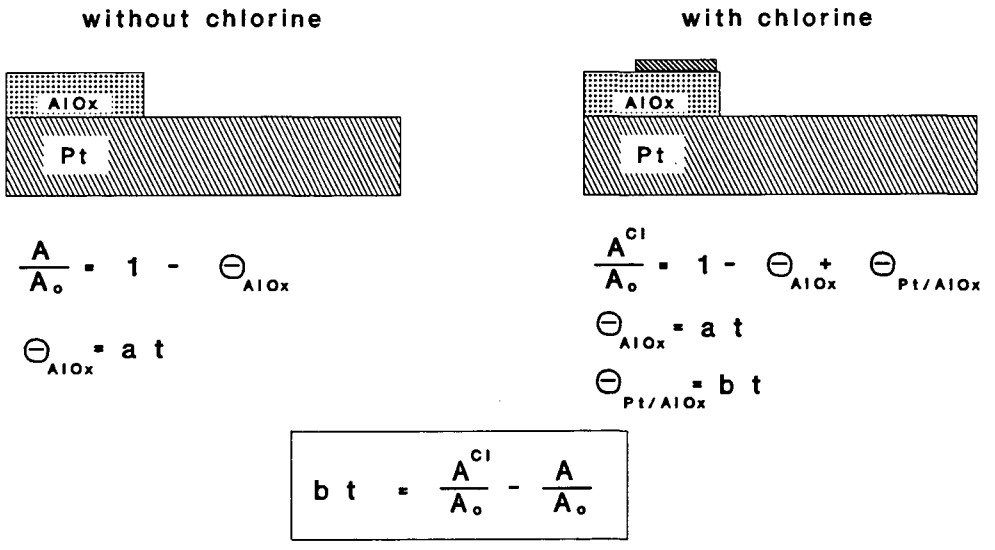

Figure 4.10 Model for 'redispersion' of AlO_x/Pt catalysts.

deposition, is a linear function of the deposition time and that the deposition rate of AlO_x (a in the model) is constant. The total platinum surface area has two contributions: uncovered platinum foil and the newly formed platinum islands on the AlO_x. In this model b is the rate of formation of the platinum layer on the AlO_x islands. Using the boxed expression in Fig. 4.10 (from Figs. 4.7 and 4.9) we can calculate b for the annealed and sputtered platinum foil. The values are 8×10^{-3} A_o^a/min and 2.5×10^{-3} A_o^s/min, respectively, where A_o^a and A_o^s are the initial surface areas of the annealed and sputtered platinum foil. The absolute surface areas are not known, but the A_o^s/A_o^a ratio can be calculated from CO TPD and equals to 1.4. Thus the rate of formation of platinum islands is about a factor of two larger on annealed platinum foil. One would expect that the formation of platinum-chlorine(-oxygen) species is enhanced on a more open, sputtered surface so it appears that the mobility of such species is smaller.

In Fig. 4.11 we show the selectivity of MCP hydrogenolysis over our model catalysts prepared on annealed platinum foil in the absence and in the presence of chlorine. The proportion of the 2MP, 3MP and nHx changes with reaction time and the activity decreased rather dramatically. In this discussion we consider only initial

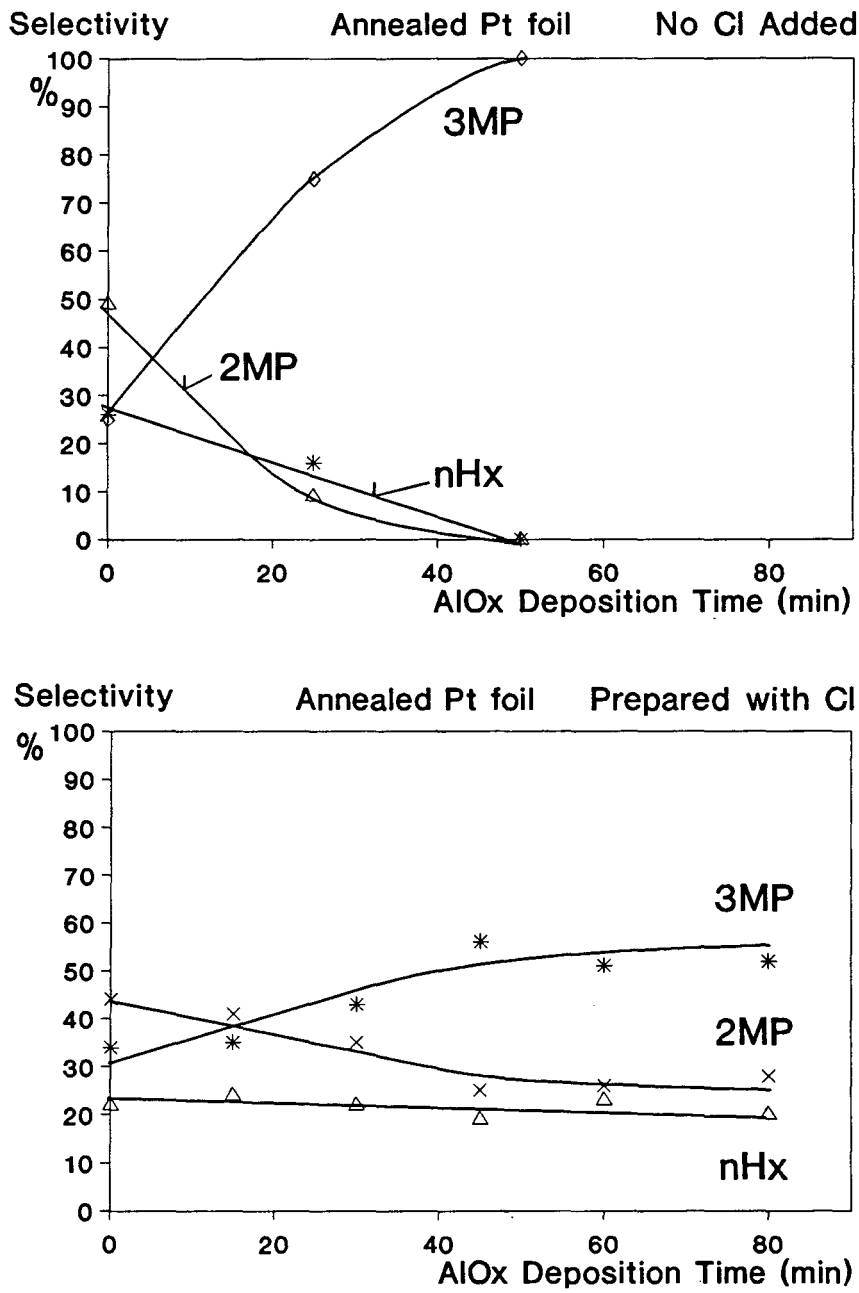

Fig. 4.11 Selectivity of MCP hydrogenolysis over model catalysts prepared on an annealed platinum foil in the absence and in the presence of chlorine. (T=620 K, p_{H2}=1 atm, H_2/MCP=240)

rates and initial selectivities. The change of selectivity pattern with conversion will be discussed in Chapter 4.4, where we compare these 'inverse' catalysts with the ones prepared by platinum vapor deposition on AlO_x/Au.

Over clean platinum foil, the initial selectivity pattern is different from the reported selectivities for supported platinum catalysts [17]. It cannot be described as a linear combination of two hypothetical selectivity patterns (selective and statistical) and the fraction of the nHx is much higher than expected. Which means that the ring opening mechanism is mechanism C described by Gault [17] and it involves the consecutive isomerization of acyclic products. We calculated the thermodynamic equilibrium compositions for the three hexane isomers. In Fig. 4.12 we plot this calculated thermodynamic product distribution with the hypothetical and experimental selectivities reported in the literature as well as the initial distribution found in this work. We also find that the selectivities are temperature dependent which further supports the contention that the ring opening mechanism on clean platinum foil is mechanism C. According to this mechanism the lifetime of the surface intermediates is long enough that an equilibrium mixture of the acyclic

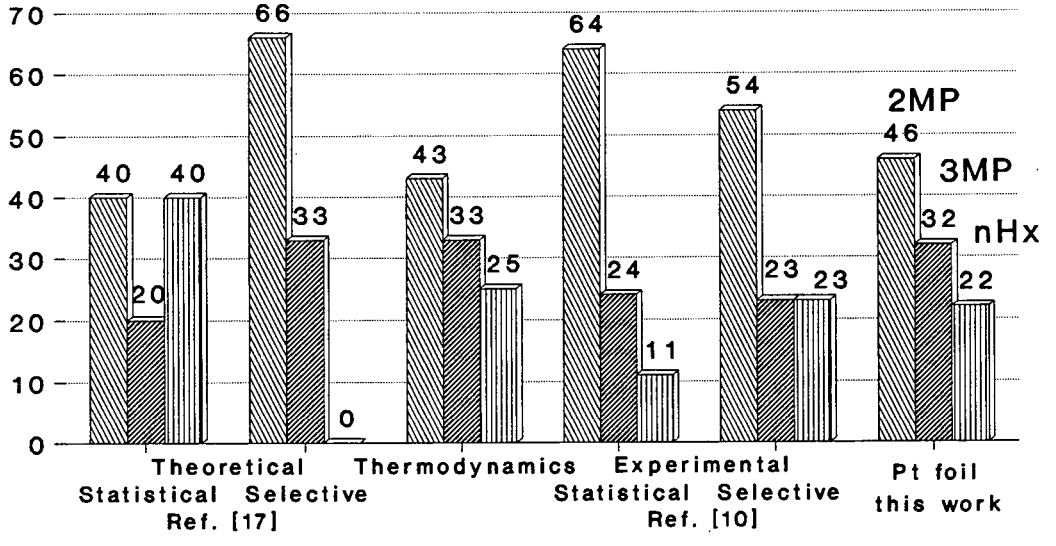

Fig. 4.12 Comparison of MCP ring opening selectivities on platinum.
3MP = 3-methyl-pentane, 2MP = 2-methyl-pentane and nHx = n-hexane.

products can form. The rate limiting step is most probably the desorption of the hexanes.

As we deposit alumina on the platinum foil the product distribution changes rather dramatically (Fig. 4.11). According to Kramer and Zuegg [16] the MCP hydrogenolysis proceeds on both the metal particles and at the boundary of the particles and the support. Based on their findings, we expected that the product distribution would shift from the thermodynamic distribution toward a more characteristic statistical one, since by depositing alumina we gradually increase the length of the boundary. This is clearly not the case. As we increase the AlO_x coverage on chlorine free platinum foil more and more 3MP forms, and the fraction of the 2MP and nHx decreases.

As we have mentioned the selectivities change with time also. But even at higher conversion (reaction time), there is significant deviation from the expected linear combination of selective and non-selective mechanisms. (See Chapter 4.4.)

The chlorine does not influence the initial selectivity trends (Fig. 4.11), probably because it leaves the surface almost instantaneously under reaction conditions. It is interesting that initially the selectivities change with increasing amount of AlO_x, but as the number of surface platinum atoms becomes constant, the selectivity pattern remains unchanged. If our platinum migration model is correct this implies that the reaction takes place on two distinct areas. On the platinum foil between the AlO_x islands and on the platinum atoms (maybe particles) on the AlO_x.

In the absence of chlorine the alumina islands get larger and finally coalesce. Just before the complete coalescence of the islands only small platinum ensembles are available for reaction. The MCP molecule, due to steric hindrance, can approach these small platinum ensembles such that only the C-C bond opposite to the methyl group can interact with them. This interaction results in the cleavage of this C-C bond, and the sole product is 3MP.

On samples prepared in the presence of chlorine, it is likely that platinum species migrate on top of the AlO_x islands. After the deposition of a monolayer

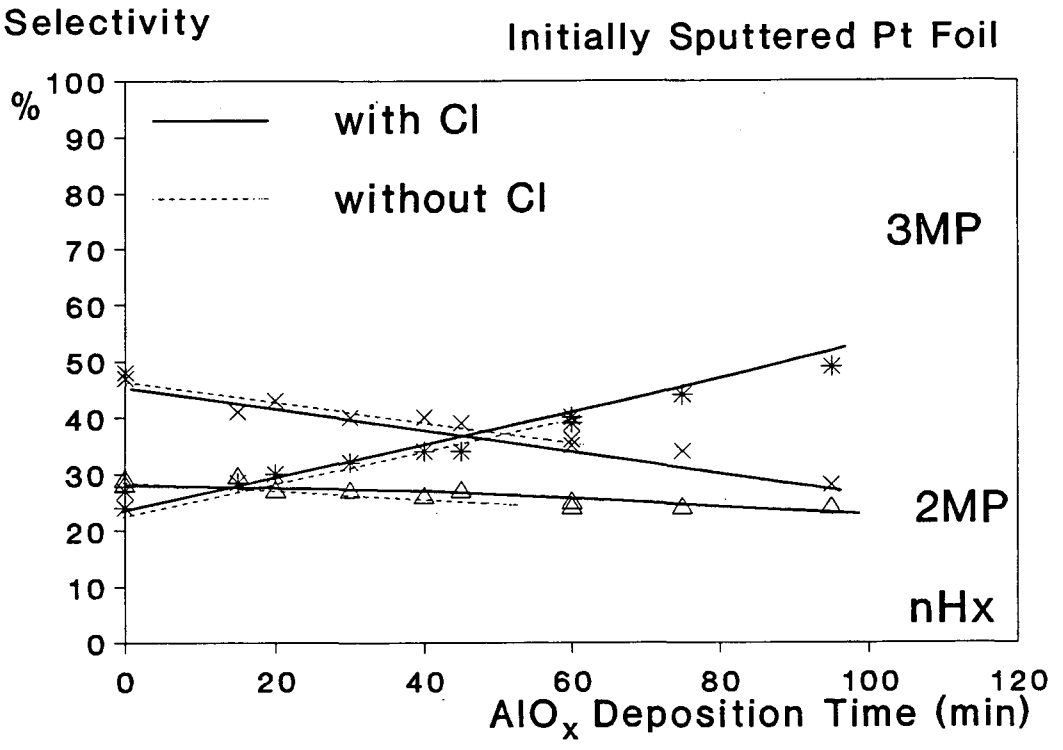

Fig. 4.13 MCP selectivity over model catalysts prepared on sputtered platinum foil in the presence and in the absence of chlorine.

equivalent of alumina (40-50 min) the surface platinum atoms are located mostly on the alumina. Based on the selectivities we can conclude that the ensembles on top of the alumina are similar to the ones on the platinum foil between the alumna islands. But because the steric hindrance is not as pronounced as between the islands an intermediate product distribution is observed, an intermediate between the thermodynamic and the geometrically selective distributions.

The product distribution for catalysts prepared on sputtered platinum foil is shown in Fig. 4.13. The trends are similar here to the ones observed on annealed foils. The 3MP selectivity increases, the 2MP selectivity decreases with increasing AlO_x coverage and the nHx selectivity is almost independent of the amount of alumina deposited.

These selectivity changes on the sputtered platinum substrate are not as dramatic as on the annealed foil. On the annealed foil we have assumed that the increase in 3MP selectivity is due to the steric hindrance at close to full AlO_x coverage. Thus 3MP selectivity can be a measure of the accessibility of platinum atoms. As we increase the coverage on the sputtered foil the number of platinum ensembles with limited accessibility slowly increases. There is no difference in selectivity pattern between catalysts prepared in the absence and in the presence of chlorine primarily because it is removed from the surface under reaction conditions. So any effect it might have, has to be indirect, through the size of the platinum ensembles exposed. And it seems that there is no difference in this respect between samples with and without chlorine. The surface platinum atoms on the rough surface probably have similar properties to platinum atoms that have migrated on top of the alumina islands.

We have shown that the 'inverse' AlO_x/Pt catalysts exhibit some similarities to the practical catalysts. When the model catalysts are prepared in the presence of chlorine the platinum surface area is always higher after a given amount of alumina is deposited.

4.3 $Pt/AlO_x/Au$ and $Pt/Cl/AlO_x/Au$

We want to compare our model AlO_x/Pt catalysts to the more realistic model system of $Pt/AlO_x/Au$. In the previous chapter we saw that the product distribution on AlO_x/Pt catalysts was different from the reported distributions of alumina supported platinum particles [10,17]. In the case of catalysts prepared in the presence of chlorine, unusually high 3MP selectivity was observed at high alumina coverages. If our interpretation of these results that platinum atoms migrate on top of the alumina islands, in the presence of chlorine, is correct, one would expect a similar product distribution when platinum is deposited on

AlO_x/Au. In addition we would like to compare oxygen and oxygen+chloroform treatments as to their ability to increase the platinum surface area.

4.3.1 Experimental

Aluminum was deposited on a clean gold foil (0.025 mm) mounted on two 0.51 mm diameter gold wires in the presence of $1x10^{-8}$ torr oxygen for 120 minutes. To make sure that the aluminum is fully oxidized the sample was heated to 570 K in $1x10^{-5}$ torr oxygen for 10 minutes. After this deposition procedure no gold could be detected by AES.

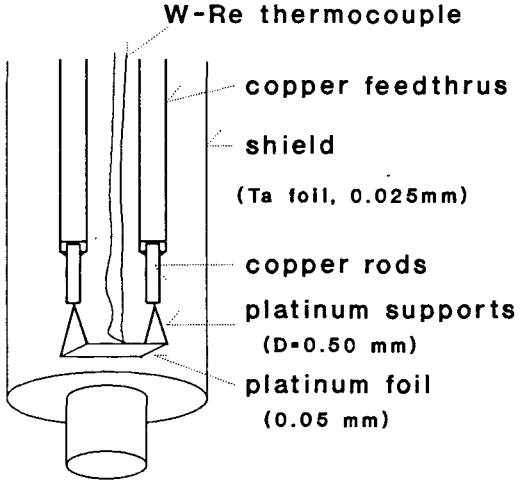

Fig. 4.14 Platinum source.

The platinum source consisted of a 3x15x0.051 mm platinum foil (99.99%) mounted on two platinum wires (Fig. 4.14). The platinum foil was outgassed by heating to 1600-1700 K after the first introduction to the UHV chamber for at least 72 hours. During outgassing occasionally (4-5 times) oxygen was introduced into the chamber at 10^{-5} torr for one-one hour to remove carbon. After this cleaning procedure pure platinum could be deposited on the AlO_x/Au substrate. The sample to source distance was about 2 cm. The temperature of the platinum foil was kept at 1500 K at all times, and only 10 minutes before deposition was it raised to the deposition temperature (1800 K). The deposition was carried out at < $2x10^{-9}$ torr.

To investigate the effect of chlorine on the redispersion, the catalysts were exposed to 100 L chloroform at 570 K prior to the oxygen treatment. On platinum

foil this exposure was sufficient to produce a saturation Cl coverage. Under these conditions the AlO_x could not be chlorinated. Even after chloroform treatments at pressures as high as 90 torr (at 470 K), we could not detect chlorine on the surface.

In order to incorporate chlorine in the AlO_x we had to develop a more drastic method. During exposure to 6,000 L of chloroform at 570 K we turned on the ion gun (emission current 20 mA and beam voltage 300 V) to generate positively charged $CHCl_{3-x}$ and Cl species and accelerate them toward the substrate. In this process carbon also deposited on the surface, but it could be easily removed by a 1,200L oxygen treatment at 770 K. The chlorine on AlO_x/Au was stable in UHV, and even after hydrogen treatment under reaction conditions (620 K, 1 atm) 70-80% of chlorine was still present.

Three sets of experiments were carried out by repeating the following cycles.
A. $Pt/AlO_x/Au$. Deposit platinum - characterize with AES and CO TPD - run MCP hydrogenolysis (1 atm H_2, 620 K, see Chapter 4.2.1 for details)- AES, CO TPD - oxygen treatment (1,200 L, 770 K) - AES.
B. $Cl/Pt/AlO_x/Au$. Deposit platinum - AES, CO TPD - run MCP hydrogenolysis (1 atm H_2, 620 K) - AES, CO TPD - 100 L $CHCl_3$ at 570 K - oxygen treatment (1,200 L, 770 K) - AES.
C. $Cl/Pt/Cl/AlO_x/Au$. Deposit platinum on $AlO_x/Cl/Au$ - AES - MCP hydrogenolysis (1 atm H_2 at 620 K) - AES - Cl sputtering (see conditions above) - oxygen treatment (1,200 L, 770 K) - AES.

4.3.2 Results and Discussion

This platinum-on-alumina model system is probably the closest to the real life catalysts. To find out if it possesses the redispersion properties of alumina supported platinum particles we performed the following CO TPD study.

Altman and Gorte studied the temperature programmed desorption of CO from small metal particles vapor deposited on oxidized aluminum prepared on a

tantalum foil [28]. In agreement with their results, we find that the surface area of platinum is always 25-30% higher on freshly vapor deposited samples than on the same sample after subsequent TPD runs. This indicates that during the first TPD or any heat treatment in vacuum the platinum particles irreversibly aggregate to form stable particles. In this study, all of our samples (even the ones labelled as 'fresh') had been heated at least once to 800 K after deposition and before the CO TPD. CO TPD showed two features at 540 and 480 K (Fig. 4.15), at somewhat higher

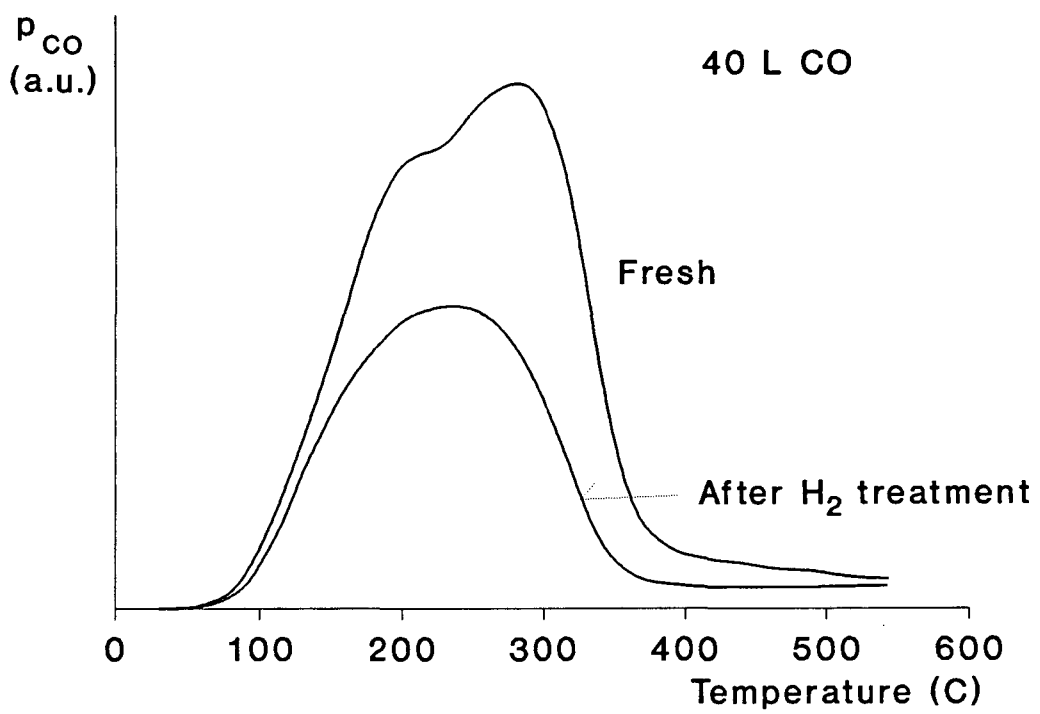

Fig. 4.15 Typical CO TPD peak shapes before and after hydrogen treatment.

temperatures than reported by Altman and Gorte [28]. They reported that the shape of the CO TPD peaks changes with particle size. Based on qualitative comparison of their results and ours we estimate that the platinum particle size is about 1-4 nm [28].

In Fig. 4.16 we show the CO TPD areas relative to the fresh (but heated once) sample after each consecutive treatment indicated. From the figure it is clear

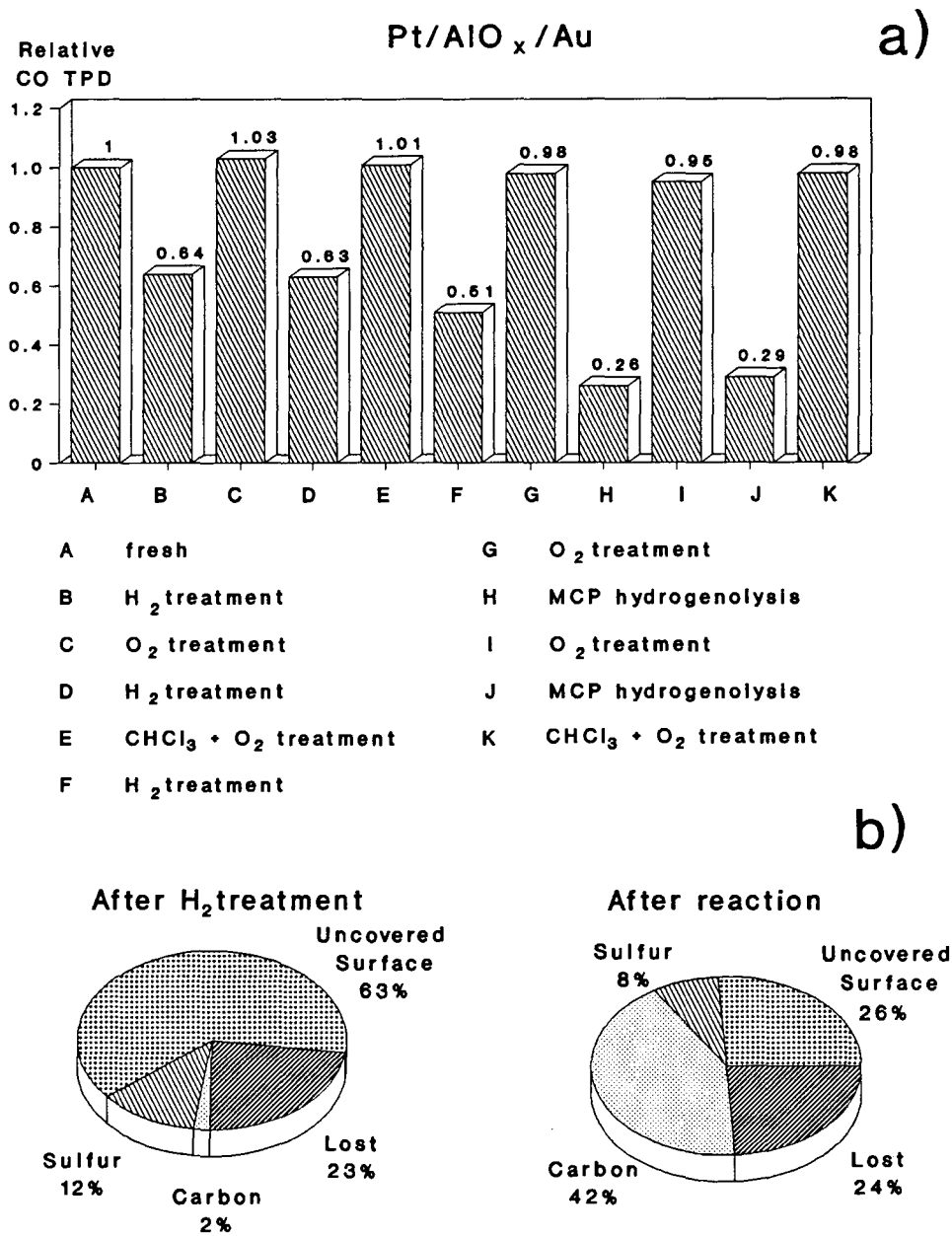

Fig. 4.16 a) Relative CO TPD areas as a function of catalyst treatments. For conditions see text. b) Total platinum surface area after hydrogen treatment and MCP hydrogenolysis. Lost surface area refers to the decrease of surface area.

that none of the regenerating treatments can increase the platinum surface area above the initial value.

Fig 4.16B: The freshly prepared sample was introduced in the high pressure cell and heated in 1 atmosphere of hydrogen at 620 K for 30 minutes. The CO TPD curves are shown in Fig. 4.15. Auger electron spectroscopy indicated that after the hydrogen treatment some sulfur and carbon was present on the sample. (The sulfur is possibly coming from sulfur containing contaminants in the hydrocarbons used in this study.) According to calibrations on single crystal surfaces [18,25] we estimate that the sulfur and carbon coverage was 12% and 2% of a monolayer, respectively. Taking into account these coverages, the total platinum surface area decreased by approximately 23%.

Fig 4.16C,D: Subsequent oxygen treatment at 770 K restores the initial surface area.

Fig 4.16E: We wanted to see if the presence of chlorine on the platinum can influence this regeneration process. We have shown that 100 L chloroform exposure at 570 K selectively deposits chlorine on the platinum. We find that the final platinum surface area after a combined $CHCl_3$ + O_2 treatment is equal to the initial area and not larger than after oxygen treatment alone. This means that saturation coverage chlorine attached to platinum does not influence the regeneration process.

Fig 4.16H: After MCP hydrogenolysis the platinum surface area is 70-75% smaller. Using Auger electron spectroscopy the carbon coverage can be estimated from the C(272 eV)/Pt(237 ev) [18] peak ratio and it is about 0.4 monolayers. After reaction ca. 0.08 monolayer of sulfur was also present. Thus, the following balance can be written: 8% is covered with sulfur, 42% is covered with carbon, from CO TPD, 26% of the platinum surface is still available, and the total platinum surface area decreased by 24%. The decrease of total platinum surface area is about the same in both cases. The pie charts on the bottom of Fig. 4.16 indicate the surface composition after hydrogen treatment and after MCP hydrogenolysis. 100% represents the total initial platinum surface area after deposition.

Fig 4.16I,J and K: Clearly, one oxygen treatment is sufficient to regenerate the catalyst surface after MCP hydrogenolysis, and the presence of chlorine does not seem to influence the regeneration process as far as the final platinum surface area is concerned.

In Figs. 4.17 and 4.18 we compare the properties of two series of $Pt/AlO_x/Au$ catalysts, with increasing platinum content, using oxygen and chloroform+oxygen regenerating procedures as described in the experimental (**A** and **B**).

With increasing amount of platinum on the AlO_x (**A.**) the platinum surface area increases, indicated by CO TPD (Fig. 4.17), AES and MCP hydrogenolysis rate (Fig. 4.18). As we change to $CHCl_3+O_2$ regeneration procedure (**B.**), however, it appears that the platinum surface area/unit amount of platinum deposited is larger. This can only be possible if the dispersion of the platinum particles is larger. And it would be in agreement with the widely believed role that chlorine plays in redispersion of platinum [10,22]. But, the MCP hydrogenolysis rate does not follow

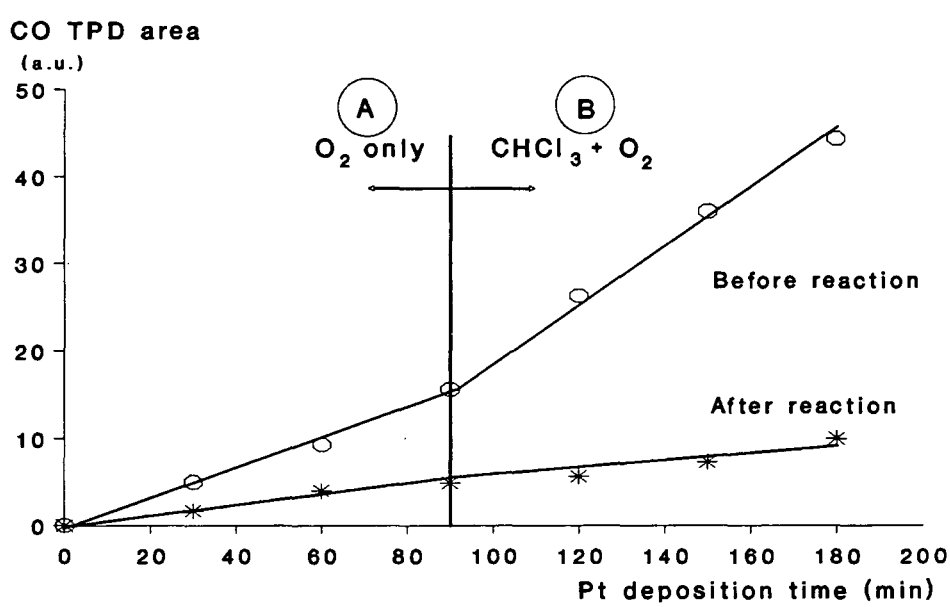

Fig. 4.17 Total CO TPD area as a function of platinum deposition time and regeneration conditions. **A** and **B** refer to sample preparation and regeneration procedures described in Chapter 4.3.1.

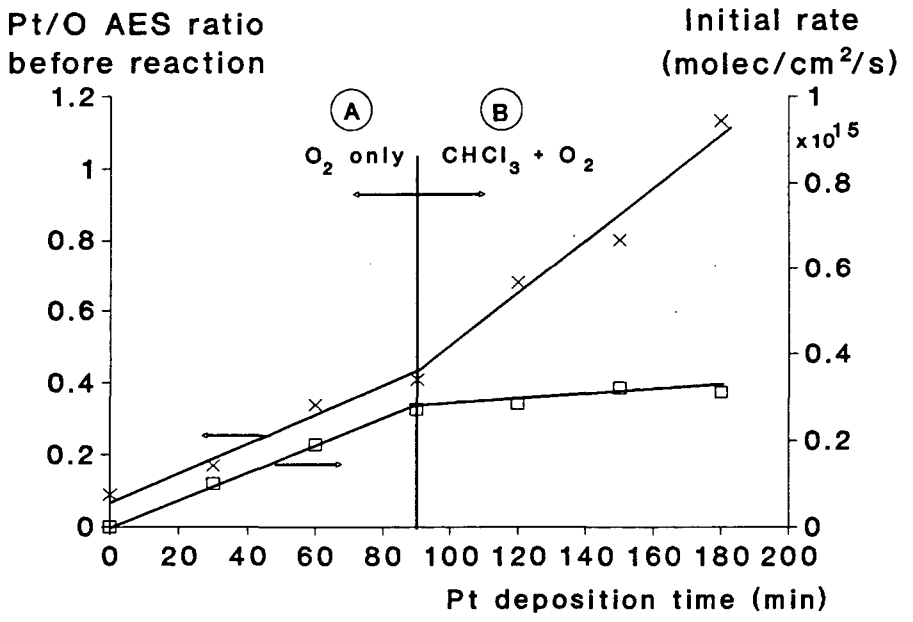

Fig. 4.18 The intensity ratio of the Pt (237 eV) and O (512 eV) Auger peaks asa function of platinum deposition time and regeneration conditions. **A** and **B** refer to sample preparation and regeneration procedures described in Chapter 4.3.1.

the same trend. It hardly increases with increasing amount of platinum (Fig. 4.17). At the same time, the platinum surface area after reaction, measured by CO TPD, (Fig. 4.22) increases independently of the type of the regeneration process.

The facts that the dispersion is higher in UHV, as indicated by CO TPD, and, yet the activity hardly increases with platinum deposition, suggest that the platinum particles are not stable in hydrogen atmosphere, if the regeneration involved the chlorination step. This instability leads to a quite rapid loss of platinum surface area in hydrogen atmosphere. In agreement with this, if we go back to Fig. 4.16, although at the time those results were discussed it did not seem significant, we find that after $CHCl_3+O_2$ treatment the platinum surface area was approximately 10% less than after oxygen treatment alone.

Assuming a constant platinum flux, from the change of slope in Fig. 4.17 we can estimate the upper limit of the change in dispersion due to chloroform regeneration. The ratio of the slopes is about two, e.i. the dispersion is about twice

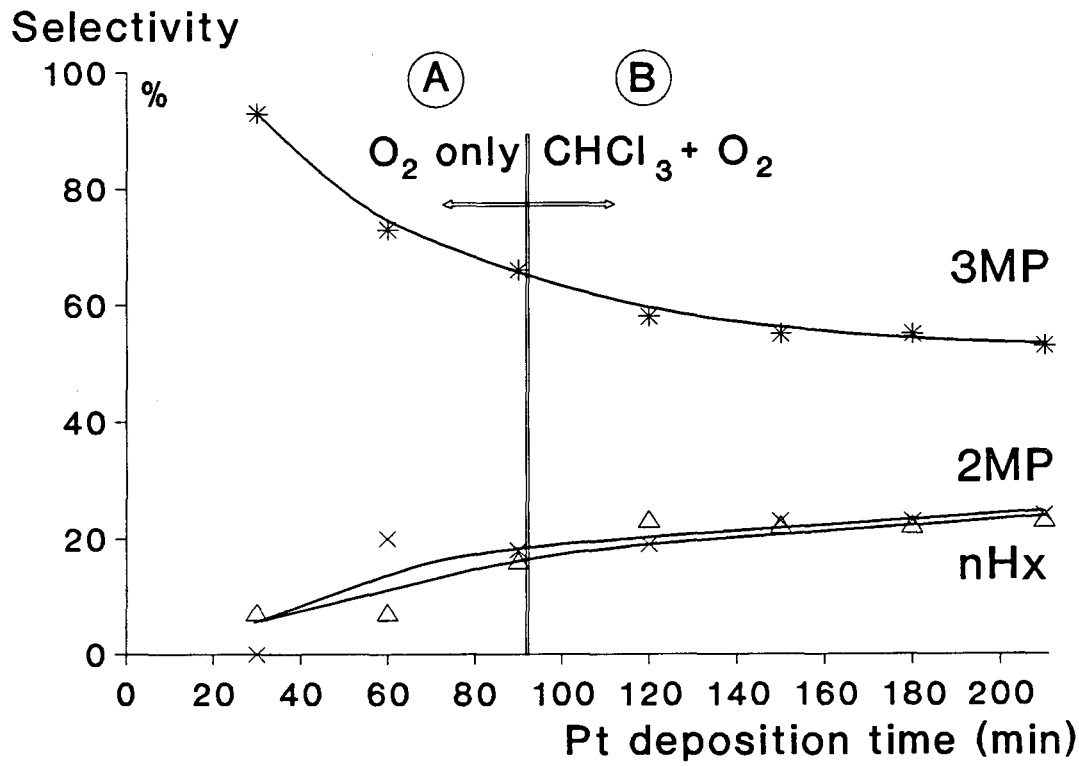

Fig. 4.19 Product distribution for methyl cyclopentane (MCP) hydrogenolysis over model Pt/AlO$_x$/Au catalysts. **A** and **C** refer to sample preparation and regeneration procedures described in Chapter 4.3.1.

of that of the oxygen regenerated samples. This is the upper limit because it has been suggested [27] that the stoichiometry of adsorption is not CO : Pt = 1 : 1 on highly dispersed platinum particles, but can be 20-30% higher.

Why is it that we did not see an increase in surface area in the previous experiment when we were studying the redispersion properties of larger platinum particles? Since there was no difference between the final platinum surface area after oxygen and oxygen+chloroform regeneration, it appears that chlorine cannot redisperse already existing larger particles. But it *can* stabilize small particles and it prevents aggregation. This latter effect can be observed in UHV only, and these smaller particles are much less stable in hydrogen.

The product distribution of MCP hydrogenolysis is shown in Fig. 4.19a Initially, when only small platinum particles are present the sole product is 3MP.

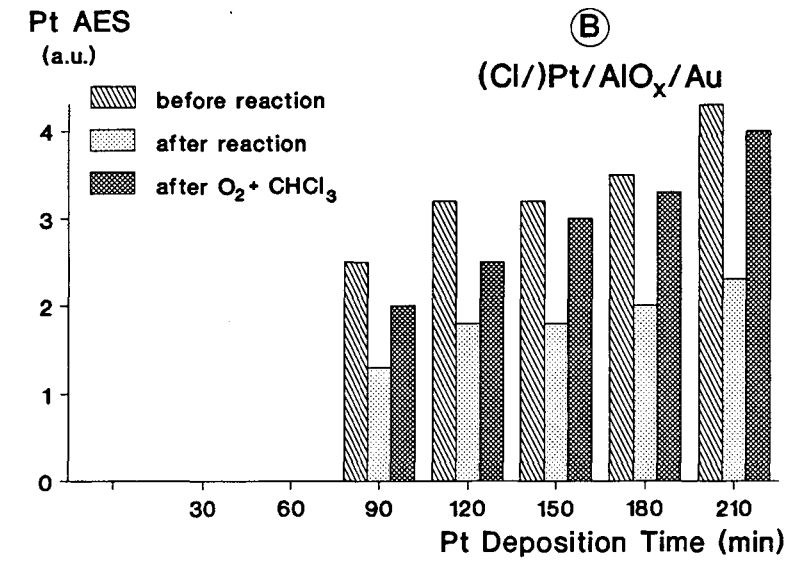

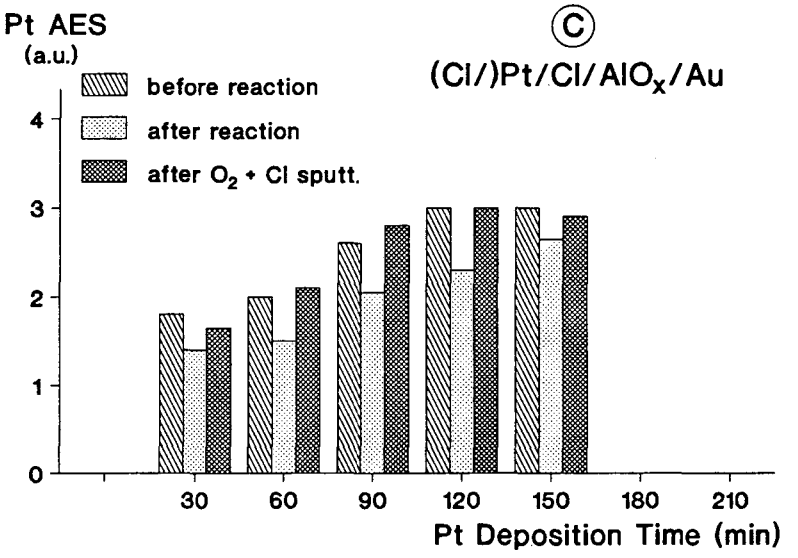

Fig. 4.20 The intensity of the Pt (237 eV) peak before reaction, after reaction and after regeneration as a function of deposition time. **B** and **C** refer to sample preparation and regeneration procedures described in Chapter 4.3.1.

As the platinum concentration increases the selectivity toward 3MP decreases. It is interesting that the trend here is just the opposite of what we saw in the 'inverse' system. There, the initial product distribution on clean platinum was close to the equilibrium mixture of hexanes (Fig. 4.11b), and as we increased the AlO_x coverage on an annealed foil the 3MP selectivity increased. We will return to the comparison of the two model AlO_x/(Cl/)Pt and (Cl/)Pt/AlO_x/Au systems in Chapter 4.4.

In Fig. 4.20 some Auger results are shown to compare catalysts that have chlorine on the platinum only, and ones that have chlorine on both the alumina and the platinum. The intensity of the platinum Auger peak after reaction (second bar) in all cases decreases due to carbon deposition and change in the platinum surface area. The catalyst was then regenerated, the Auger spectra were taken (third bar) and the next deposition took place. From the comparison of the two figures, it is clear that the presence of chlorine on the alumina has an effect on the amount of

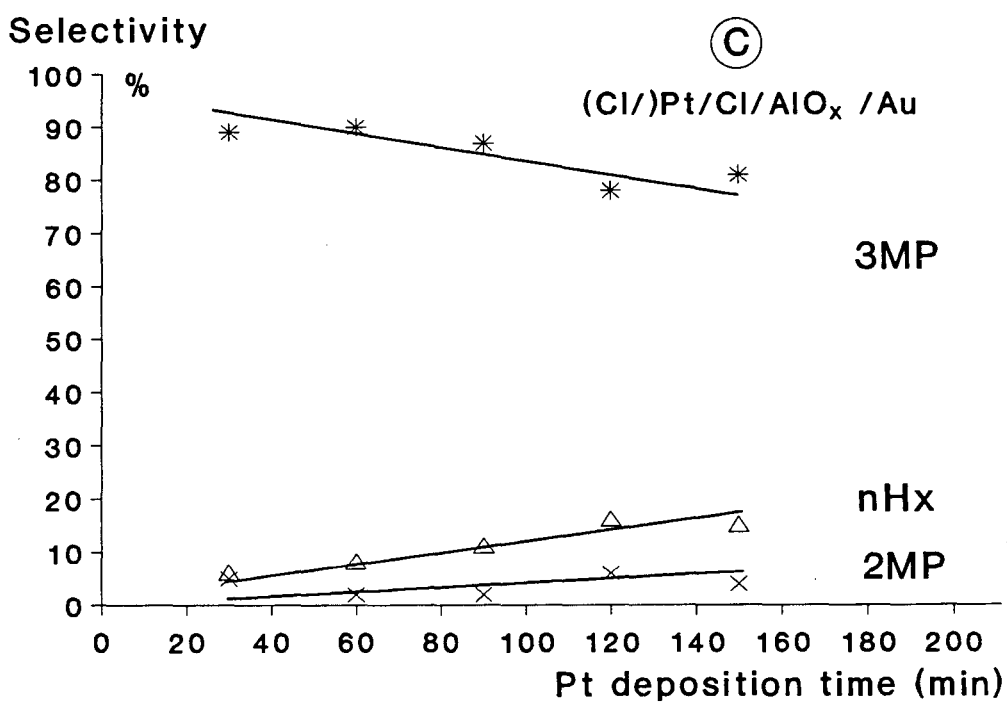

Fig. 4.21 MCP ring opening selectivity on (Cl/)Pt/Cl/AlOx/Au model catalysts as a function of platinum deposition time.

platinum present after reaction. It is interesting that the 'loss' of platinum due to carbon deposition and sintering is less pronounced if chlorine is present on the alumina. This suggests that the chlorine on the alumina plays a role in stabilizing the platinum particles. As we saw, under reaction conditions, chlorine on the platinum increases the tendency for sintering.

It seems that chlorine has a dual effect on the platinum surface area. If it is attached to alumina it stabilizes the particles and helps to maintain dispersion in UHV. On the other hand, if it is attached to the platinum, as we increase the amount of platinum, larger and larger particles form, indicating that chlorine, in this case, enhances the mobility of the platinum species in hydrogen.

The role of chlorine on the alumina as a stabilizing component can be inferred from the product distribution as well (Fig. 4.21). We saw that, possibly due to geometric effects, small platinum ensembles selectively produce 3MP. The 3MP selectivity remains high and does not decrease as rapidly as in the absence of chlorine with increasing amount of platinum.

Chlorine on the alumina influences the regeneration process too (Fig. 4.20b). A complete regeneration can only be achieved if chlorine is present on both the alumina and the platinum before reaction. In this case the before and after reaction surfaces are identical by CO TPD and AES.

4.4 Pt/(Cl/)AlO_x/Au and AlO_x/(Cl/)Pt - Summary

In surface science studies, it is more convenient to use 'inverse' catalytic systems instead of their 'real life' counterparts. By investigating both in this study, we can point out the similarities and differences between them.

As we have mentioned in Chapter 4.2.2, the ring opening selectivities change as the reaction proceeds. In Fig. 4.22 we plot the 3MP/2MP and the 2MP/nHx ratios for all experiments, as a function of conversion for the three systems: AlO_x/Pt, Pt/AlO_x/Au and Pt/Cl/AlO_x/Au.

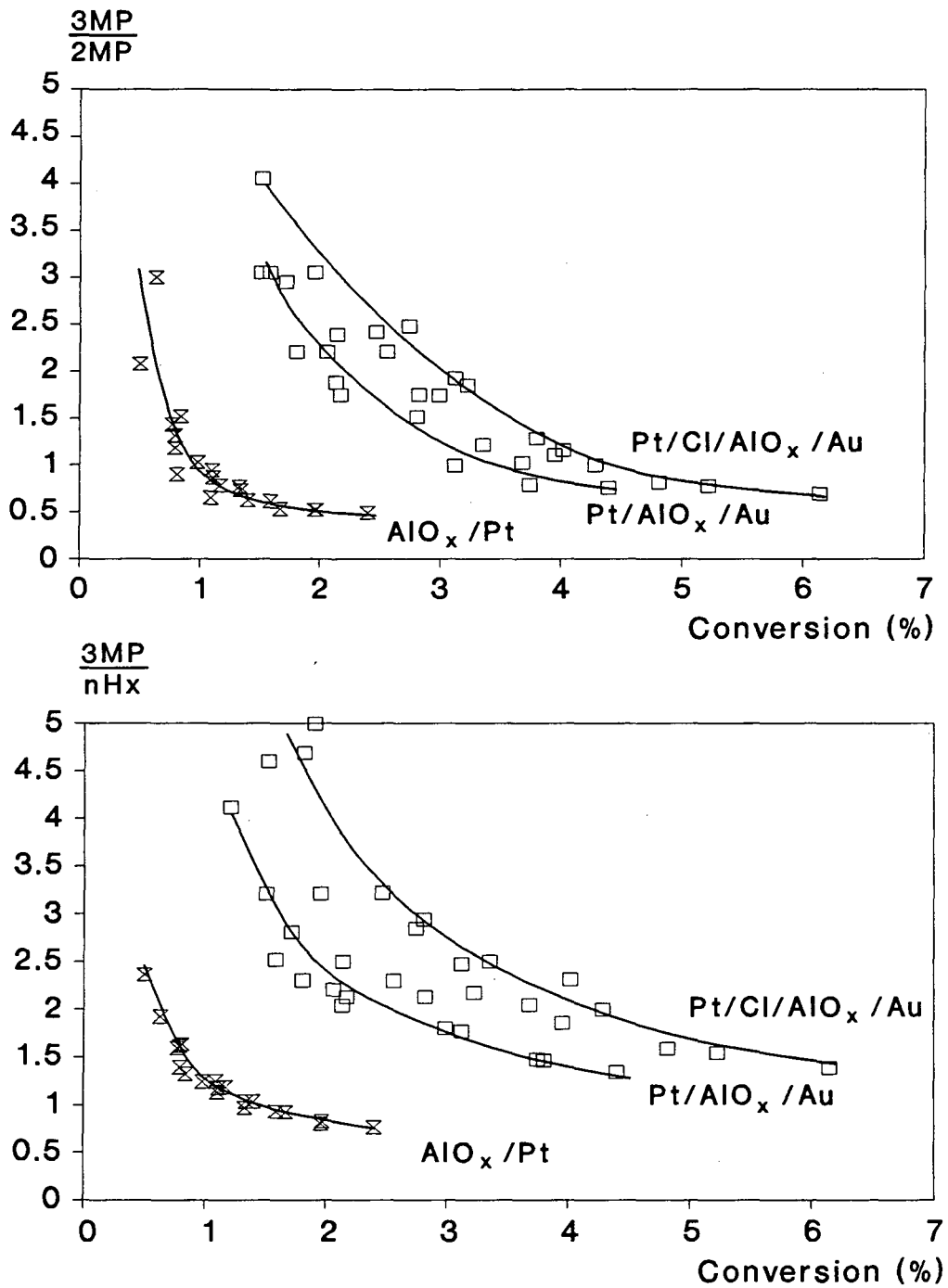

Fig. 4.22 3MP/2MP and 3MP/nHx ratios for catalysts AlO_x/Pt, Pt/AlO_x/Au and Pt/Cl/AlO_x/Au as a function of MCP conversion.

At low conversions 3MP dominates the products. It is remarkable that all three systems behave very similarly in the limit of zero conversion. It is difficult to extrapolate what the selectivity pattern is in this limit, but 75-100% 3MP, 0-15% 2MP and 0-15% nHx is our best estimate. This low conversion is realized if small platinum ensembles are exposed on the surface of either alumina-on-platinum or platinum-on-alumina. Because of steric hindrance, the C-C bond opposite to the methyl group can interact with these small ensembles and the major product is 3MP. We can speculate that acid-base interaction between the proton on the tertiary carbon atom and a coordinatively unsaturated aluminum ion in the AlO_x layer assists this mechanism. This selectivity pattern has not been reported in the literature.

As the reaction proceeds the 3MP selectivity decreases, and even catalysts that initially produced exclusively 3MP start to generate the other two hexane isomers (Fig. 4 22). This shift of selectivity in time can be due to changing surface composition of the platinum particles (product poisoning or carbon deposition), to change in the platinum surface area or to the restructuring effect of hydrogen. If the reaction is interrupted and restarted without cleaning, the product distribution is the same as on the fresh and clean sample. This indicates that the carbon deposits or the change in the particle size cannot be held responsible for the changes in the selectivity pattern. It appears then that either reversible product poisoning or hydrogen induced changes in the local structure of the platinum surface causes the selectivity to change with time. The high conversion limits for the systems are summarized in Table I.

The selectivity patterns for the selective and statistical ring opening of the MCP postulated by Gault and co-workers [14,15,17] are indicated in Fig. 4.1. According to these schemes n-hexane forms only in the statistical process (mechanism A). Thus, assuming the 3MP : 2MP : nHx = 1 : 2 : 2 ratio, we can calculate the selectivity of the 'selective' process (Table I).

From the results it is clear that there is a significant difference between the platinum-on-alumina and the alumina-on-platinum model catalysts. In case of the

Table I.

	Observed high conversion limit %	Ring opening Statistical %	Ring opening Selective %
AlOx/Pt			
3MP	19	15	4
nHx	30	30	0
2MP	51	30	21
		75	25
Pt/AlO_x/Au			
3MP	25	12	13
nHx	25	25	0
2MP	50	25	25
		62	38
Pt/Cl/AlO_x/Au			
3MP	22	18	4
nHx	35	35	0
2MP	43	35	8
		88	12

inverse system (AlO_x/Pt) the product distribution cannot be described as a linear combination of the two postulated distribution at any conversion which is indicative of 'mechanism C' [14,15,17]. In Chapter 4.2.2 we showed that the initial product distribution was close to the equilibrium mixture of the three hexanes. The presence of chlorine on the platinum did not influence this pattern.

On the other hand, platinum-on-alumina catalysts produced a linear combination of the two limiting distributions. Similarly to the inverse system, the chlorine did not affect the distribution if attached to the platinum. But there is a significant shift in product distribution if the alumina is chlorinated. From observed selectivities we can calculate the ratio of selective and statistical ring opening. If

chlorine is present on the AlO_x, mechanism A (statistical ring opening) accounts for 88% of the products while in its absence only 62%. This further supports our claim that the particle size is smaller in this case, because it has been generally accepted [14,15,17] that the statistical ring opening is more dominant on highly dispersed platinum.

The literature offers two explanations for this. As discussed earlier, Kramer and Zuegg [16] suggested that the platinum - alumina boundary is responsible for the statistical ring opening. While earlier studies claimed that the shift in selectivity is due to particle size effect [15]. On large particles more than one MCP molecule can adsorb. The secondary-tertiary carbon-carbon bonds are sterically hindered and the products are mainly 2MP and 3MP. On small particles, only one MCP molecule can interact with one platinum atom of a small particle and the probability of the cleavage of the C-C bonds is purely statistical.

We have prepared platinum-on-alumina samples with a broad range of platinum loading. Although we do not have direct measure of the particles size, we believe that chances are that the same dispersion was achieved both ways, prepared in the absence of chlorine on the alumina and in the presence of chlorine on alumina. Yet, the selectivity pattern for the two sets of catalysts is significantly different (Fig. 4.22). Thus, we believe that the shift in selectivity from a more characteristic 'statistical ring opening is due to the presence of chlorine on the alumina.

Anderson and co-workers [3] studied the MCP hydrogenolysis on titania and silica supported platinum particles. They find that Pt/TiO_2 catalysts are more selective for nHx than Pt/SiO_2 catalysts. In essence accepting Kramer and Zuegg [16] explanation for the shift in ring opening selectivity, they explain the results in terms of the difference between the support - platinum boundary. On Pt/TiO_2, there are Ti^{3+} ions, Lewis acid sites, at the interface. The hydrogen atom on the tertiary carbon in a MCP molecule adsorbed near the boundary can interact with a Ti^{3+} site. And this interaction leads to a higher nHx selectivity. Since silica does

not exhibit Lewis acidity the ring opening mechanism is the selective mechanism B [3].

As we discussed in the introductory chapter of this thesis, it is well known that chlorination increases the acidity of aluminas (see refs. [29b] and [30a] in Chapter 1). Thus it is possible that the shift in the selectivity toward a 'more statistical' ring opening (Table I.) is due to the enhanced Lewis acidity at the interface.

The other goal of this study has been to investigate the role of chlorine in the platinum - alumina interaction. We have found that the properties of (Cl/)Pt/AlO_x/Au and AlO_x/(Cl/)Pt systems converge. The initial ring opening selectivities become very similar (55% 3MP, 20-25% nHx and 20-25% 2MP) if chlorine was present on the platinum during preparation (Figs. 4.12 and 4.19). This is an additional piece of information that supports the notion that chlorine aids the transport of platinum atoms on top of the AlO_x islands on annealed platinum.

Just like in the case of practical catalysts, if platinum particles are supported on AlO_x/Au, the platinum surface area decreases under reaction conditions. This decrease can be due to 1) sintering [5], 2) migration of partially reduced alumina species on top of the platinum particles [26] or 3) incorporation of platinum particles in the alumina lattice [29].

We have found that the initial surface area can be regained in an oxygen treatment and the presence of chlorine is not necessary on the platinum. Ruckenstein *at al.* [24a] reported that a sintered platinum catalyst can be regenerated in oxygen treatment in the absence of chlorine. The redispersion of platinum particles can be caused by the fracture of platinum particles or spreading of partially oxidized platinum species. They point out that the redispersion can be explained on the basis of wetting properties of platinum and alumina.

From basic surface thermodynamics it is known that at equilibrium, surfaces are covered with the component that has the lowest surface free energy. Metals, in general, have high surface tensions, but, as it was demonstrated by Buttner *at al.* [30], the surface tension of metals depends on the oxygen partial pressure. For

example the surface tension of silver is three times higher in vacuum than in 1 atm of oxygen. As a general trend it has been observed that the surface tension of oxides is lower than that of the corresponding clean metal.

Heating in oxygen, thus, partially oxidizes the platinum surface and, as a result, the platinum particles will spread on the alumina [24]. The trend that the platinum surface area is always higher if chlorine is present on the platinum surface during preparation implies that the chlorinated platinum species tend to cover the surface. There is no data available on the surface tension of platinum halides, but our experimental results suggest that the decreasing order of surface free energies is as follows Pt > PtO_x > AlO_x > $Pt(O_x)Cl_y$.

Although it has not been our principle goal to investigate how the selectivity of the minor products changes with coverage, here we report these selectivities in Table II. Especially the formation of ring enlargement products, such as

Table II.

	C1-C2[a)]	C3-C5	cC6[b)]	Hexanes
	Selectivity %			
$AlO_x/Pt_{sputtered}$	2.4	7.0	0.9	89.7
$AlO_x/Pt_{annealed}$	1.0	4.0	0.9	94.1
$Pt/AlO_x/Au$	1.4	8.5	2.2	87.9
$Pt/Cl/AlO_x/Au$	0.9	3.5	1.4	94.2
Pt(111)[c)]	0.6[d)]	0.3[e)]	0.8[f)]	-
Pt(557)[c)]	0.4[d)]	0.4[e)]	2.2[f)]	-

Table II. MCP hydrogenolysis selectivities at 620 K, H_2/MCP=240

a) from hydrogenolysis of surface carbonaceous deposit only C1 and C2 associated with C4 and C5 have been subtracted from the total C1+C2

b) cyclohexane + benzene, c) calculated from Table I in Ref. [31],

d) methane only, e) all <C6, f) benzene only

cyclohexane and benzene, deserves attention. On single crystal surfaces, Zaera *at al.* [31] found very low benzene selectivities. It has been suggested [32,33] that the enlargement of the cyclopentane ring does not occur on platinum single crystals because this reaction requires the presence of acid centers on the support. In our model systems, although the H_2/MCP ratio (ca. 240) has been higher than in those studies, we do not observe any major changes in the ring enlargement selectivity as a function of coverage (AlO_x on Pt or Pt on AlO_x/Au). But it appears that the selectivity toward cyclic products tends to be higher when platinum particles are supported on alumina, implying that perhaps interactions between particles and the support rather than between bulk platinum and alumina can promote this reaction channel. Further studies aimed at this aspect of the platinum alumina interactions should be carried out at lower H_2/MCP ratio.

References

1. a) Williams, K. J., Salmeron, M., Bell, A. T. and Somorjai, G. A., *Surf. Sci.*, **204**, L745 (1988).
   b) Levin, M., Salmeron, M., Bell, A. T., Somorjai, G. A., *J. Catal.*, **106**, 401 (1987).
2. Vurens, G. H., Salmeron, M., and Somorjai, G. A., *Progr. Surf. Sci.*, **32**(3-4), 333 (1989).
3. Anderson, J. B. F., Burch, R., and Cairns, J. A., *J. Catal.*, **107**, 351-363 (1987).
4. a) Trimm, D. L., *Appl. Catal.*, **5**, 263 (1983).
   b) Froment, G. F., *in* "Catalyst deactivation," Eds. Delmon, B. and Froment, G. F., p. 1, Elsevier, Amsterdam, 1980.
   c) Butt, J. B., *in* "Catalyst deactivation," Eds. Delmon, B. and Froment, G. F., p. 21, Elsevier, Amsterdam, 1980.
5. a) Straguzzi, G. I., Aduriz, H. R., and Gigola, C. E., *J. Catal.*, **66**, 171-183 (1980).
   b) Lee, T. J. and Kim, Y. G., *J. Catal.*, **90**, 279 (1984).
   c) Nakamura, M., Yamada, M., and Amano, A., *J. Catal.*, **39**, 125 (1975).
6. a) Hogin, D. R., Morbeck, R. C., and Sanders, H. R. U.S. Patent 2,916,440 (1959).
   b) Coe, R. H., and Randlett, M. E., U.S. Patent 3,278,419 (1966).
   c) Menon, P. G. and Froment, G. F., *J. Catal.*, **59**, 138 (1979).
7. White, D., Baird, T., Fryer, J. R., Freeman, L. A., Smith, D. J., and Day, M., *J. Catal.*, **81**, 119 (1983).
8. a) Beck, D. D. and Carr, C. J., *J. Catal.*, **110**, 285-297 (1988).
   b) Rickard, J. M., Genovese, L., Moata, A., and Nitsche, S., *J. Catal.*, **121**, 141 152 (1990).
9. Dautzenberg, F. M. and Wolters, H. B. M., *J. Catal.*, **51**, 26 (1978.

10. Lieske, H., Lietz, G., Spindler, H., and Völter, J., *J. Catal.,* **81**, 8-16 (1983).
11. Schwab, G. M. and Pitsch, E., *Z. Phys. Chem. B*, **1**, 385 (1928).
12. Tauster, S. J., Fung, S. C., and Garten, R. L., *J. Amer. Chem. Soc.*, **100**, 170 (1978).
13. Baker, R. T. K., Tauster, S. J. and Dumesic, J. A. eds. "Strong Metal-Support Interactions," ACS Symposium Series, no. 298, ACS, Washington, D.C., 1986.
14 a) Maire, G., Corolleur, C., Juttard, D., and Gault, F. G., *J. Catal.*, **21**, 250 (1971).
b) Corolleur, C., Gault, F. G., and Beranek, L., *React. Kinet. Catal. Lett.,* **5**, 459 (1976).
c) Bragin, O. V., Karpinski, Z., Matusek, K., Paal, Z., and Tétényi, P., *J. Catal.*, **56**, 219 (1979).
15. Maire, G., Plouidy, G., Prudhomme, J. C., and Gault, F. G., *J. Catal.*, **4**, 556 (1965).
16. a) Kramer, R. and Zuegg, H., *J. Catal.*, **80**, 446-456 (1983).
b) Kramer, R. and Zuegg, H., "8th ICC, Berlin, 1984," Vol. 5, p. 275. 1984.
17. Gault, F. G., *Adv. Catal.*, **30**, 1-95 (1981).
18. Davis, M. S., Ph. D. Thesis, University of California, Berkeley, 1981.
19. Cocke, D. L., Johnson, E. D., and Merrill, R. P., *Catal. Rev.- Sci. Eng.*, **26(2)**, 163-231 (1984).
20. Parmaliana, A, Frusteri, F., Mezzapica, A, and Giordano, N., *J. Catal.*, **111**, 235-242 (1988).
21. Argile, C., and Rhead, G. E., *Surf. Sci. Rep.*, **10**, 277-356 (1989).
22. Foger, K. and Jaeger, H., *J. Catal.*, **92**, 64-78 (1985).
23. Vatolin, N. A. and Timofeev, *Dokl. Phys. Chem.*, **302**, 827-830 (1988).
24. a) Ruckenstein, E. and Chu, Y. F., *J. Catal.*, **59**, 109-122 (1979).
b) Baker, R. T. K., *J. Catal.*, **63**, 523-525 (1980).
25. Kim, C. and Somorjai, G. A., to be published
26. a) Den Otten, G. J. and Dautzenberg, F. M., *J. Catal.*, **53**, 116-125 (1978).
b) Kunimori, K, Ikeda, Y., Soma, M., and Uchijima, T., *J. Catal.*, **79**, 185-195

(1983).

27. Rotermund, H. H. and Jacobi, K., *Surf. Sci.*, **126**, 32 (1983).
28. Altman, E. I. and Gorte, R. J., *Surf. Sci.*, **172**, 71-80 (1986).
29. Gonzalez-Tejuka, L., Arka, K., Namba, S., and Turkevich, J., *J. Phys. Chem.*, **81**, 1399 (1977).
30. Buttner, F. H., Funk, E. R., and Udin, H., *J. Phys. Chem.*, **56**, 657 (1952).
31. Zaera, F., Godbey, D and Somorjai, G. A., *J. Catal.*, **101**, 73-80 (1986).
32. Brandenberger, S. G., Callender, W. L., and Meerbott, W. K., *J. Catal.*, **42**, 282 (1976).
33. McVicker, G. B., Collins, P. J., and Ziemiak, J. J., *J. Catal.*, **74**, 156 (1982).

LAWRENCE BERKELEY LABORATORY
CENTER FOR ADVANCED MATERIALS
1 CYCLOTRON ROAD
BERKELEY, CALIFORNIA 94720